In presenting the dissertation as a partial fulfillment of the requirements for an advanced degree from the Georgia Institute of Technology, I agree that the Library of the Institute shall make it available for inspection and circulation in accordance with its regulations governing materials of this type. I agree that permission to copy from, or to publish from, this dissertation may be granted by the professor under whose direction it was written, or, in his absence, by the Dean of the Graduate Division when such copying or publication is solely for scholarly purposes and does not involve potential financial gain. It is understood that any copying from, or publication of, this dissertation which involves potential financial gain will not be allowed without written permission.

7/25/68

A SYSTEMS STUDY OF THE TYPEWRITER CONSIDERED AS A FLUIDIC SYSTEM

A THESIS

Presented to

The Faculty of the Graduate Division

by

Richard Austin Whisnant

In Partial Fulfillment

of the Requirements for the Degree

Doctor of Philosophy

in the School of Mechanical Engineering

Georgia Institute of Technology

June, 1970

A SYSTEMS STUDY OF THE TYPEWRITER

CONSIDERED AS A FLUIDIC SYSTEM

Approved:

Chairman

Date approved by Chairman: 5/20/70

ACKNOWLEDGMENTS

I wish to express my appreciation to all those who have contributed to the successful completion of this thesis. The problem of this thesis was suggested by Dr. S. L. Dickerson, and his advice and encouragement as thesis advisor is gratefully acknowledged. The helpfulness of the other members of the thesis committee, Drs. J. R. Baumgarten, P. V. Desai, A. G. Hansen, and J. B. Peatman is greatly appreciated.

My graduate program was made possible through the financial assistance of a National Defense Education Act Fellowship, for which I wish to thank both the taxpayers of the United States who provided the funds and the School of Mechanical Engineering and its Director, Dr. S. P. Kezios, for making them available to me.

I also wish to thank the members of the staff of the School of Mechanical Engineering who aided in the construction of the model, and to Mr. Hopkins and Mr. Thomas of Dittler Brothers, Inc. of Atlanta, who provided photoetching facilities.

The completion of my graduate program would not have been possible without the love, patience, understanding and hard work of my wife, Elaine. I shall always be grateful for her contribution to this endeavor. The patience and understanding of my daughters, Lisa and Kathy, was an inspiration to be remembered always.

TABLE OF CONTENTS

LIST OF TABLES

LIST OF ILLUSTRATIONS

SUMMARY

The intent of this study was to investigate the typewriter as a fluidic system to determine its degree of feasibility, to optimize its performance according to an established criterion of success and to demonstrate a representative method of attack in designing such a system.

In this thesis, fluidic devices were utilized to perform all of the essential functions of a typewriter which incorporated impact printing and mechanical digital actuators for type selection using a single type carrier. The analysis was carried out by breaking the overall typewriter system into subsystems and considering each subsystem in relation to the overall system design criteria of minimum power consumption and maximum typing speed. The subsystems considered were (1) the keyboard and fluidic interface, (2) the character selection encoder, (3) the sequence control, (4) the type head positioning mechanism, (5) the printing mechanism, (6) the carriage and (7) a power supply consisting of a compressor and accumulator.

Each of the subsystems was modeled either mathematically or with alternative designs and the subsystem configurations which best satisfied the overall design criteria were established. These preferred configurations were then incorporated into a computer design program so that numerical values of the essential parameters could be chosen and the effect of variations in these parameters could be determined.

Finally, a demonstration model incorporating the fluidic portions of the design and basic mechanical features was constructed and tested. The study concludes that a fluidic typewriter with the features mentioned above is feasible at typing rates up to approximately 30 characters per second with power consumption on the order of one-third horsepower. Actuator size, power consumption and fluidic time delays become limiting factors at about this speed. A maximum of 110 fluid amplifiers would be required for a complete machine having stationary keys, and these amplifiers would be of more or less conventional design. The size of the amplifiers, actuators, compressor and other components would be such as to allow a commercially competitive design from the size and weight standpoint. The use of the diaphragm instead of Coanda amplifiers can reduce the power consumption of the actuator drives by an order of magnitude or more, and they are essential to the design.

The work related to this thesis was not intended to produce a commercial device, but was intended to probe in a quantitative fashion the feasibility of such a development.

GLOSSARY OF ABBREVIATIONS

a	Y^2_w
a	length
b	blade width of compressor
c	speed of sound
d	width of power jet nozzle
e	base of Naperian logarithms
f	f (•), function defined by context
g	acceleration due to gravity
h	height of power jet nozzle
i	subscript
i	current analog
j	subscript
k	equivalent spring constant
l	length
n	integer exponent
n	number of amplifiers
n	number of compressor blades
p	pressure
q	flow, volume/time
r	pneumatic resistance
r	radius
s	Laplace transform complex frequency
t	time

v	velocity at nozzle throat
w	energy per cycle
$\hat{w}$	minimum value of w
x	piston displacement
y	motion coordinate
z	motion coordinate
A	piston area
A_D	compressor displacement area
B	$W(\tau - 1)/\pi R^2$
C	flow coefficient
C_A	accumulator analog capacitance
D	$q_m T/A$
E	equivalent pressure head, feet
F	implicit function
F	logical variable
G	implicit function
G_p	pressure gain, P_o/P_c
H	implicit function
I	moment of inertia
I	current analog
K	parameter, Equation (23)
KE	kinetic energy required to print
M	logical variable
M	m/T^3
N	logical variable

N_m	Mach number
P	$p_m q_m$
P_c	control pressure
P_c	compressor source pressure
P_o	output pressure
P_s	supply pressure
P_t	throat pressure
Q	parameter, Equation (22)
Q_c	control flow, volume/time
Q_s	supply flow, volume/time
R	$q_m \sqrt{m}/A$
R	gas constant (53.3)
R	flow resistance
Re	Reynolds number
R_o	diaphragm amplifier ridge resistance
S	rotational speed, rev/min
S_N	specific speed
T	time for actuator forward stroke
T_r	time for actuator total motion
T_s	power jet supply temperature
U	volumetric flow, ft^3/sec
V	$m[x(T)]^2/T^2$
V_D	compressor volume displacement
W	$p_m q_m T$
Y	$p_m A/\sqrt{k}$

α	bit designation
β	key designation
γ	specific weight
δ	damping ratio, Equation (94)
ϵ	$\sqrt{2KE}$
ζ	parameter, Equation (56)
η	amplifier aspect ratio, h/d
θ	angle
λ	rA^2/m
ν	function of time, Equation (154)
ξ	ridge position parameter
π	3.14159...
ρ	fluid density
σ	pressure recovery, P_o/P_s
τ	T_r/T
ϕ	$\omega_n T$
ω	$\sqrt{k/m}$
ψ	angle, Equation (91)

Subscripts: Alphabetic subscripts on these symbols are defined from context. Single numerical subscripts (e.g., w_1) refer to subsystem numbers in Figure 3. Double numerical subscripts denote quantities within a subsystem (e.g., r_{15} is radius one of subsystem five).

CHAPTER I

INTRODUCTION

Systems Analysis

The solution of engineering problems has generally been achieved by stating the problem as accurately as possible based on given information, and then choosing a solution from among the body of scientific and engineering facts available. The selection of an optimum solution has seldom been an objective, and optimum solutions were generally achieved by evolution rather than formal means. On the whole, this approach has been very successful. However, the rapidly expanding fund of knowledge in science and technology has, in recent years, made available more and more solutions to a given problem. This expansion has also provided means to solve problems which were previously too complex to consider. This trend in science and engineering has lead to the development of an approach which is known as systems analysis, complex system design, and similar terms.

The basic idea of such an approach to a problem is first to state the objectives which the system is to achieve and to place some relative value on these objectives. Then possible solutions are proposed, and these solutions are expressed in terms of models which may be physical, mathematical or organizational. Next the external factors which influence the performance of the system in obtaining its objectives are met. The various parameters inherent in the models may be

adjusted to improve their performance until the best system is achieved as determined by the established objectives or performance criteria.

This rather general approach takes many forms as it is applied in different situations. Closed loop automatic control incorporates the essential features in a very well developed body of mathematical and physical knowledge. More recently, optimal control theory has provided concepts with broad application of more general nature. The systems approach is also being utilized in the evaluation of manufacturing facilities and business systems, in the modeling of economic systems, and in the evaluation of environmental, transportation and weaponry systems.

It is the intent in this investigation to utilize the basic ideas of systems analysis described above as they apply in a specific design situation, that of designing a fluidic typewriter. Before going into more detail as to how this will be accomplished, some preliminary remarks on fluidics are in order.

Fluidics

In the period since 1960, a number of devices have been developed which provide logical, control, sensing, and amplification functions using gases or liquids as the working medium. The term fluidic is generally used to denote devices or systems which have no moving parts and accomplish their function through momentum interaction and other fluid flow phenomena. An exception to this definition which is closely related and of interest in this investigation

is the diaphragm amplifier, and it will be described subsequently.

The most prominent fluidic devices of interest here are those employing the Coanda effect described by Henri Coanda[9]*. The wall attachment (Coanda) effect is described by Warren [30] and numerous others. The Coanda effect is utilized in several devices providing logical functions [15]. Since it is well known that all logical functions can be accomplished with combinations of NOR elements [20], a fluidic NOR element is described as shown in Figure 1 [6]. The power jet fluid is applied at P. The wall (a) and cavity (b) restrict and allow, respectively, entrainment such that the flow is out of the NOR output if there is control input at neither C1 nor C2. If there is control flow at C1 or C2, it is introduced into the separation bubble so that the power stream switches to the OR output port. It is also possible to replace the cavity (b) with a wall similar to (a). With control ports on each side, the element becomes bistable and can be used as a memory element.

When the device controls power from a separate source, as the NOR gate described above, it is termed an active element. There are also passive fluidic devices, such as the AND gate in Figure 1, which operate on the signal fluid alone [15]. If either input A or B is present alone, there is no output from the AND port. If both A and B are present, the momentum of each interacts to direct the stream out the AND port.

---

*Numbers in brackets refer to the articles in the Bibliography.

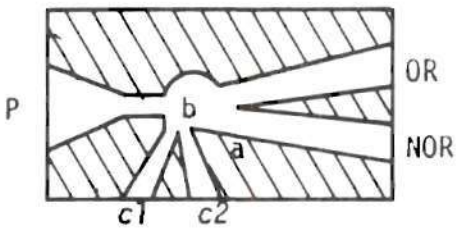

Active NOR Element

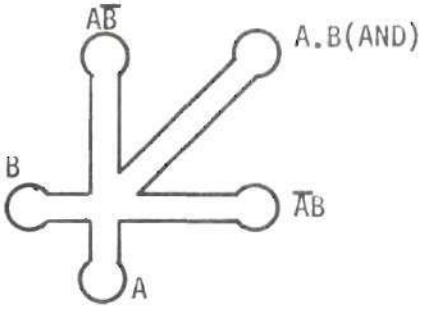

Passive AND Element

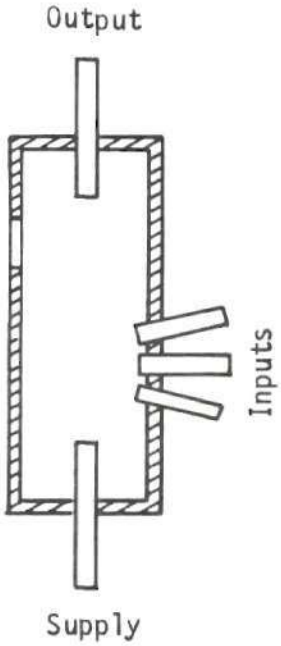

Turbulence Amplifier

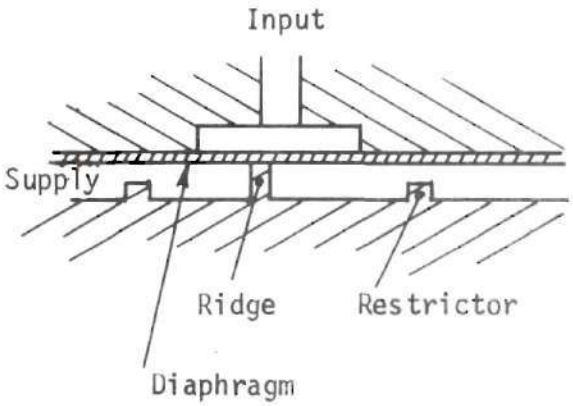

Diaphragm Element

Figure 1. Conceptual Fluidic Elements

The turbulence amplifier shown in Figure 1 operates on the principle of pressure recovery of a laminar jet [5]. Flow to one or more of the input ports causes transition to turbulent flow and a reduction in output pressure. Logically, the device corresponds to a NOR gate.

The diaphragm element, also shown in Figure 1, is a device which incorporates a moving part in the sense that the diaphragm stretches and moves away from the ridge. However, it is capable of very fast response and has the interesting feature of consuming no power when cut off. The diaphragm element can be used as a NOR gate or an amplifier, as described by Jensen, et. al. [16]. It consists of a cavity intercepted by a ridge and covered with a diaphragm of thin plastic film. Above the diaphragm is a control cavity. The variation of pressure in the control cavity varies the flow area between the ridge and the diaphragm, providing a change in output flow.

The intent of this investigation is to consider the applicability of these and related fluidic devices to the typewriter. Before proceeding, it is of interest to look at the typewriter from the historical viewpoint.

Historical Background on Fluid Actuated Typewriters

The machine that today is known as the typewriter had its beginning in 1714 when an English engineer, Henry Mill, was granted a patent [8]. The typewriter appeared in America in 1829 when William A Burt patented his typographer. The first practical commercial device was developed by Christopher L. Shoales in 1867 and was

called the typewriter from then on. The use of fluids as a working medium appeared in 1894 in a patent by William Raab [1]. This machine had bulbs for keys, each connected to a tube with a bulb on the opposite end. Compressing the "key" propelled a stencil onto the paper. Carl Weiss patented in 1895 [2], a typewriter with a cylindrical, rotating type carrier which was motor driven. The keys appear to be similar to Raab's and operated an escapement device to select the character. Beginning in 1901, Max Soblik patented several typewriters which made use of a source of compressed air, had cylindrical, rotating type carriers and means to actuate the type through air cylinders actuated by the keys [3].

None of these machines had any fluid amplification characteristics in the sense of present day fluidic devices. Not until 1967, did a typewriter incorporating a fluidic amplifier appear in the patent literature [4]. This machine seems to incorporate many of Soblik's ideas, but adds the feature having keys which are valves and actuate the control ports of fluidic amplifiers; in this case, one-shot multivibrators. This particular typewriter utilizes fluidic amplifiers only for the purpose of actuating a stop to cause a character to be printed from a cylindrical, rotating type wheel, the rest of the mechanisms being entirely mechanical. A single-stage fluid amplifier is connected to each key to provide this function.

Objectives of this Investigation

It is apparent that the logical and amplification capabilities of fluidic devices could be applied to the typewriter, as well as to

other business machines which have similar operations requiring human-mechanical interfacing. It is also apparent that the typewriter is a fairly complex device and that a general systems analysis approach to the problem would be helpful. It is, therefore, the intent of this study to investigate the typewriter as a fluidic system to determine its degree of feasibility, to optimize its performance according to an established criterion of success and to demonstrate a representative method of attack in designing such a system.

CHAPTER II

SYSTEM DEFINITION

Typewriter Functions

In order to consider the applicability of fluidics to the typewriter, it is first necessary to state the functions which a typewriter performs. The study will be limited to impact printing, and no attempt to develop novel methods of printing will be made.

The most basic typewriter function is, of course, to drive a type-face against the output medium (paper, stencil, mat, etc.) when a key is depressed. In order to print more than one character, the printing point must move. This requires that either the paper or the type-face must move after printing. The carriage motion thus forms the second important function. To print more than one line, the output medium must be advanced, requiring a third function. Also the typing point must be returned to the beginning of the line, necessitating a carriage return function. The typewriter (and the similar tele-typewriter) has a multiplicity of keys and corresponding type-faces. The office typewriter generally has 44 keys with both upper and lower case, and the tele-typewriter generally has a slightly fewer number of characters. A basic function of the typewriter, then, is to select the proper character when the key or keys are depressed. To print a blank, the space bar, is also necessary.

There are numerous other functions or features of the typewriter.

Impact printing typewriters usually employ ribbon as a means of ink supply. The ribbon advance and positioning is another function. Some typewriters also provide for multicolor printing with the ribbon mechanism. It is also usual to provide variable margin stops and means to position these, as well as intermediate stops to assist in tabulation and mechanisms for setting these stops. These are other necessary functional parts of the typewriter.

In both "manual" typewriters (powered entirely by the operator) and "electric" typewriters (having additional sources of energy) many of the functions are performed by complex mechanical linkages with their various interlocks and sequencing features, some of which might advantageously be replaced by fluidics, and some might just as well remain mechanical. The first task of this study is to consider the more basic and complex of the typewriter functions in the light of the capabilities of fluidics, to determine which functions can be accomplished with fluidics, and to arrive at a general system model.

Overall Model Guidelines

The Coanda or wall attachment effect provides fluidic devices which are essentially digital. That is, their outputs are either on or off, in one state or another, rather than varying smoothly from one state to another. The diaphragm devices mentioned previously may also have this switching characteristic. One of the basic functions listed previously was the selection of the character to be typed when the corresponding key is depressed. A means of providing this function fluidically would be to code the characters numerically and have each

key generate a number to select the character. The digital nature of the fluidic devices is well adapted to this function.

In conjunction with this character selection, there are several possible mechanical means of conveying the type-face itself to the paper. The familiar type-bar machines (both manual and electric) have each key connected mechanically and individually to a bar carrying the type-face. Such an arrangement requires, at most, power amplification between the key and the type bar. While fluidic elements can provide this, such an arrangement would not take full advantage of fluidic capabilities. The scheme employing a type carrier or head with all the type-faces on this single member, which is positioned in various ways with respect to the print position to select the character, is another possibility. The type carrier may be planar, cylindrical, spherical, etc., in shape, with motion commensurate with the shape. Also, the printing motion may be provided in various ways. Such devices are actually older than the type-bar arrangement. For instance, the type carrier may be cylindrical or spherical with a rotary and/or axial motion for type selection. Printing can be accomplished by moving the type carrier itself to the paper, either by driving its support forward or by striking a floating carrier with a "hammer". It is also possible to have the faces propelled individually to the paper. These, along with carriers having two-axis planar motion have all been used in various machines for many years. This single type carrier arrangement is best adapted to the fluidic coding discussed above.

Therefore, in this study the single-type carrier of cylindrical or spherical shape will be considered. Character selection will be

accomplished with pneumatic digital actuators of the multipiston type to be described later, the motion of the actuators being determined by a numerical code generated fluidically from a standard keyboard arrangement. It is felt that this will make maximum use of the fluidic devices and demonstrate their effect on the system most completely.

It is apparent from the previous discussion that there are several basic functions of the typewriter, and they are considered here to be the input or key function, the type selection function, the printing function, the carriage motion function, and in the case of powered machines, an energy source function. The proper sequential operation of these functions is usually carried out on manual or electric typewriters by arrangements of linkages, clutches, stops and escapements which tend to be quite complex. Due to the digital or logical character of Coanda fluidic devices these sequencing operations can be carried out, in large measure, without moving parts. Therefore, a fluidic control or sequencing function also is basic to the typewriter's overall system.

These will be considered the basic functions and will be dealt with extensively. The other functions; such as advancing of the paper, ribbon positioning, margin setting, tabulation, etc.; are much less complex and will not be considered in this analysis.

General System Model

In keeping with the desire to make a systematic analysis, the remarks concerning the basic functions of the typewriter can be summarized and formalized in a model or functional block diagram,

such as Figure 2. Each of the functions can be translated into a block containing hardware, whose form is yet to be specified in detail, and whose interaction with other blocks can be determined. The general features of the typewriter are thus displayed beginning with mechanical inputs from an operator and some source of pneumatic power, such as a compressor. These inputs are converted to pneumatic signals to activate the fluidic functions of control, character selection and positioning, and printing, which are then reconverted to mechanical motions to provide the output of characters printed on the paper. It is in this context of considering the fluidic typewriter as a mechanical-fluidic-mechanical conversion device consisting of functional subsystems that the present analysis may have more general application to other similar systems. Some general guidelines as to the hardware corresponding to the functions have already been given in the previous section. Further definition will be delayed pending a discussion of measures of success for the design achieved.

Design Criteria

In order to investigate the degree of applicability of fluidics to the typewriter, and in some measure to other similar machines, it is first necessary to define a criterion of success so that alternatives may be weighed in proper perspective. There are a number of fairly obvious criteria which can be used to judge a typewriter design; cost (both initial and operating), print quality, speed capability, noise level, overall weight and volume, power consumption and visual appearance.

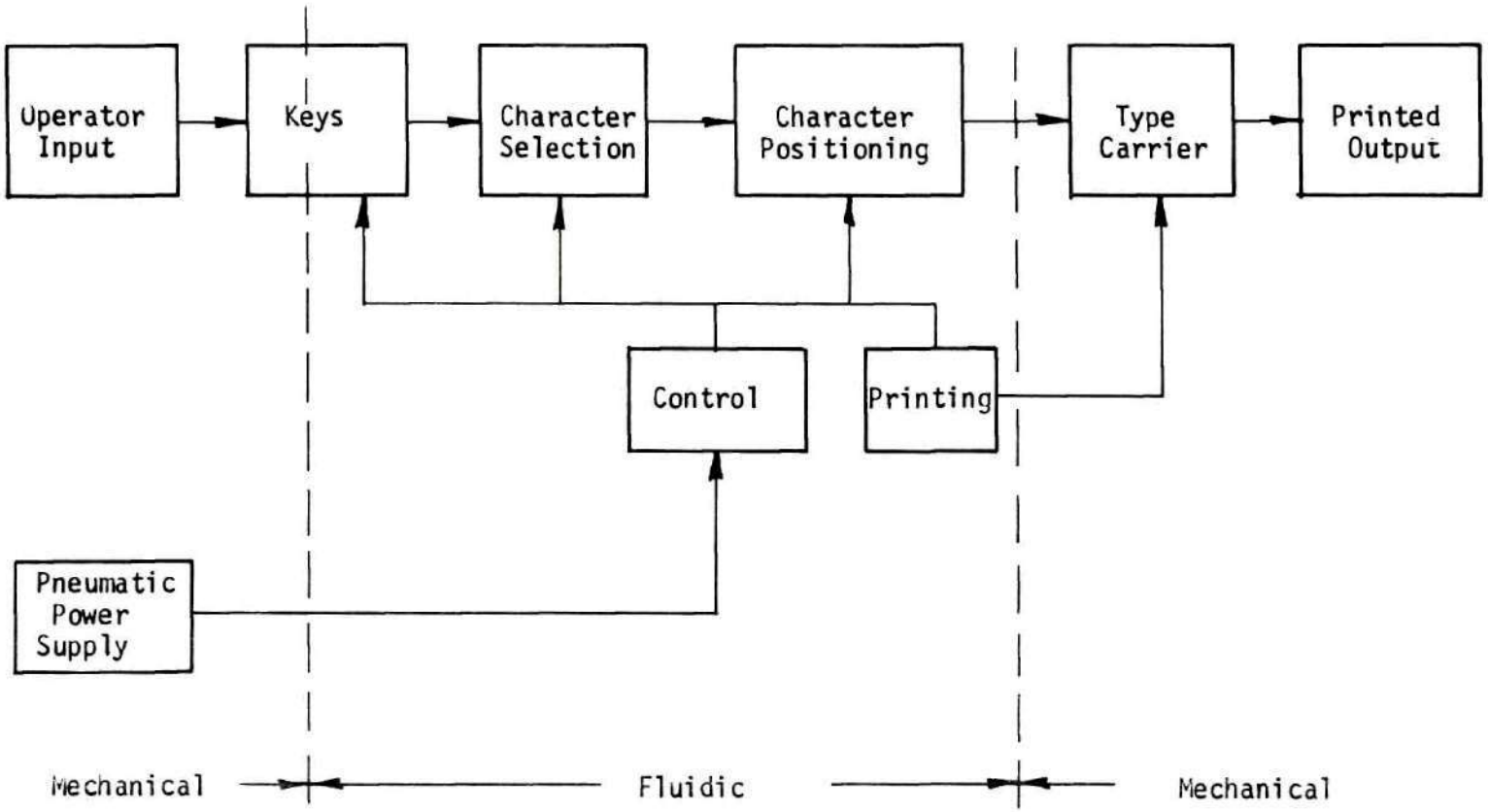

Figure 2. General System Model

For instance, first cost as a criterion has only limited significance outside of a well-defined manufacturing environment where labor, material and overhead costs are precisely known. However, it is possible in this problem to estimate the cost of the components of the fluidic typewriter which are peculiar to it and to estimate their possible significance in terms of the selling price of a competitive typewriter. That is, if the cost of such fluidic elements is 10 per cent of the selling price, the design is much better than if it is 90 per cent of that price.

Operating cost as a criteria is easier to compute and to utilize as a design criterion. In terms of power required (which costs, say 1.5¢/kwh), a typewriter drawing one kilowatt would cost about $30 per year to operate. There is another way in which power may be used as a criterion. If the device requires more than 15 amperes at 115v, then it cannot be plugged into a normal office or household outlet, since 15 amps is the design current for most such circuits, thus, 1725 watts is something of a break point in power consumption and may serve as a constraint at some point in the design. Furthermore, power consumption has implications with regard to the criteria of noise, speed and weight which may not be as readily formulated, but are nonetheless real.

Print quality is certainly an important criterion for measuring performance. Many factors influence print quality (which includes legibility, uniformity of density, spacing, type design, ribbon design, etc.) and most of these are considered outside the scope of this thesis. According to Greenblott [13], satisfactory printing will be achieved if

the printing element (and its associated structure) strikes the paper with a kinetic energy of 10^5 ergs. This will be taken in this thesis as a firm design criterion or constraint where it applies.

Speed capability as expressed in number of characters printed per second is another valid way to judge a design. Typists in general may type at rates of 60 words per minute or five characters per second. The maximum is about ten per second for human operators. Likewise, computer terminals, teletypewriters and the like, operate at about 10 - 15 characters per second. So a fluidic typewriter, to be feasible, must approach these speeds and exceed them if possible, depending on whether other criteria are met or not.

For office and business use, the noise level of the typewriter is certainly a factor. However, the prediction of noise level for an initial design is not very practicable. Nevertheless, noise may be one of the more critical problems in a fluidic typewriter, since all Coanda type elements are vented and there will be air exhausting from cylinders as well. Since the amount of acoustic power available for noise generation is directly related to pneumatic power consumed, reduction of power may have significance here, as well as from the cost and size standpoints.

The weight, size and visual appearance of the typewriter are other criteria which would become important before a saleable design were achieved. For example, a typewriter weighing 500 pounds would hardly be acceptable, but the value of reducing weight from 50 to 40 pounds is hard to assess in the context of the proposed work. Size and appearance are, of course, important from the standpoint of

marketing and utilization.

These comments on design criteria and how they relate to the overall typewriter design are summarized in Table 1.

It is apparent that there are many factors involved in judging whether an acceptable and/or preferable design has been achieved. Some can be expressed precisely in numerical terms, while others depend on esthetic appeal. Still other factors are influenced by manufacturing limitations and competition in the market. In carrying out an analysis in an academic environment these latter factors cannot be evaluated as accurately as can the quantitative factors. This seeming limitation is not as bad as it may appear for two reasons. First, it is not possible to consider such criteria as manufacturing cost, size, appearance, etc. until the system has been established which meets the functional requirements and performs adequately, as measured in some quantitative fashion. This analysis is intended to establish such a system and, in that sense, is preliminary to consideration of such factors of manufacturing cost or esthetic appeal. This is not to say that these factors are completely ignored, but that they are subordinate at this early stage. Secondly, the criterion of power consumption which is a quantitative measure, has implications with regard to many of the other criteria. For example, minimizing power consumption tends to minimize the number of fluidic devices, which in turn reduces manufacturing cost, size, weight and noise, and improves reliability. Reduction in size, weight and noise level makes design for esthetic appeal and conservation of space easier. However, if the minimization

Table 1. Relation of Design Criteria and Overall Objective

Criterion	Relation to Objective
Initial Cost	Estimated cost of fluidic components relatively small part of typewriter selling price
Operating Cost	Proportional to power cost
Print Quality	Determined by kinetic energy of 10^5 ergs
Speed Capability	At least 10 characters per second, greater if other factors allow
Noise	Proportional to power consumption
Weight	Comparable to competitive typewriter
Volume	Comparable to competitive typewriter
Appearance	Must be capable of neat appearance

of power consumption is carried to its ultimate, the result is zero power and no capability to type. It is desirable that the typing speed capability be as high as possible, both to provide competitive advantage where the machine may be applied as a teletypewriter or computer terminal and to explore the maximum capability of the fluidic system.

Based on these considerations, the overall design criterion for this analysis of the fluidic typewriter will be to maximize speed and minimize power consumption, consistent with the constraints imposed by the model guidelines discussed previously and with mechanisms chosen

to couple with the fluidic and pneumatic components.

Method of Attack

In general, the attack will be to separate the physical mechanisms of the typewriter into subsystems. A subsystem will be defined as a device or devices performing a definite, specifiable function on given inputs and producing given outputs. Design criteria will be established for each subsystem which contribute to the achievement of the overall design goal. The parameters which govern the subsystem performance will be identified and their values established by modeling the subsystem and determining the parameter values which best satisfy the subsystem criterion. Where trade-off situations among parameter values can be identified, these will be carried out.

The subsystems to be considered are illustrated in Figure 3, which shows each subsystem as a block with an indication of the information or signal flow, as well as the power flow between them. The broken line enclosing the carriage with the type head position and print subsystems is an indication that some or all of these may be part of the carriage, as determined by further analysis. The numbers one through ten on the blocks distinguish the subsystems and will be utilized in the notation of subsequent discussions.

In the succeeding chapters each subsystem will be considered in detail and then the overall model formulated in order to analyze the typewriter as a complex system.

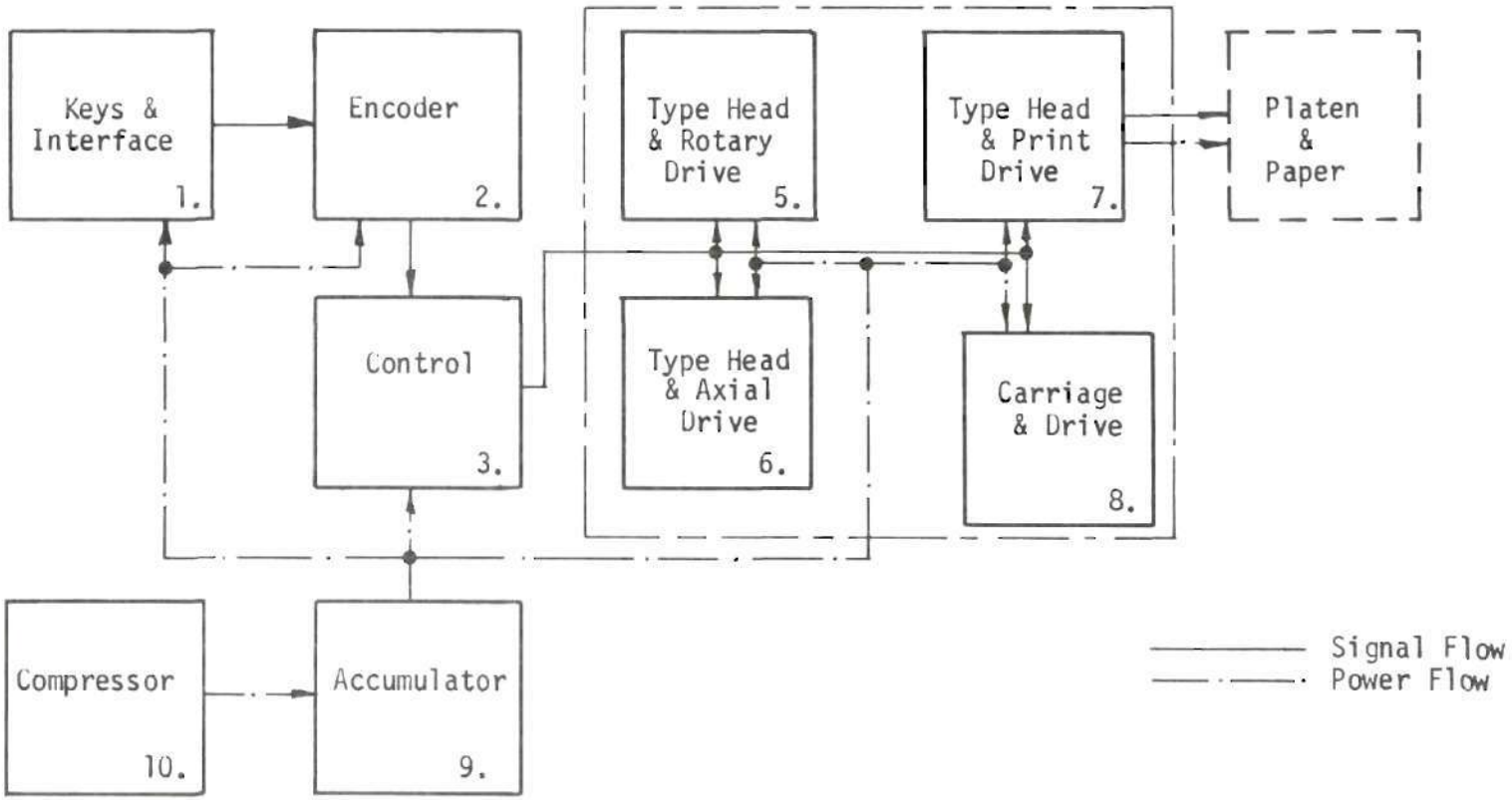

Figure 3. Functional System Model

CHAPTER III

PRINT SUBSYSTEM OPTIMIZATION

Definition of the Problem

As was observed in Figure 3, the flow of information is from the keys to the paper and the last operation in typing a character (excluding carriage motion) is to cause the print head to strike the paper. The form and characteristics of the print drive subsystem will than have an influence on the prior subsystems which interface with it, and these in turn on the ones prior to them. It is thus logical to consider first the print drive subsystem and to define its configuration and parameters.

The print drive subsystem consists basically of the type head; its supporting structure, which is free to move so that the type head strikes the paper; a pneumatic cylinder to drive the structure; one or more fluid amplifiers to supply air pressure to the cylinder; and a return spring, if required.

The first task is to define a criterion by which to judge the possible configurations. Essentially, the criterion is that when the subsystem is actuated, a character of acceptable print quality appears on the paper at the proper place. However, it is difficult to design to such a specification, except by experimentation with hardware. What is needed is some quantitative characteristic of the subsystem which can be related to the parameters involved. In a study of a computer

line printer, Greenblott [13] showed for a metal hammer striking a six-part form (i.e. original and five copies) against a metal type-face, the kinetic energy required for acceptable printing was about 100,000 ergs. For a one-part form, the energy was 28,300 ergs. In engineering units 100,000 ergs is approximately 0.088 in.lb. Since the typewriter under consideration here also prints by impact under similar conditions, the objective of acceptable printing will be equated with the achievement of 100,000 ergs of kinetic energy. The design criterion will, therefore, be that the type head and its support structure achieve 100,000 ergs of kinetic energy just before striking the paper, and do so in a manner consistent with the overall objective of minimum input power and maximum typing speed.

Possible Configurations

The mechanical portions of this subsystem consist of the type head mounted on a movable structure which is coupled by some mechanical linkage to a moving piston. Regardless of the form of the linkage, it is possible to represent this mathematically as a reflected or equivalent mass connected directly to the piston, so long as there is a linear relationship of input to output motion. The numerical value of the equivalent mass will depend on both the mass of the moving parts and the kinematic relations of the moving parts.

The fluidic portions of the subsystem consist of the one or more fluidic elements directly driving the piston. The fluidic element required here would be a digital or switching type element, which would apply pressure on command to the cylinder for a given time and then

reset. The three types of elements mentioned in Chapter I were the turbulence amplifier, the Coanda amplifier and the diaphragm amplifier. The output pressure from the turbulence amplifier is on the order of a few tenths of a psi [5], [31], [32], and is not considered suitable for this application. Output pressures for the Coanda and diaphragm devices are much higher (1 - 5 psi).

There are several possible combinations of these basic components, six of which are shown in Figure 4, along with some of the nomenclature to be used. Subsequently, they will be referred to as Case a, Case b, etc. Some general observations on the features and relative merits of each case can be made. One of the most important observations is that the Coanda elements (Case a and b) consume the pneumatic power supplied to the power jet continuously, regardless of the action of the driven piston and mass, whereas the diaphragm elements (Cases c to f) consume power only when there is flow over the ridge to move the cylinder. This tends to reduce the power consumption of the subsystem. There are, of course, different numbers of amplifiers required for the various cases, which has implications for the cost and reliability of the machine.

The basic difference in Cases a and b is that in Case a the piston is driven forward to print and returned by a spring, whereas in Case b the piston is driven by the amplifier in both directions. The potential energy stored in the spring during piston motion must also be supplied by the amplifier, possibly resulting in a larger amplifier than Case b. The spring constant could be adjusted to compensate for this to some extent, but the total response time would be different.

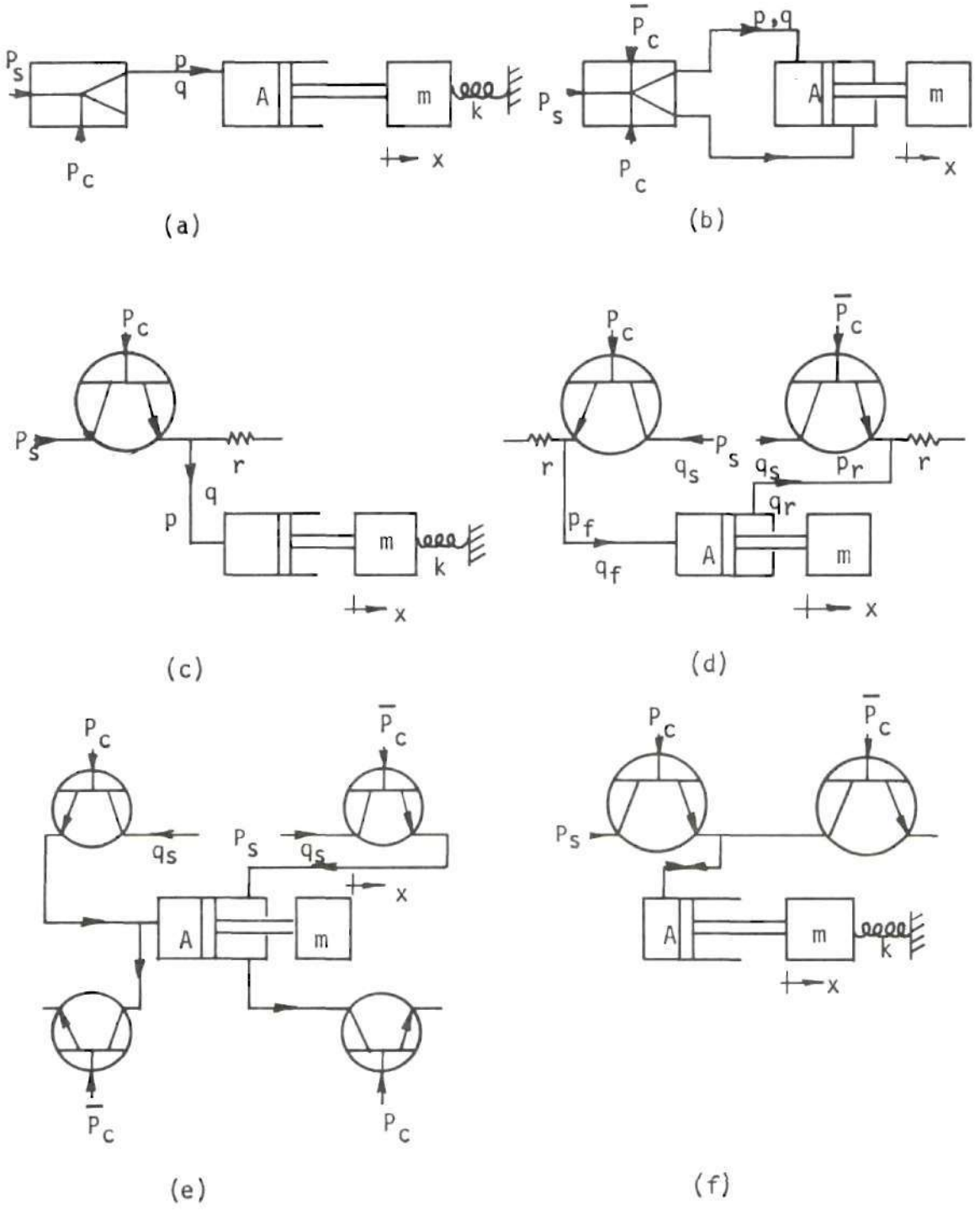

Figure 4. Print Subsystem Configurations

The diaphragm element of Case c uses power only when driving the cylinder, as opposed to Case a. However, only part of the power drives the cylinder, the rest being dissipated through the exhaust resistance r. The resistance r is needed to provide pressure to drive the cylinder. It is possible that Case c will have lower power consumption than Case a, particularly at low typing speeds.

By using two diaphragm elements as in Case f, the power loss in the resistance r of Case c can be eliminated. In Case f, as in all the cases, P_C, the control pressure, is treated as a Boolean variable and $\overline{P}_C$ indicates the negated value of P_C. Thus, when P_C is off the supply pressure P_S is applied to the piston only since $\overline{P}_C$ is on and the exhaust is blocked. During exhaust, the ridge restriction is very low and the exhaust is essentially unrestricted.

Case d shows the use of two diaphragm amplifiers to drive the piston in either direction. It has the same disadvantage as Case c in that part of the flow is dissipated through the resistance r which is necessary for exhaust in both directions. In addition, each end of the cylinder is under pressure at the being of the opposite stroke, which tends to reduce the effective pressure. This can be eliminated, along with the loss through r, at the cost of two more diaphragm elements, as in Case e. Case f eliminates the resistance losses in both directions with two amplifiers, but returns with a spring.

These more or less qualitative remarks furnish some background for choosing a print drive configuration. However, it is necessary to consider each system quantitatively as well in order to determine

which will best satisfy the overall design objective. Each case will be represented mathematically, the design criterion stated mathematically, and the combination of physical parameters which best satisfies the criterion determined.

Case a

The equation of motion for the piston, mass and spring of Figure 4a, assuming the spring massless and the piston mass included in m, is

$$m\ddot{x} + kx = pA \qquad x(0) = 0,\ \dot{x}(0) = 0 \tag{1}$$

where friction in the cylinder has been neglected. If it is assumed that the output characteristic of the Coanda amplifier can be approximated by a straight line and that the line friction loss and delay are small, then the output pressure is given by

$$p(t) = -\frac{P_m}{q_m} q(t) + p_m \tag{2}$$

Now since the pressure is low at the amplifier output, assume incompressibility, so that

$$\dot{x}A = q(t) \tag{3}$$

Substitution of Equation (2) and (3) into Equation (1) will yield

$$\ddot{x} + \frac{\rho_m A^2}{q_m m}\dot{x} + \frac{k}{m}x = \frac{\rho_m A}{m} \qquad (4)$$

with the same initial conditions.

The assumption of small delay time between the switching of the amplifier output and application of pressure to the cylinder needs to be considered briefly. Schuder [33] has given a solution for the problem of a step input to a transmission line connected to a fixed volume. The published discussion of this paper by D. C. Union gives a simpler relationship, which is sufficient for the present purpose. Since the dimensions of the typewriter would limit the length of any transmission line to about one foot, the pure delay for the pressure pulse would be about one millisecond. Furthermore, since the piston does not move instantaneously, the cylinder volume is practically constant for a short time. If, for example, a line ten cm. long with an internal diameter of two mm. is connected to a volume of seven $cm.^3$, a delay of approximately one millisecond occurs between application of pressure to the line and the attainment of applied pressure in the cylinder according to Union's equation. A total delay on the order of two milliseconds is small for typing speeds of about ten characters per second (100 ms. per character), so that the assumptions of Equation (2) are reasonable.

The equation of motion for the forward motion of the print drive is given by (4). At the time of impact, t = T, the forward motion stops and the type head and its support are returned by the action of the

spring, the amplifier output having been switched off. The cylinder exhausts through the amplifier output port, which is vented, and presents a low impedance which is neglected here. The equation of motion for the return stroke is ($t \geq T$)

$$m\ddot{x} + kx = 0 \qquad x(T) = x_o\,,\ \dot{x}(T) = 0 \tag{5}$$

The boundary conditon on $\dot{x}$ reflects the assumption that the type head does not rebound after impact with the platen. Some rebound is to be expected, so that in terms of the time required to return the type head to its original position, the assumption is a conservative one.

In order to apply the design criterion of maximum speed and minimum power to this subsystem, some quantitative expression of it is needed. First, note that the power consumed is given by the product of pressure and volume flow to the amplifier power jet. The power jet flow and pressure are some fraction of q_m and p_m, respectively, and therefore the product $p_m q_m$ is indicative of the power consumption. As noted before, it is not practical to minimize power alone or to maximize speed alone. However, if the product

$$w = p_m q_m T_r \tag{6}$$

is formed as the function to be minimized, where T_r is total time for forward and reverse motion, then the design objective tends to be satisfied. Observe that minimizing T_r tends to maximize typing speed

since the smaller is T_r, the more characters can be typed in a given time. Also observe that since w has the dimensions of force times length, or work, minimizing w minimizes the work of a given print operation.

To summarize the problem, then, it is desired to minimize w in Equation (6) subject to the dynamic constraints of Equations (4) and (5), with the additional objective of achieving a fixed kinetic energy

$$KE = 0.5\, m\, [\dot{x}(T)]^2 \tag{7}$$

at the end of the forward stroke.

The minimization of w can be carried out as follows: The Laplace transform of Equation (4) leads to

$$x(s) = \frac{p_m A}{k} \quad \frac{1}{s\left(s^2 + \frac{p_m A^2}{q_m m} + \frac{k}{m}\right)} \tag{8}$$

The transform of Equation (3) gives

$$q(s) = sAx(s) \tag{9}$$

Define $\epsilon(t)$ by

$$\epsilon(t) = (2KE)^{0.5} \tag{10}$$

Then from (7)

$$\epsilon(t) = m^{0.5}\dot{x}(t) \tag{11}$$

and combining this with (3) gives

$$q(t) = Am^{-0.5}\epsilon(t) \tag{12}$$

The Laplace transform of (12) can be combined with equations (8) and (9) to yield

$$\epsilon(s) = \frac{\rho_m A}{m^{0.5}}\left(s^2 + \frac{\rho_m A^2}{q_m m}s + \frac{k}{m}\right)^{-1} \tag{13}$$

At this point the analysis divides into three sub-cases corresponding to the complex, real and equal, and real and unequal roots of the quadratic factor in equation (13). Considering first the complex roots, the inverse transform of (13) evaluated at t = T gives

$$\epsilon(T) = \frac{\rho_m A}{m^{0.5}} \frac{\left[\exp\left(-\frac{\rho_m A^2 T}{2q_m m}\right)\right]}{\left[\frac{k}{m} - \left(\frac{\rho_m A^2}{2q_m m}\right)^2\right]^{0.5}} \sin\left[\left(\frac{k}{m} - \frac{\rho_m A^2}{2q_m m}\right)T\right] \tag{14}$$

where $\epsilon(T)$ is known.

Now consider Equation (5), whose solution is

$$x(t') = \cos\left(\frac{k}{m}\right)^{0.5} t' \qquad t' \geq T \tag{15}$$

Let $t = t - T$ and evaluate (15) at $t = T_r$, which gives

$$x(T_r - T) = x(T)\cos\left[\left(\frac{k}{m}\right)^{0.5}(T_r - T)\right] \tag{16}$$

But at $t = T_r$, $x = 0$ and Equation (16) is satisfied for these conditions only when

$$\left(\frac{k}{m}\right)^{0.5}(T_r - T) = \frac{\pi}{2} \tag{17}$$

It would be convenient to have the ratio

$$\tau = \frac{T_r}{T} \tag{18}$$

and combining (17) and (18) the result is

$$\tau = \frac{\pi}{2T}\left(\frac{m}{k}\right)^{0.5} + 1 \tag{19}$$

This last equation furnishes a relation between the forward and return stroke times and the physical system (m and k) which will prove useful.

It is now desired to relate the quantity to be minimized, w, to the relations developed from the constraints, namely Equations (14) and (19). If the definitions of Y and R are made as

$$Y = \frac{P_m A}{k^{0.5}} \qquad R = \frac{g_m m^{0.5}}{A} \tag{20}$$

then it can be shown that

$$F(w,Y) = \frac{Y}{Q} \exp(-K) \sin\left[\frac{\pi Q}{2(\tau-1)}\right] - \epsilon(T) \tag{21}$$

where

$$Q = \left[1 - \frac{\pi^2 Y^4 \tau^2}{16 w^2 (\tau-1)^2}\right]^{0.5} \tag{22}$$

and

$$K = \frac{\pi^2 Y^2 \tau}{8 w (\tau-1)^2} \tag{23}$$

An outline of the development of Equation (21) is given in Appendix A.

The quantities Y and R have an interesting physical interpretation. The maximum potential energy of the subsystem is proportional to $kx^2(T)$. Expressing x(T) as force divided by k, where the force is proportional to $P_m A$, results in

$$Y \sim \sqrt{\text{maximum potential energy}}$$

Similarly, since the maximum kinetic energy is proportional to $m\dot{x}^2(T)$, by using Equation (3) it is seen that

$$R \sim \sqrt{\text{maximum kinetic energy}}$$

The quantities Y and R of Equation (20) are thus related to the

energies of the subsystem at the end of the forward stroke.

It is seen that for any given value of τ Equation (21) gives w as an implicit function of one variable, Y. Since F(w,Y) is identically zero, it can be shown that

$$\frac{dw}{dY} = - \frac{\partial F/\partial Y}{\partial F/\partial w}$$

For w to be minimum with respect to Y, dw/dY = 0, which implies that at the minimum

$$\left.\frac{\partial F}{\partial Y}\right)_{\hat{w}} = 0 \tag{24}$$

and

$$\left.\frac{\partial F}{\partial w}\right)_{\hat{w}} \neq 0 \tag{25}$$

Carrying out the operation of Equation (24), the relation

$$\tan\left[\frac{\pi}{2}\left(\frac{Q}{\tau-1}\right)\right] = \left[\frac{16(\tau-1)^3 Q}{\pi^3 \tau^2 a^2} - \frac{4(\tau-1)Q}{\pi \tau a} + \frac{2(\tau-1)}{\pi Q}\right]^{-1} \tag{26}$$

is obtained, where

$$a = \frac{Y^2}{w} \tag{27}$$

Since Q and K can be expressed in terms of a and τ alone, Equation (26) can be solved numerically for a, the corresponding Q and K substituted in (21) to get Y, and the minimum value of w, $\hat{w}$, then gotten from (27). The process can be repeated for various values of τ to give a curve of w versus τ.

Equation (25) results in the relation

$$\frac{\partial F}{\partial w} = \frac{\exp(-K)\pi^2 Y^3 \tau}{8w^2(\tau-1)^2 Q}\left\{\frac{\pi Y^2 \tau}{4w(\tau-1)Q}\cos\left[\frac{\pi Q}{2(\tau-1)}\right] + \sin\left[\frac{\pi Q}{2(\tau-1)}\right] - \frac{Y^2\tau}{2wQ^2}\sin\left[\frac{\pi Q}{2(\tau-1)}\right]\right\} \neq 0 \tag{28}$$

The solutions to (24) must satisfy (28). Presentation of the results is delayed until after consideration of the sub-cases for real roots.

Returning to Equation (13) and assuming real and unequal roots for the quadratic factor, the inverse transform gives (when evaluated at t = T) the same result as (14) with sine replaced by hyperbolic sine

$$\epsilon(T) = \frac{\rho_m A}{m^{0.5}} \frac{\exp\left(-\frac{\rho_m A^2 T}{2q_m m}\right)}{\left[\frac{k}{m} - \left(\frac{\rho_m A^2}{2q_m m}\right)^2\right]^{0.5}} \sinh\left[\left(\frac{k}{m} - \frac{\rho_m A^2}{2q_m m}\right)T\right] \tag{29}$$

Then following the same procedure that lead to Equation (21), it can be shown that

$$G(w,Y) = \frac{Y}{J}\exp(-K)\sinh\left[\frac{\pi J}{2(\tau-1)}\right] - \epsilon(T) \tag{30}$$

where

$$J = \left[\frac{\pi^2 Y^4 \tau^2}{16 w^2 (\tau-1)^2} - 1\right]^{0.5} \tag{31}$$

and K is as defined in Equation (23). To find the minimum value of w with respect to Y for any given τ, the procedure is the same as that leading to Equation (26). The conditions to be satisfied are

$$\left.\frac{\partial G}{\partial Y}\right)_{\hat{w}} = 0 \tag{32}$$

and

$$\left.\frac{\partial G}{\partial w}\right)_{\hat{w}} \neq 0 \tag{33}$$

Evaluation of (32) leads to the relation

$$\tanh\left[\frac{\pi J}{2(\tau-1)}\right] = \left[\frac{4(\tau-1)J}{\pi a \tau} - \frac{16(\tau-1)^3 J}{\pi^3 a^2 \tau^2} + \frac{2(\tau-1)}{\pi J}\right]^{-1} \tag{34}$$

where a and J have been defined previously. Since J and K can be expressed in terms of a alone for any given τ, Equation (34) can be solved numerically for a, the corresponding J and K substituted into (30) to get Y, and the minimum w gotten from (27). Repeating the process for several values of τ will allow plotting $\hat{w}$ versus τ.

Evaluation of equation (33) leads to

$$\frac{\partial G}{\partial w} = \frac{\pi^2 Y^3 \tau \exp(-K)}{8 w^2 (\tau-1)^2 J} \left\{ -\frac{\pi Y^2 \tau}{4 w (\tau-1) J} \cosh\left[\frac{\pi J}{2(\tau-1)}\right] + \frac{Y^2 \tau}{2 w J^2} \sinh\left[\frac{\pi J}{2(\tau-1)}\right] + \sinh\left[\frac{\pi J}{2(\tau-1)}\right] \right\} \neq 0 \tag{35}$$

Returning once again to Equation (13), the sub-case of real and equal roots of the quadratic (critical damping) is considered. The inverse transform evaluated at t = T yields

$$\epsilon(T) = \frac{\rho_m A T}{m^{0.5}} \exp\left[-\left(\frac{k}{m}\right)^{0.5} T\right] \tag{36}$$

Using the relations of (19) and (20) and the additional fact that for critical damping Y/R = 2, it is possible to arrive at

$$H(w, Y) = \frac{2w}{Y\tau} \exp\left(-\frac{2w}{Y^2 \tau}\right) - \epsilon(T) \equiv 0 \tag{37}$$

Again, the minimum of w with respect to Y for any given τ is defined by

$$\left.\frac{\partial H}{\partial Y}\right)_{\hat{w}} = 0 \tag{38}$$

and

$$\left.\frac{\partial H}{\partial w}\right)_{\hat{w}} \neq 0 \tag{39}$$

Since w = 0 is excluded by physical considerations, Equation (38) results in

$$\frac{4w}{\tau Y^2} = 1 \tag{40}$$

If this is substituted into (36), along with Y and R from (20), the result is

$$\hat{w} = [\epsilon(T)]^2 e \tau \tag{41}$$

However, from Equations (19) and (20), it can be shown that

$$\tau = \frac{\pi Y^2 \tau}{4w} + 1 \tag{42}$$

If (40) and (42) are combined, the result is

$$\tau = 4.142\cdots \tag{43}$$

so that the final result for $\hat{w}$ is

$$\hat{w} = 11.21 [\epsilon(T)]^2 \tag{44}$$

when critical damping is specified.

It is fairly simple to show that Equation (39) is satisfied. If the differentiation is carried out and Equations (40) and (43)

substituted appropriately, the result is

$$\frac{\partial H}{\partial w} = 0.147\, Y^{-1}$$

and since Y is, from physical considerations, never infinite, Equation (39) is satisfied.

As previously stated, the solutions for $\hat{w}$ when the roots are complex or real and unequal must be found numerically. The computations were carried out with the aid of a programmable electronic calculator, and the solutions for all three sub-cases underdamped, critically damped and overdamped are presented in Figure 5.

It is of interest to note that there is a minimum of w with respect to τ at approximately $\tau = 2.6$, which is in the range representing the complex roots or underdamped portion of the curve. In the interval $2.6 < \tau < 5.0$ (approximately) Equations (26) and (34) did not yield solutions. However, this is not unexpected from the physical standpoint, since it turns out to be the transition from underdamped to overdamped, and the solution for w from the critically damped case falls in this interval. A smooth curve is faired through this interval to give a complete picture of the value of $\hat{w}$, representing the minimum energy expended in typing one character for Case a of Figure 4.

It is of interest to note the value of the damping coefficient corresponding to the minimum at $\tau = 2.6$. It can be shown that the damping coefficient can be expressed by

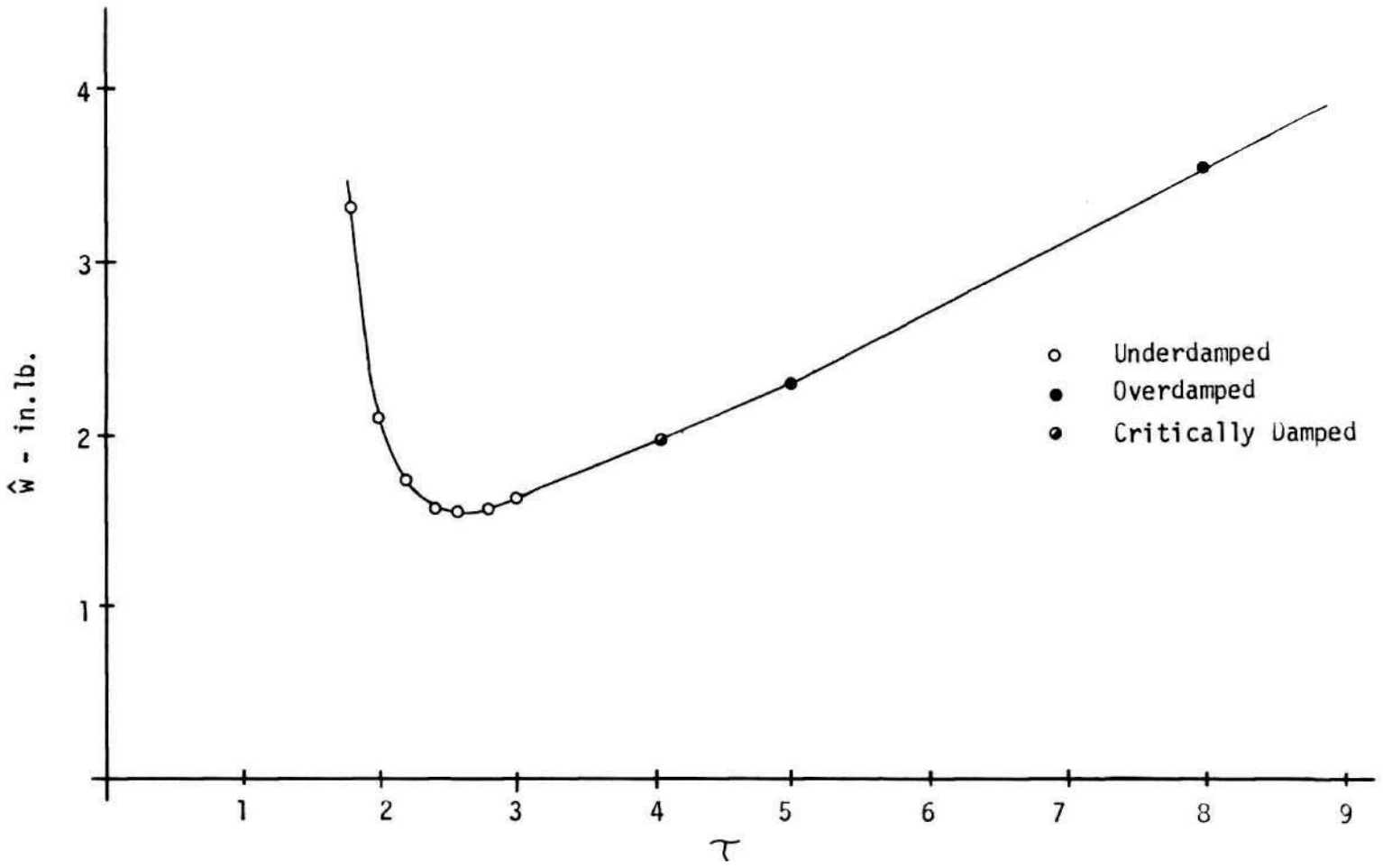

Figure 5. Minimum Work for Printing, Case a

$$\delta = \frac{Y}{2R}$$

and the value at $\tau = 2.6$ turns out to be $\delta = 0.63$.

Case b

This configuration as shown in Figure 4 drives the piston in both directions with the amplifier. The equation of motion in either direction is

$$m\ddot{x} = pA \qquad x(0)=0, \quad \dot{x}(0)=0 \tag{45}$$

As before, friction in the cylinder is neglected, as well as flow restriction in the exhaust direction. Assuming a linear amplifier output characteristic as in Equation (2) and incompressible flow as in Equation (3), the equation of motion becomes

$$\ddot{x} + \frac{p_m A^2}{q_m m}\dot{x} = \frac{p_m A}{m} \tag{46}$$

The boundary conditions again reflect the assumption of no rebound, and since the motion is the same in both directions, τ has the single value $\tau = 2$. A further result of the similar forward and return strokes is that the work per cycle can be expressed by combining $\tau = 2$ with Equations (6) and (18) to get

$$w = 2 \rho_m q_m T \tag{47}$$

which is the function to be minimized. As in all cases, the design must satisfy Equation (7). By the same reasoning as in Case a, the solution to (46) can be expressed as

$$\epsilon(T) = \frac{m^{0.5} q_m}{A} \left[1 - \exp\left(- \frac{\rho_m A^2 T}{q_m m} \right) \right] \tag{48}$$

By substituting R from (20), it can be shown that

$$w = 2 R^2 \ln \left[\frac{R}{R - \epsilon(T)} \right] \tag{49}$$

Since w here is only a function of R, the minimum value is found by setting the derivative equal to zero. The resulting expression is

$$2 \ln \left[\frac{1}{1 - \epsilon(T)/R} \right] - \frac{1}{1 - \epsilon(T)/R} + 1 = 0$$

Numerical solution for $\epsilon(T)/R$ results in

$$R = 1.4 \epsilon(T)$$

and when substituted into (49), along with Equation (10), the final solution for the minimum value of w is

$$\hat{w} = 9.86\,KE$$

For KE = 100,000 ergs, the minimum value of w is

$$\hat{w} = 0.863 \text{ in. lb.} \tag{50}$$

which is about one-half the minimum for Case a.

Case c

If the Coanda amplifier of Case a is replaced by a diaphragm element, there exists a possibility for reduced power since the power flow is cut off during the return stroke. This configuration is shown in Figure 4c.

On the forward stroke the equation of motion is given by Equation (1). However, the assumption here is that the ridge resistance is negligible and thus p is a constant, P_s. In this case, the solution to (1) is

$$x(t) = \frac{P_s A}{k}\left[1 - \cos\left(\frac{k}{m}\right)^{0.5} t\right] \tag{51}$$

The return motion due to the spring is described by ($t > T$)

$$m\ddot{x} + kx = -qrA \qquad x(T) = x_o,\ \dot{x}(T) = 0 \tag{52}$$

with the assumption of incompressibility as in Equation (3), (52) becomes

$$m\ddot{x} + \frac{r A^2}{m} + \frac{k}{m} x = 0 \tag{53}$$

Because the driven mass must return to x = 0 in a finite time, the only permissible solution to this equation corresponds to that for complex roots for the characteristic equation (i.e., underdamped).

The quantity to be minimized, work required to print, can be expressed as

$$w = P_s \int_0^T q_s \, dt \tag{54}$$

since the power flow exists only on the forward stroke. The value of the integral is the total flow, so that (54) can be expressed for incompressible flow as

$$w = P_s \left[A x(T) + \frac{P_s}{r} T \right] \tag{55}$$

The problem, as before is to minimize w subject to the constraints of (51) and (53), as well as the desired kinetic energy of (7).

In order to get a form for (55) which can be minimized a solution for (53) is needed. A useful form is given by Kuo, [34], p. 122 ff. With the definitions

$$\omega_n = \left(\frac{k}{m}\right)^{0.5} \qquad \zeta = \frac{rA^2}{2(mk)^{0.5}} \tag{56}$$

the required solution is

$$x(t') = x_o \exp(\zeta \omega_n t') \left\{\cos(\omega_n \sqrt{1-\zeta^2}\, t') + \frac{\zeta}{\sqrt{1-\zeta}} \sin(\omega_n \sqrt{1-\zeta^2}\, t')\right\} \tag{57}$$

where $t = t - T$.

With the further definition of

$$\phi = \omega_n T \tag{58}$$

the evaluation of (57) at $t = (T_r - T)$, (i.e., $t = T_r$), gives

$$x_o \exp[\phi \zeta(\tau-1)] \left\{\cos[\phi(\tau-1)\sqrt{1-\zeta^2}] + \frac{\zeta}{\sqrt{1-\zeta^2}} \sin[\phi(\tau-1)\sqrt{1-\zeta^2}]\right\} = 0$$

From physical considerations, the term in braces must be zero, which leads to an expression for ϕ in terms of τ and ζ,

$$\phi = \frac{1}{(\tau-1)\sqrt{1-\zeta^2}} \tan^{-1}\left(-\frac{\sqrt{1-\zeta^2}}{\zeta}\right) \tag{59}$$

By taking the first derivative of x(t) in (51) and combining with (10) and (58), it can be shown that

$$[\epsilon(T)]^2 = \frac{P_s^2 A^2}{k} \sin^2\phi \tag{60}$$

Further, by combining (56), (58) and (60), it can be shown that

$$\frac{P_s^2 T}{r} = \frac{[\epsilon(T)]^2}{\sin^2\phi}\left(\frac{\phi}{2\zeta}\right) \tag{61}$$

Going back to (55), then, and making proper substitutions from (51), (60) and (61), the expression for w becomes

$$w = \frac{[\epsilon(T)]^2}{\sin^2\phi}\left[1 - \cos\phi + \frac{\phi}{2\zeta}\right] \tag{62}$$

By substituting for ϕ from Equation (59), a relation for w as function of one variable, ζ, for any given τ is obtained. Since $0 < \zeta < 1$ is required by the necessity of an underdamped solution for (53), it is possible to solve numerically for $w/[\epsilon(T)]^2$ for various values of using (59) and (62). This procedure can be carried out by choosing a value for τ and plotting $w/[\epsilon(T)]^2$ for values of ζ, as in Figure 6.

Fortunately, these curves have a minimum value for $w/[\epsilon(T)]^2$ and this minimum can be plotted as a function of τ as in Figure 8, which compares the six cases of this chapter.

Case d

It is possible that an improvement on Case b might be a similar

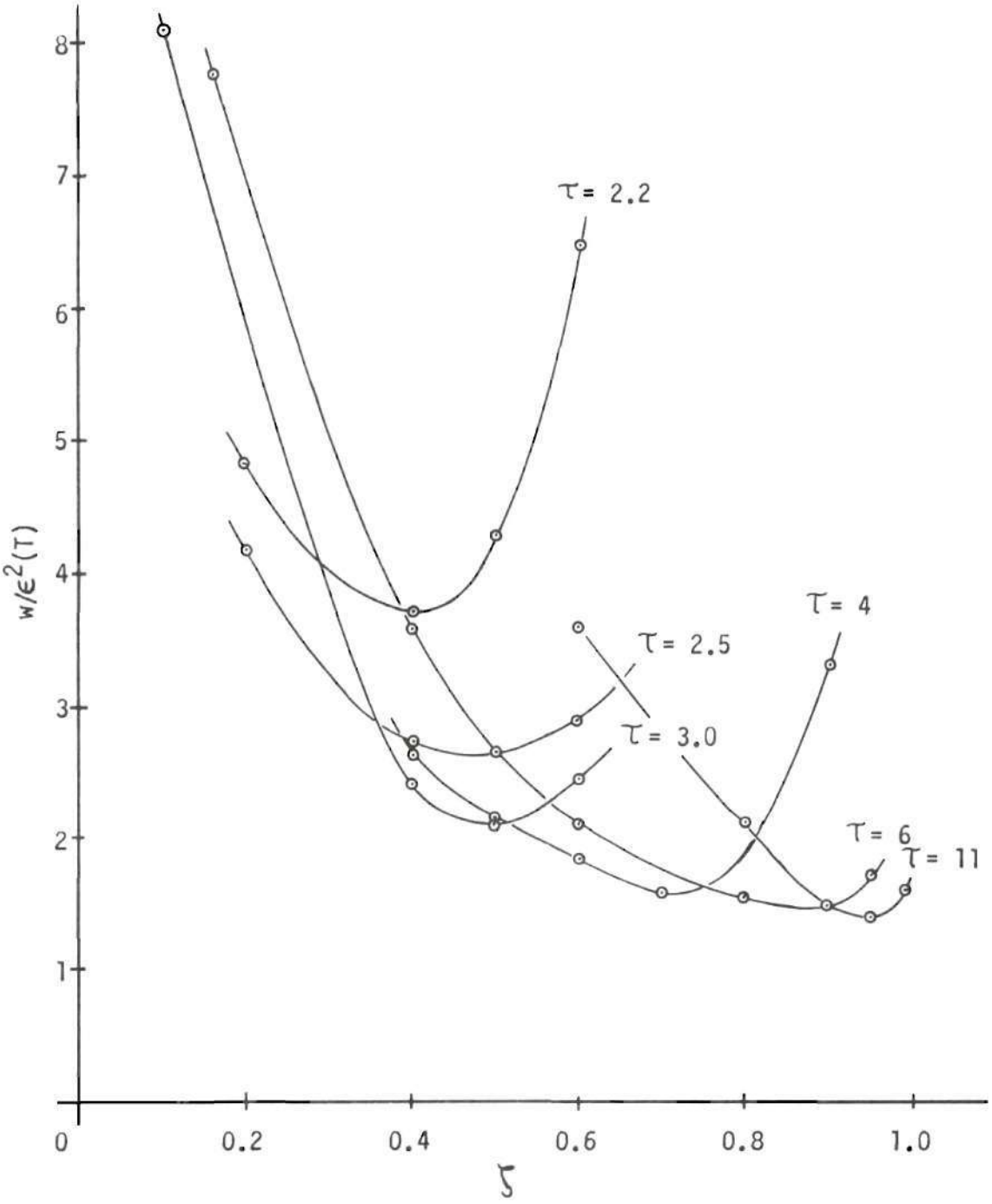

Figure 6. Minimum Value of $w/\epsilon^2(T)$, Case c

arrangement, with diaphragm elements instead of Coanda elements. This is shown in Figure 4d. As in Case b, the forward and return equations of motion are the same, so that the only value for τ is $\tau = 2$. The equation of motion for the forward stroke may be expressed as

$$m\ddot{x} = (p_f - p_r) A \tag{63}$$

where

$$p_r = q_r r \tag{64}$$

Since the restriction of the ridge is neglected, $p_f = P_s$, and for incompressible flow Equation (3) applies. Thus Equation (63) becomes

$$\ddot{x} + \frac{rA^2}{m} \dot{x} = \frac{P_s A}{m} \qquad x(0)=0,\ \dot{x}(0)=0 \tag{65}$$

The solution to this equation can be written

$$x(t) = \frac{P_s A}{m\lambda^2} \left[\exp(-\lambda t) + \lambda t - 1\right] \tag{66}$$

where

$$\lambda = \frac{rA^2}{m} \tag{67}$$

The function to be minimized is, again, the work required for the forward and return motion, which is given by

$$w = P_s \int_0^{Tr} q_s \, dt \tag{68}$$

Since the flow during both motions goes either to the cylinder or through the resistance r, Equation (68) can be written

$$w = 2P_s \left[Ax(T) + \frac{P_s}{r} T \right] \tag{69}$$

In order to reduce w in (69) to a function of one variable, Equation (66) is differentiated with respect to t and combined with Equation (10) to give

$$\epsilon(T) = \frac{P_s m^{0.5}}{rA} \left[1 - exp(-\lambda T) \right] \tag{70}$$

Then by substituting (66) and (70) into (69) w can be expressed by

$$w = \frac{2 [\epsilon(T)]^2}{1 - exp(-\lambda T)} \left[exp(-\lambda T) + 2\lambda T - 1 \right] \tag{71}$$

Since $\epsilon(T)$ is known, the minimum value of w can be found by setting the derivative with respect to λT to zero. The numerical solution to the expression for λT thus obatined is $\lambda T = 1.23$. Substitution of this value into Equation (71) gives the minimum value of w as

$$\hat{w} = 1.24 \text{ in.lb.} \tag{72}$$

This is a larger value of w than for Case b as seen from Equation (50).

Case e

It is apparent from the first four cases (a - d) that despite the assumption of no piston sliding friction, there are still damping terms in the equations of motion due either to required line resistances or amplifier output characteristics. The last two cases to be considered give two means of eliminating all damping terms in the equations of motion under the other previous assumptions. The first, Case e, as shown in Figure 4e uses four diaphragm elements so that air is both supplied to and exhausted from both sides of the piston with no restriction.

The equation of motion in the forward direction is

$$m\ddot{x} = P_s A \qquad x(0)=0, \ \dot{x}(0)=0 \tag{73}$$

and its solution is

$$x(t) = \frac{P_s A}{m}\left(\frac{t^2}{2}\right) \tag{74}$$

It is necessary to satisfy the kinetic energy requirement, and from Equations (7), (10) and (74) it can be shown that

$$\epsilon(T) = \frac{P_s A T}{m^{as}} \tag{75}$$

It is desired to minimize the work in both directions, and the total work w can be written

$$w = P_s \int_0^{T_r} q_s \, dt \tag{76}$$

Since all input flow goes to the cylinder, w becomes (for incompressible flow)

$$w = 2 P_s A x(t) \tag{77}$$

Substituting from (74) and (75) the result is

$$\hat{w} = [\epsilon(T)]^2 = 2KE$$

which becomes

$$\hat{w} = 0.177 \text{ in. lb.} \tag{78}$$

when the value of KE is substituted. This is the lowest value of w obtained so far. However, the system has inherent a value of $\tau = 2$, and it has already been seen that the minimum of w can depend on τ where a spring return is used.

Case f

The other method of elimination damping loss using diaphragm elements is shown in Figure 4f. This configuration uses one element to supply the forward stroke power and the other to give an unrestricted

exhaust during return by the spring. The forward stroke equation of motion is

$$m\ddot{x} + kx = P_s A \qquad x(0) = 0,\ \dot{x}(0) = 0 \tag{79}$$

and its solution is

$$x(t) = \frac{P_s A}{k}\left[1 - \cos\left(\frac{k}{m}\right)^{0.5} t\right] \tag{80}$$

For the return stroke, the equation of motion is the same as Equation (5), whose solution leads to the expression for τ in (19). As in the previous cases, it is desired to minimize the work and satisfy the kinetic energy requirement. The energy w can be expressed for this case as

$$w = P_s \int_0^T q_s \, dt$$

and with incompressible flow becomes

$$w = P_s A x(T) \tag{81}$$

By differentiating (80) and using Equations (3), (7) and (10), it can be shown that

$$\epsilon(T) = \frac{P_s A}{k^{0.5}} \sin\left(\frac{k}{m}\right)^{0.5} T \tag{82}$$

By combining Equations (19), (56) and (58) it can be shown that ϕ can also be expressed as

$$\phi = \frac{\pi}{2(\tau-1)} \tag{83}$$

and substituting from (19), (80), (82) and (83) into (81), w can be expressed by

$$w = \frac{[\epsilon(T)]^2}{\sin^2\phi}\left[1-\cos\phi\right] \tag{84}$$

Thus w is function only of ϕ and its minimum can be found by setting the derivative with respect to ϕ to zero. This results in

$$\sec\phi + \cos\phi = 2$$

which is satisfied by

$$\phi = 2n\pi \qquad n=0,1,2,\cdots$$

Equation (83) implies that w has a minimum only as τ approaches infinity. By taking

$$\lim_{\phi \to 0^+} w = 0.5\,[\epsilon(T)]^2 \tag{85}$$

in Equation (84), it is seen that

$$\lim_{\tau \to \infty} w = KE \tag{86}$$

where KE is, of course, the required kinetic energy to print. The result of Equation (86) shows that if a sufficiently long time is allowed for the return stroke, the required energy approaches the least possible, that being only that required to achieve the printed character. For values of τ which are practical, the minimum value of w is given by (84). This curve is plotted in Figure 7, and shows that an improvement on Case e can be obtained at values of τ which are reasonable.

Selection of Print Drive Subsystem

From the values of minimum work or energy derived for the six configurations of Figure 4, a comparison can be made based on the compilation of these results shown in Figure 8. These results are all for KE of 100,000 ergs. For other values of KE, the values of $\hat{w}$, are proportional to KE.

Each of the three configurations with spring return show a variation of $\hat{w}$ with τ. This is reasonable since increasing τ implies longer return time for a given forward time and requires less energy stored in the spring. However, for Case a, the Coanda amplifier has a constant power consumption and this is reflected in the shape of the curve, which has a minimum at $\tau \simeq 2.6$, whereas Case c and f decrease continually as τ increases.

Due to the definition of τ in Equation (18), $\tau = 2$ represents equal forward and return strokes. Thus, Cases b, d and e are shown in Figure 8 as single points at $\tau = 2$.

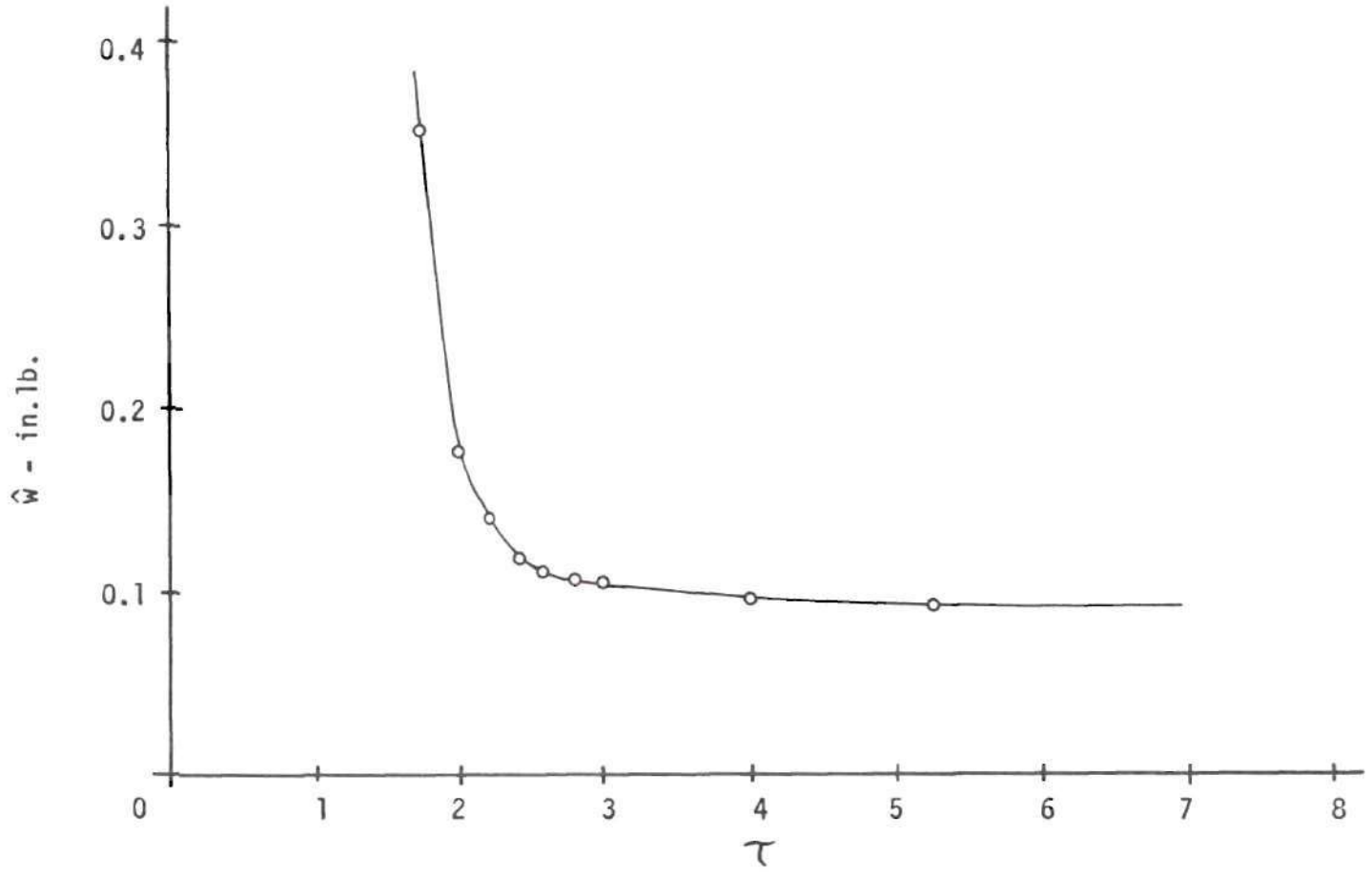

Figure 7. Minimum Work for Printing, Case f

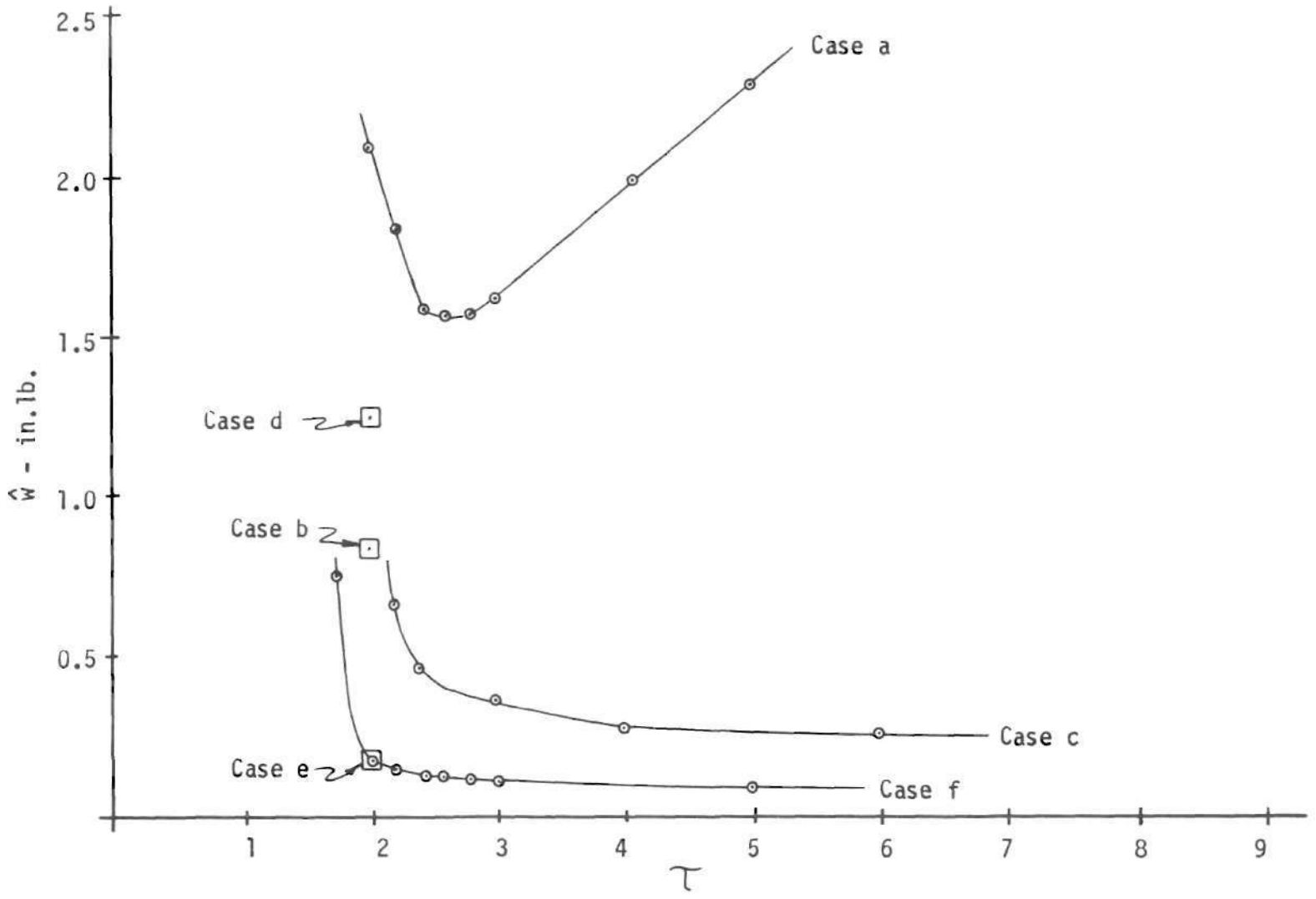

Figure 8. Minimum Work for All Print Subsystem Configurations

It is easily seen that the configuration which best satisfies the criterion of minimum power consumption is the last, Case f, using two diaphragm elements with a spring return. This configuration has a power consumption of more than an order of magnitude less than Case a. The significance of this power saving for the overall system will become apparent later. Case f also has the advantage of a spring return so that τ can be varied if that seems advisable from timing considerations. The disadvantages of Case f are that it uses two amplifiers as opposed to Case c, its closest competitor in power consumption, and that the diaphragm amplifiers have a moving mechanical part, the diaphragm. However, the diaphragm should present few problems from the standpoint of wear, speed of response or size, and the additional amplifier results in less than half the power consumption of Case c.

Therefore, the configuration of Case f will be used in the further consideration of the overall typewriter as the printing drive subsystem corresponding to block seven of Figure 3.

CHAPTER IV

POSITION DRIVE SUBSYSTEM OPTIMIZATION

Definition of the Problem

In addition to the print drive, two final elements in the logical flow of information in Figure 3 are those which provide rotary and axial motion to the type head for selections of the character to be printed. The rotary and axial drives provide the same basic function, that of converting a set of pressure signals to corresponding mechanical motion of a given magnitude, the motion being accomplished in some fixed time, and a return to some initial or home position. While the mechanical linkage will be different for the two, it is still possible to model them in the same sense as the print drive in Chapter III, in which case they are indistinguishable.

Thus, this chapter will be concerned with what amounts to a motion transducer converting pressure to a fixed mechanical motion as mentioned in Chapter II. The action of a key will be converted to a set of digital pressure signals which specify the amount the type head must be moved (axially or rotationally). The motion is to be accomplished by connecting the pressure pulses to a digital actuator, as in Figure 9. The actuator, which is illustrated here as being binary coded, consists of a series of pistons moving in a single cylinder with their axial motion constrained by a set of stops such that the forward motion of each piston relative to the piston behind it is weighted in

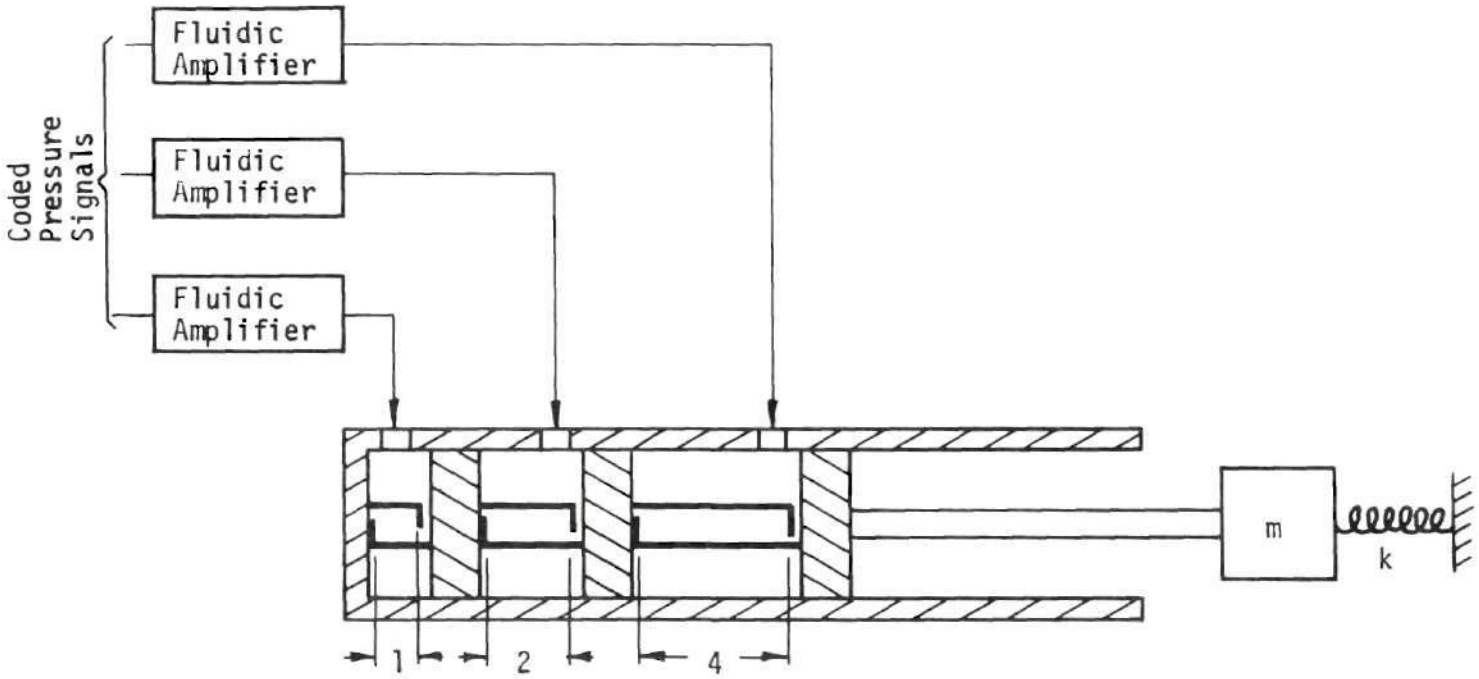

Figure 9. Position Drive and Digital Actuator

the same manner as the binary number system (i.e., 1, 2, 4, 8, 16,...). Motion of any piston is transmitted to the driven mass, and the individual motions are additive, so that the motion of the driven system has a relative magnitude equal to the magnitude of the binary number represented by the input pressure pulses. The driven mass has 2^n positions, where n is the number of pistons. The return motion is shown as being spring driven. It would also be possible to return the actuator to the zero or home position with air pressure by enclosing the open end of the cylinder. This digital actuator and the associated driving fluidic amplifiers, along with the connected mechanical linkage and the type head itself, constitute the position drive subsystem. It should be emphasized that codes other than binary can be used for the actuator.

As will be seen, there are several possible configurations which could be utilized here, and a criterion for determining the best one is needed. Since the overall criterion is to minimize power and maximize speed, the best system is the one which moves the driven mechanical load to the desired position in a specified time using the least power. As in the print subsystem, the objectives of maximum speed and minimum power can be achieved by minimizing the work required to accomplish the specified motion and return.

Possible Configurations

Examination of Figure 9 will show that the pistons of the actuator do not move simultaneously. For instance, if the high-order piston (rightmost in Figure 9) is the only one pressurized, it alone

drives the load. However, if all three are pressurized, the high-order piston moves through its stroke first, and then pulls the next piston after it, which then pulls the low-order piston. This is due to the balanced forces on the lower-order pistons. Other combinations of piston motion are obvious. Thus, the load driven by fluidic amplifier may vary during one operation of the actuator and from operation to operation. If the load represented by the pistons is small (as it turns out to be), this variation can be neglected for this initial analysis and the position drive system represented simply by a single piston driven by the fluid amplifier and driving the equivalent or reflected mass, m.

These remarks then allow the use of the six possible configurations shown in Figure 4 to be studied as position drive subsystems. The only difference is that here the constraint is to achieve a given magnitude of motion at time t = T instead of achieving a given kinetic energy. These configurations will again be referred to as Cases a - f, and each will be modeled mathematically and the most suitable one chosen. The general remarks concerning them in Chapter III apply here as well.

Quantitative Evaluation of Possible Configurations

Design Criterion

Since the configurations of Figure 4 were first developed in Chapter III, the equations of motion and the other pertinent relations developed there will be used in this chapter where they apply. The assumptions upon which they are based and the rationale of their

development will not be repeated in this chapter. Instead, the development of each case will be presented more concisely with appropriate reference to previous equations.

Again, it is necessary to have a quantity to be minimized which reflects the minimum power and maximum speed criterion. In the calculations for w in Chapter III, the constraint of given kinetic energy at time t = T was used as expressed by Equation (7). This energy constraint resulted in the ability to minimize w as a function of τ only. Note that Equation (7) actually places a restriction on the product $m[\dot{x}(T)]^2$. However, in the present problem the actual constraint is only on x(T). Physically speaking then, if w is minimized, it is possible for the minimization to force T to infinity (an unacceptable result) since motion of a finite mass m over a finite distance in infinite time takes zero work. Or, if the time remains finite, the mass may be forced to zero, also unacceptable. Thus, the position drive problem is less constrained than the print drive, and in order to get the same type solution for w as a function of τ, it will be necessary to fix the value of the parameter

$$V = \frac{m[x(T)]^2}{T^2} \tag{87}$$

which has the dimension of energy or work. Note that since x(T) itself is fixed as well as the time for the forward stroke, T, Equation (87) has the effect of fixing m. The expression for w in Equation (6) can also be written

$$w = \rho_m q_m T \tau$$

If W is defined by

$$W = p_m q_m T \tag{88}$$

it is seen that, since τ and T are fixed, minimization of W is the same as minimizing w. Furthermore, again for T fixed, this is the same as minimizing

$$P = p_m q_m \tag{89}$$

Both Equations (88) and (89) prove useful in this chapter.

Case a. The equation of motion for the forward stroke is Equation (4), which includes the assumptions of a linear amplifier output characteristic, Equation (2) and incompressible output flow, Equation (3). For the return stroke, the equation of motion is Equation (5). The design constraint is that x(T) must be a known, fixed number which is determined from the dimensions of the type head and the mechanical linkage connecting it to the digital actuator. The equation of motion (4) can be solved for x(t) for the underdamped case. If the definition of the dimensionless ratio B is made as

$$B = \frac{W(\tau-1)}{\pi R^2} \tag{90}$$

then this solution at t = T can be expressed as

$$\sqrt{\frac{W}{m}}\,\frac{T}{x(T)} = \left\{\left[\frac{16B(\tau-1)^3}{\pi^3}\right]^{0.5}\left[1 - \frac{\exp\left[-\pi B/2(\tau-1)\right]}{(1-B^2)^{0.5}}\cdot \sin\left[\frac{\pi(1-B^2)^{0.5}}{2(\tau-1)} + \psi\right]\right]\right\}^{-1} \qquad (91)$$

where

$$\psi = \tan^{-1}\frac{(1-B^2)^{0.5}}{B}$$

An outline of this derivation is given in Appendix B. Since V is known, Equation (91) can be expressed as

$$\left(\frac{W}{V}\right)^{0.5} = f(B)$$

It is desired to have the minimum of W with respect to B. Observe that

$$\frac{dW}{dB} = 2(WV)^{0.5}\frac{df}{dB}$$

and for a minimum of W

$$\frac{df}{dB} = 0$$

since W and V are not zero identically. A further simplification results by letting

$$f(B) = \frac{1}{f'(B)}$$

where f'(B) is the denominator of the right side of (91), so that

$$\frac{df}{dB} = -\frac{1}{(f')^2}\frac{df'}{dB}$$

Then, since from physical considerations f'(B) cannot be zero, it is simpler to set

$$\frac{df'}{dB} = 0 \tag{92}$$

as the condition for minimum W. The result of carrying out (92) is

$$\exp\left[\frac{\pi B}{2(\tau-1)}\right] + \left[\frac{B}{1-B^2}\right]\left[\frac{\pi B}{\tau-1} + 2\right]\cos\left[\frac{\pi(1-B^2)^{0.5}}{2(\tau-1)} + \psi\right] + \left\{\left(\frac{B^2}{1-B^2}\right)^{0.5}\left(\frac{\pi}{2(\tau-1)}\right) - \frac{1+B^2}{(1-B^2)^{1.5}}\right\}\sin\left[\frac{\pi(1-B^2)^{0.5}}{2(\tau-1)} + \psi\right] = 0 \tag{93}$$

This equation can be solved numerically for B as a function of τ. The result is then substituted into Equation (91) to achieve the curve of Figure 10, where the minimum value of W, $\hat{W}$, is given for any value of V.

As in the consideration of Case a for printing in Chapter III, it would now be possible to consider the solution of the equation of motion for critical damping and for underdamped motion. However, since it was seen in Chapter III that the three solutions combined to give

a smooth curve, similar results might be expected here. Instead of considering the other two cases for positioning, a limiting case will be considered. The overdamped solution carried to its limit would have a damping ratio δ equal to infinity, where

$$\delta = \frac{\rho_m A^2}{2 q_m (m k)^{0.5}} \tag{94}$$

For δ to be very large, k must approach zero, and with no spring to return the system, τ becomes infinite. By allowing k to go to zero, the equation of motion (4) reduces to Equation (46), which also happens to be the equation of motion for Case b. Thus, it can be seen that the solution for Case b (where τ has only the value $\tau = 2$) is a limiting solution for Case a with $\tau \to \infty$. This limiting solution is shown in Figure 10 in anticipation of its derivation in the following section.

Case b. The equation of motion in both directions was given by (46). The constraints are that x(T) and T are known and the value of V is given. In this case it is convenient to minimize the function P given by Equation (89).

The solution to the equation of motion can be written as (t = T)

$$x(t) = \frac{q_m T}{A} + \frac{m q_m^2}{\rho_m A^3}\left[\exp\left(-\frac{\rho_m A^2 T}{q_m m}\right) - 1\right] \tag{95}$$

By defining D and M as

$$D = \frac{q_m T}{A} \qquad M = \frac{m}{T^3} \tag{96}$$

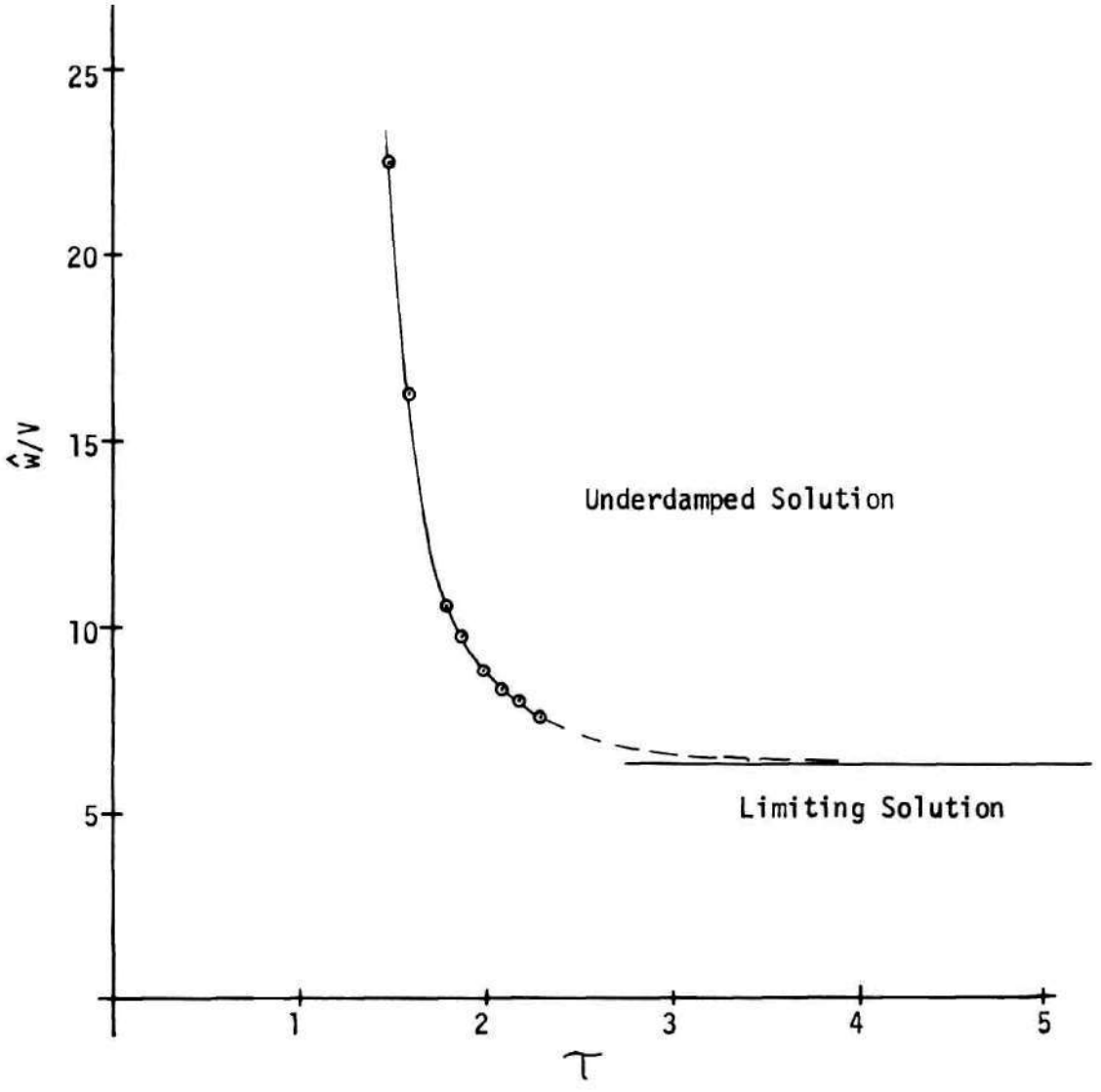

Figure 10. Minimum Work for Positioning, Case a

Equation (95) can be written to give

$$f(D,P) \equiv 0 = D + \frac{M}{D^3}\left[\exp\left(-\frac{P}{D^3 M}\right) - 1\right] - x(T) \qquad (97)$$

since M is a known constant. The conditions for a minimum of P with respect to D are then

$$\frac{\partial F}{\partial D} = 0 \qquad \frac{\partial F}{\partial P} \neq 0 \qquad (98)$$

The first of these relations results in

$$1 - \frac{3D^2M}{P} + \left[\frac{3D^2M}{P} + 2\right] \exp\frac{-P}{D^2M} = 0 \qquad (99)$$

The second gives

$$\frac{MD^3}{P}\left[-\left(\frac{1}{P} + \frac{1}{D^2M}\right)\exp\left(-\frac{P}{D^2M}\right) + \frac{1}{P}\right] \neq 0 \qquad (100)$$

Equation (99) can be solved numerically to get

$$\frac{\hat{P}}{MD^2} = 2.149 \qquad (101)$$

and by substituting this into (97) it can be seen that

$$\frac{x(T)}{D} = 0.589 \qquad (102)$$

By squaring both sides of (102), dividing (101) by the result, and then substituting the definitions of P and M, there results

$$\frac{\hat{W}}{V} = 6.2 \tag{103}$$

which gives the minimum value of W for any V. The parameter τ has the one value $\tau = 2$ for Case b. This is the result shown as an asymptotic solution for Case a in Figure 10.

It can be shown that Equation (100) is always satisfied by assuming that the term in brackets is equal to zero, multiplying through by P and noting the contradiction when substitution is made from Equation (101).

Case c. The equations of motion for this case are the same as in Chapter III, Case c. The solution to the forward motion equation is given by (51) and the solution to the return Equation (53) leads to Equation (59) as before. The constraints are that x(T) and T are known and the value of V is known, which of course implies that m is fixed. The quantity to be minimized is given by Equation (55).

Equation (55) can be reduced to a form from which a minimum can be found by first multiplying out and eliminating T and r in the second term by substitutions from Equations (58) and (56) to get

$$w = P_s A x(T) + \frac{P_s^2 A^2}{k}\left(\frac{\phi}{2\mathcal{S}}\right)$$

Then Equation (51) evaluated at t = T can be used to eliminate $P_s A$,

resulting in

$$w = \frac{k[x(T)]^2}{[1-\cos\phi]^2}\left[1-\cos\phi+\frac{\phi}{2\zeta}\right]$$

and by substitution from (56), (58) and (87) the result is

$$w = \frac{V\phi^2}{[1-\cos\phi]^2}\left[1-\cos\phi+\frac{\phi}{2\zeta}\right]$$

Finally, ϕ can be eliminated by substitution from (59) to give

$$\frac{w}{V} = \left[\frac{\tan^{-1}(\sqrt{1-\zeta^2}/\zeta)}{(\tau-1)\sqrt{1-\zeta^2}}\right]^2\left[1-\cos\frac{\tan^{-1}(\sqrt{1-\zeta^2}/\zeta)}{(\tau-1)\sqrt{1-\zeta^2}}\right. \qquad (104)$$
$$\left.+\frac{\tan^{-1}(-\sqrt{1-\zeta^2}/\zeta)}{2\zeta(\tau-1)\sqrt{1-\zeta^2}}\right]\left[1-\cos\frac{\tan^{-1}(\sqrt{1-\zeta^2}/\zeta)}{(\tau-1)\sqrt{1-\zeta^2}}\right]^{-2}$$

which is a function of ζ only for a given τ, V being fixed as before.

This last equation can be solved numerically by graphing w/V versus ζ for various values of τ, which is shown in Figure 11. These curves have a minimum value and these minima are plotted in Figure 13.

Case d. The equation of motion in the forward direction is given by Equation (65) whose solution is (66). For this configuration the forward and return motions are the same and $\tau = 2$ only. Again x(T) and V are known constants. The function to be minimized is given by Equation (68) or (69). The equation for w can be expressed in a form suitable for minimization by multiplying out (69) and eliminating P_s, A, and r by substituting from Equations (66) and (67). The result

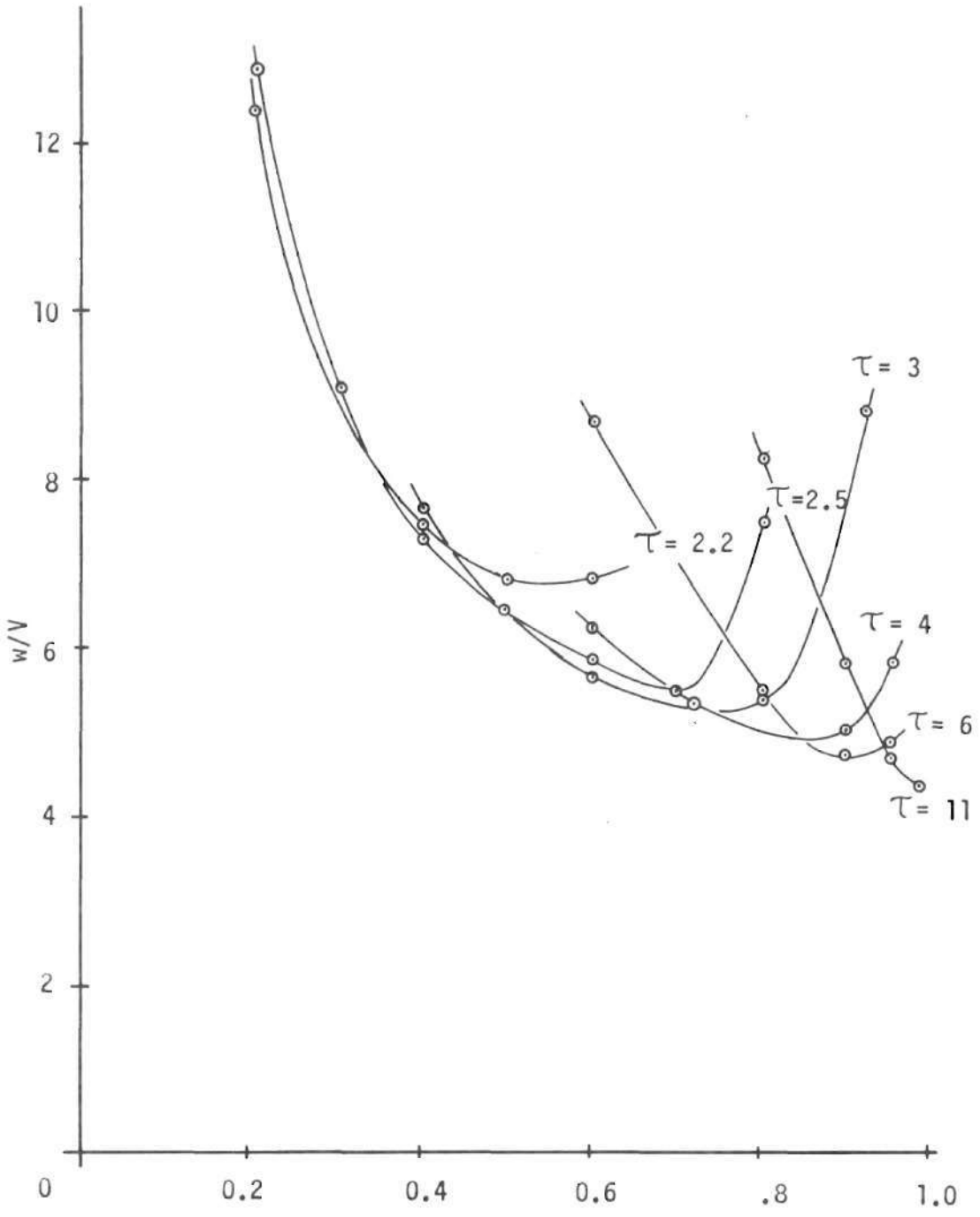

Figure 11. Minimum Values of w/V, Case c

of these operations is

$$w = 2V \frac{\lambda T \exp(-\lambda T) + 2\lambda^3 T^3 - \lambda^2 T^2}{[\exp(-\lambda T) + \lambda T - 1]^2} \tag{105}$$

This allows the minimum of w to be found by setting

$$\frac{dw}{d(\lambda T)} = 0$$

The result of this operation is a transcendental expression which can be solved numerically for

$$\lambda T = 1.565 \tag{106}$$

Substituting this back into (105) gives

$$\frac{\hat{w}}{V} = 14.8 \tag{107}$$

which is plotted in Figure 13 with the other six cases of this chapter.

Case e. The equation of motion was given in Chapter III by Equation (73) with its solution (74). Again, the design constraints are that x(T), T and V are known constants. The total work done, which is to be minimized, was given by (77) as

$$w = 2P_s A x(T)$$

Substituting for $P_s A$ from (74), the direct result is

$$\frac{\hat{w}}{V} = 4 \tag{108}$$

which is shown in Figure 13.

Case f. The equation of motion in the forward direction was given by Equation (79) and its solution by (80). In this case the return equation of motion was given by Equation (5) whose solution lead to the relation for τ in Equation (19). The design constraints for this case, as for all the position drive configurations are that x(T), T and V are known constants. The work function to be minimized is that given by Equation (81) as

$$w = P_s A x(T)$$

By substituting for $P_s A$ from Equation (80) and using ϕ from Equation (58), w becomes

$$w = \frac{V\phi^2}{1-\cos\phi} \tag{109}$$

Thus, w is a function of ϕ only and the minimum can be found by setting the derivative to zero. Carrying this out leads to the relation

$$\phi \sin\phi + 2\cos\phi - 2 = 0 \tag{110}$$

which has the solution

$$\phi = \pm n\pi \qquad n = 0, 1, 2, \cdots \tag{111}$$

Since this solution for ϕ leads to an indeterminate expression for w in (109), the minimum for w is found by taking

$$\lim_{\phi \to 0} w = 2V \tag{112}$$

However, Equation (83) implies that as $\tau \to \infty$, $\phi \to 0$, so that the result of (112) is valid for $\tau \to \infty$. For finite values of τ, the minimum value of w is simply that given by Equation (109). This Equation for w is plotted in Figure 12.

Selection of Position Drive Subsystem

A compilation of the results for minimum work or energy for each of the six cases of Figure 4 used as position drives for positioning the type head is shown in Figure 13. In all cases V as defined by Equation (87) is assumed known. It is obvious that the configuration of Case f requires the minimum energy and is the best from that standpoint. It has the disadvantage of requiring two diaphragm elements which have a moving part. However, the reduction of power by a factor of approximately three over the Coanda devices of Case b justifies the use of the Case f configuration. Therefore, for the final drive stage in positioning the type head the configuration of Case f in Figure 4 will be used.

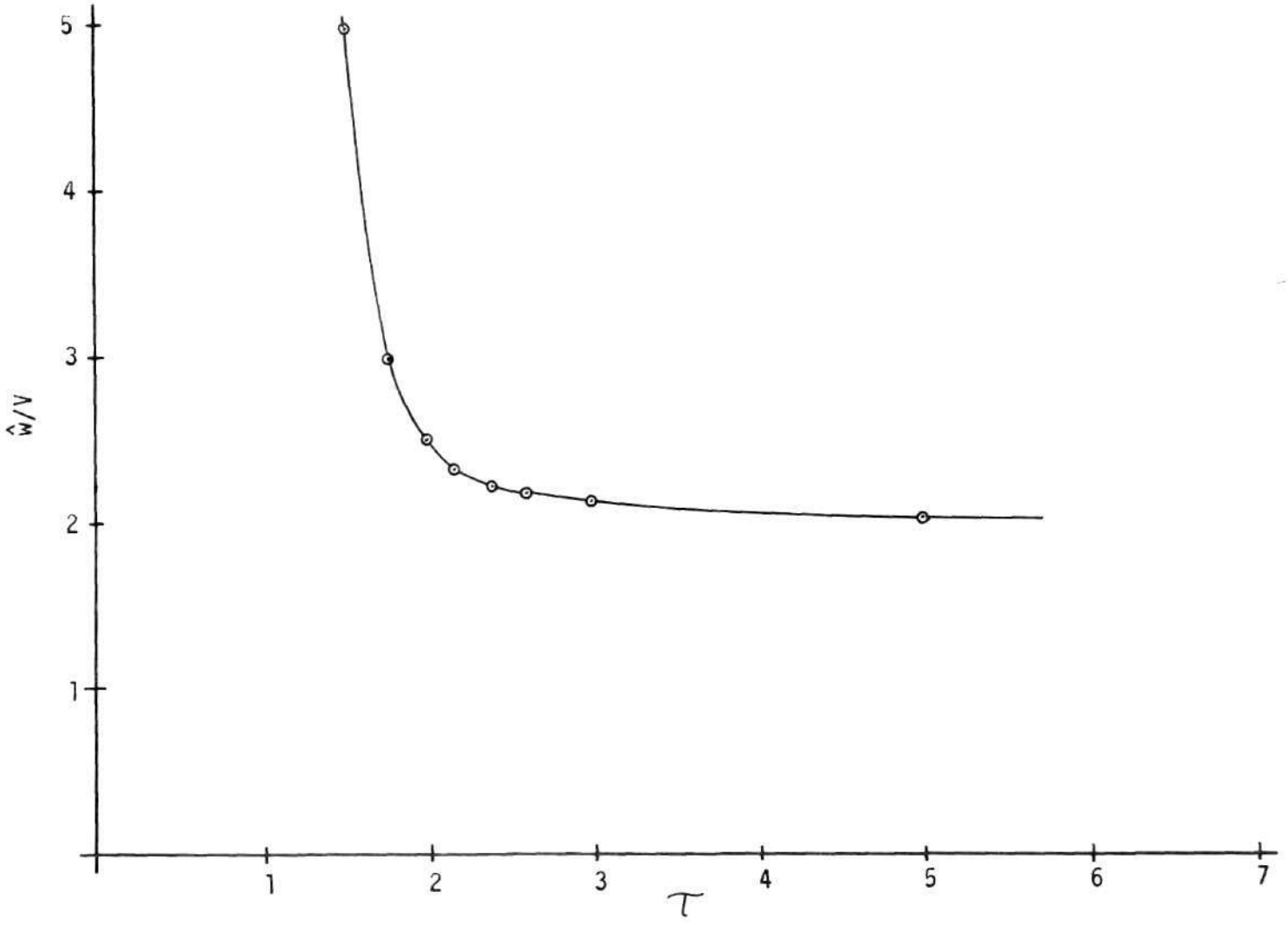

Figure 12. Minimum Work for Positioning, Case f

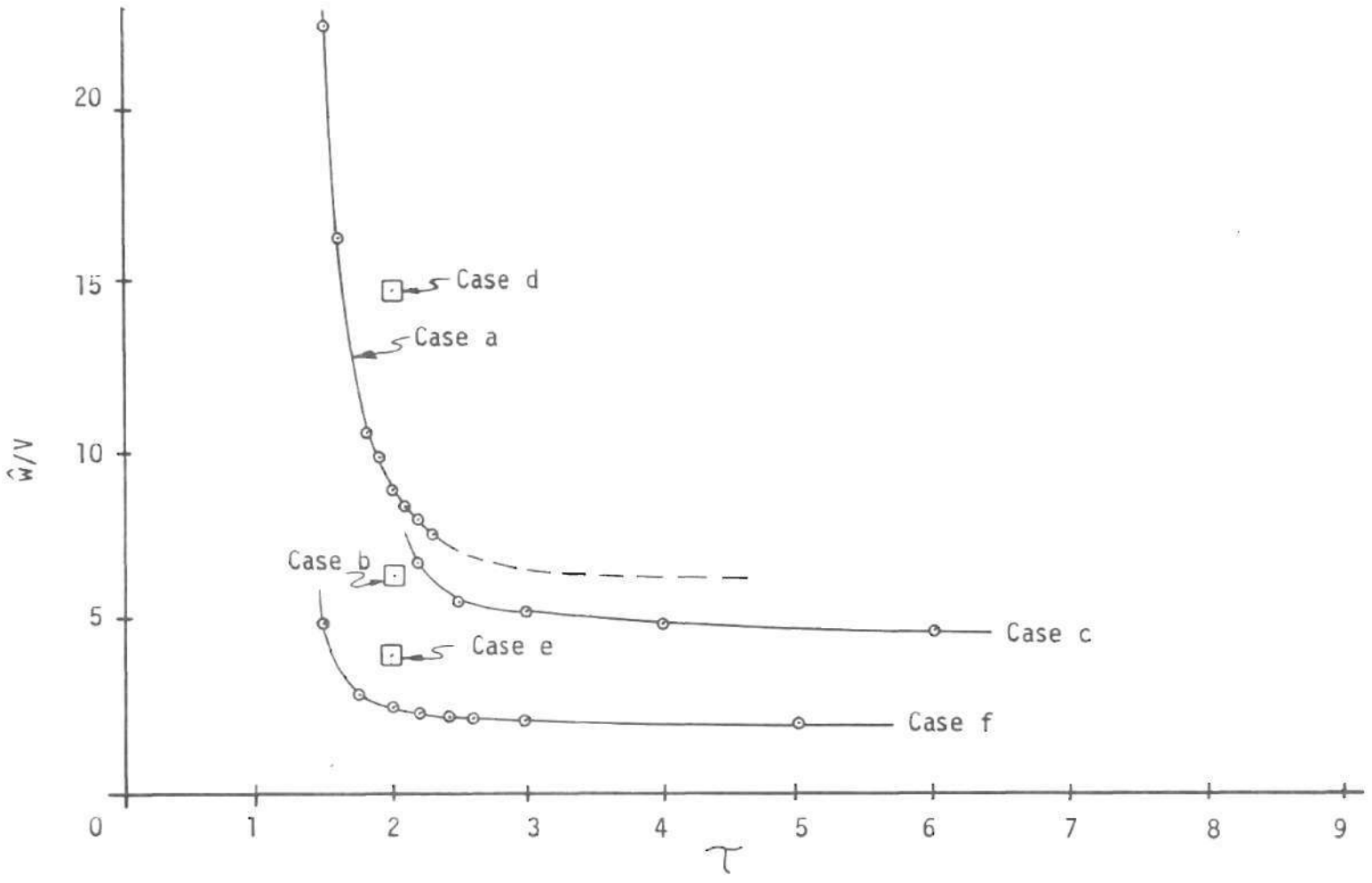

Figure 13. Minimum Work for All Position Subsystem Configurations

CHAPTER V

CONTROL SUBSYSTEM

Introduction

The discussion in the latter two sections of Chapter II pointed out the need for a control subsystem to coordinate the operation of the other subsystems. In this chapter the requirements on this control subsystem will be formulated and several alternatives evaluated.

To begin with, the overall sequence of events in typing is that a key is first actuated and this results in the typeface striking the paper, followed by a carriage motion to the next print space. For those familiar with the less modern manual type-bar machine, it will be remembered that striking a second key too quickly after the first resulted in jammed type-bars. This points out the fact that the cycle of mechanical operations resulting from key actuation require a certain minimum time, whether the typewriter be manual, electric or fluidic, before another cycle can be initiated. It is one of the functions of the control subsystem to ensure that the cycle of events necessary to print a character is carried out when a key is actuated and also to prevent unwanted interruption of that cycle if a second key is actuated too soon. The other function is to determine the sequence and initiate the operation of the type head position drives, the print drive and the carriage motion, and to reset these subsystems ready for another cycle. The minimum time required to complete the cycle of

events discussed here will be referred to as the cycle length.

The fact that the timing must prevent any action from a second key struck too quickly seems to imply that it might be possible to strike a key which would do nothing, mechanically speaking, and thus omit a letter on the paper. This is not quite true, because a basic requirement of a well designed typewriter would be that its cycle length be shorter than that corresponding to the typist's effort, so that when operated at the maximum expected typing speed and at a reasonably smooth rate the machine would always be ready for the next cycle. If there is a moving key, which need not be the case with a fluidic typewriter, the keys can be mechanically interlocked so that only one at a time can be moved, but even that does not guarantee error-free typing.

It might also be noted here that the digital encoding of the keys provides a natural means of automatic operation of the fluidic typewriter from coded information, such as paper tape. In such a case, the information would be received at a constant rate just slower than that corresponding to the cycle length, and the difficulties discussed above would not exist.

In summary, the control subsystem accepts coded information generated by the key action, initiates operation of each of the drive subsystems in proper sequence, prevents interruption of this sequence, and returns the whole machine to its rest state ready to repeat the cycle.

Possible Modes of Operation

It is evident that the control subsystem is in essence a digital information processor in the same, if less complex, sense as numerical

controllers for machine tools, process controllers and similar applications. That is, digitally coded information is input to the processor and a sequence of computational or logical operations performed upon it, and control action taken on the basis of the information or computations. In that context there are two general modes of operation which might be considered in utilizing the input. These are the synchronous and asynchronous modes.

In the synchronous mode of operation, every logical or control action is done on a time basis. In digital computers this time basis is often provided by a constant frequency oscillator whose output pulse train is used to drive gates or master-slave flip-flops which allow logical operations to proceed in synchronism with the clock. Such elaborate measures are not deemed necessary for the typewriter, since it would require the clock-oscillator circuit and additional gating. It is possible to provide time base control using R-C time constants instead of a clock and the term synchronous mode is used here to denote such a means of control.

In the asynchronous mode the logical and control operations are sequenced on the basis of the completion of other logical operations without regard to how quickly or slowly they occur. This definition is not exactly the same as in other digital applications, but it does denote the absence of time base control. In the present application the operations to be sensed are the motion of the mechanical subsystems (i.e., position, print and carriage). Some additional considerations important to the design of the control circuitry can be discussed with the aid of Figure 14.

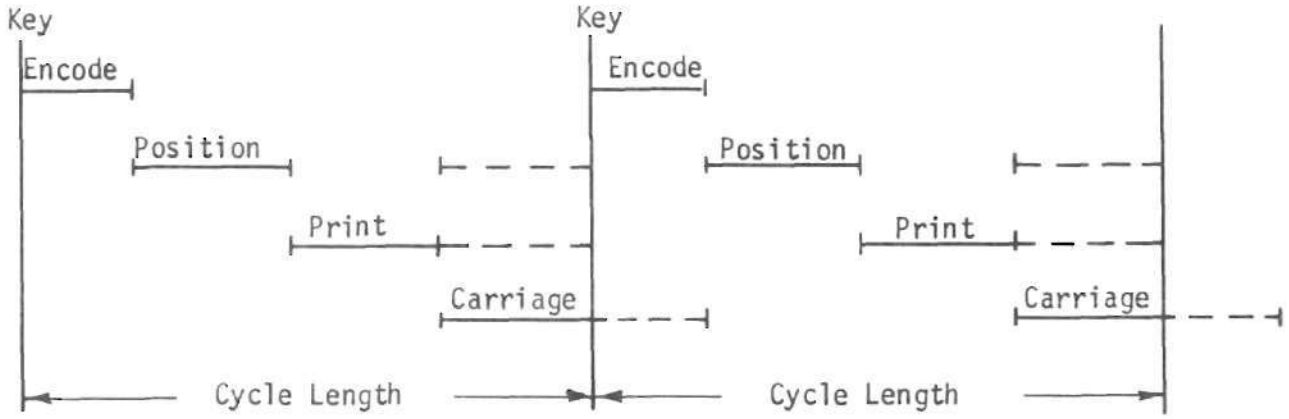

(a) Asynchronous Mode

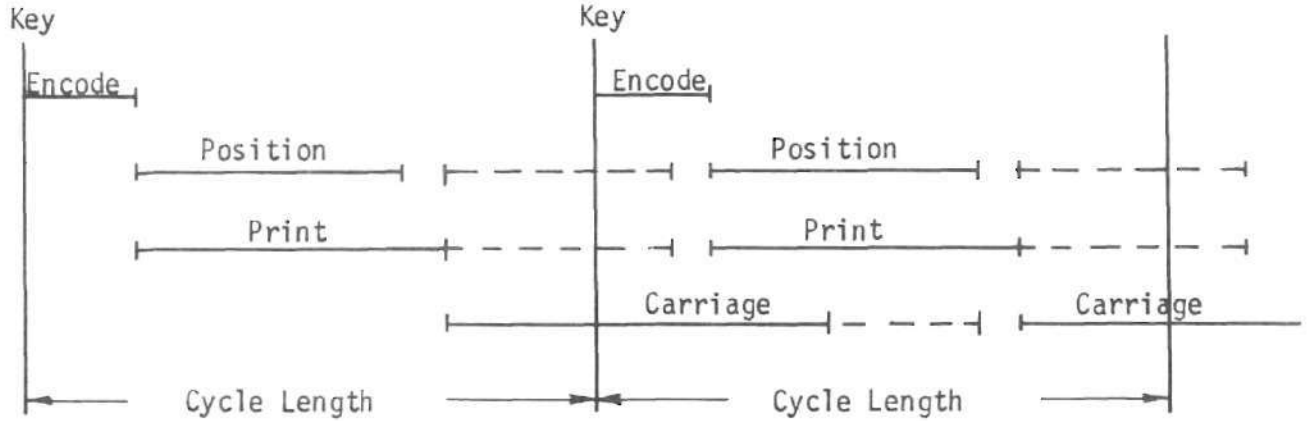

(b) Synchronous Mode

Figure 14. Basic Timing Diagrams

Beginning with the asynchronous mode of Figure 14a, assume that a period of more than a cycle length has elapsed since a key has been actuated and that two keys are actuated one after the other at the minimum allowable interval (cycle length). A short period must be allowed for propagation of the signals generated to the fluidic devices driving the actuators. This time is lumped under "Encode" in Figure 14. These signals, which are the six-bit position code or signals derived from the code, then actuate the digital actuators to select the character. The time required for any fluidic switching and the mechanical motion is the solid "Position" line in the diagram. Once this motion is complete, as indicated by some means of sensing, the print motion is initiated. The sensing of the successful completion of the printing, as indicated from the motion of the type head structure, then allows the pressure to be removed from both the positioning and printing pistons so that they reset, as indicated by the dashed lines in the diagram. Also, at this instant the carriage motion is initiated and it is completed at the end of the print cycle. It is also possible to require reset of the carriage actuating mechanism within the print cycle, but this is not done in Figure 14a. However, since the encoding time is likely to be quite small and repeatability of the positioning motion is important, the position and print mechanisms should be reset by the end of the cycle.

A similar diagram for the synchronous mode control is shown in Figure 14b. In contrast to the asynchronous mode above, if it can be assumed that the mechanical motions are repeatable to a sufficient degree so that a mechanical motion begun at the proper instant will

always be completed within a given interval, then the mechanical motions can be initiated and sequenced on a time basis. One basic advantage in this means of control can be observed in Figure 14 where there is considerable overlapping in the time allotted to each subsystem. The result is that position, print, and carriage motions can occur over longer periods of time for the same cycle length (or equivalently, the cycle length is shorter for the same subsystem actuation time), the result being that the actuators can be smaller for the same overall performance. Note that the position and print motions can begin at or near the same time so long as the position motion is accomplished first, and that their reset motions can extend into the next print cycle. The carriage motion must begin at the end of the print stroke, but its motion and reset can extend well into the next print cycle.

Fluidic Circuitry

Synchronous Mode

The synchronous mode is the simplest and it will be considered first. Figure 15 shows the circuit diagram, and each fluidic element is numbered with underlined numbers (e.g. 3) to facilitate the description of the circuit operation.

The control circuit accepts input in the form of pressure pulses from the encoder forming a six-bit binary code corresponding to the character to be printed. A seventh bit to distinguish upper and lower case is required. It is assumed to actuate a separate pneumatic-mechanical mechanism and is not considered here. As stated at the end of Chapter IV, the position drive configuration of Figure 4f is to be used.

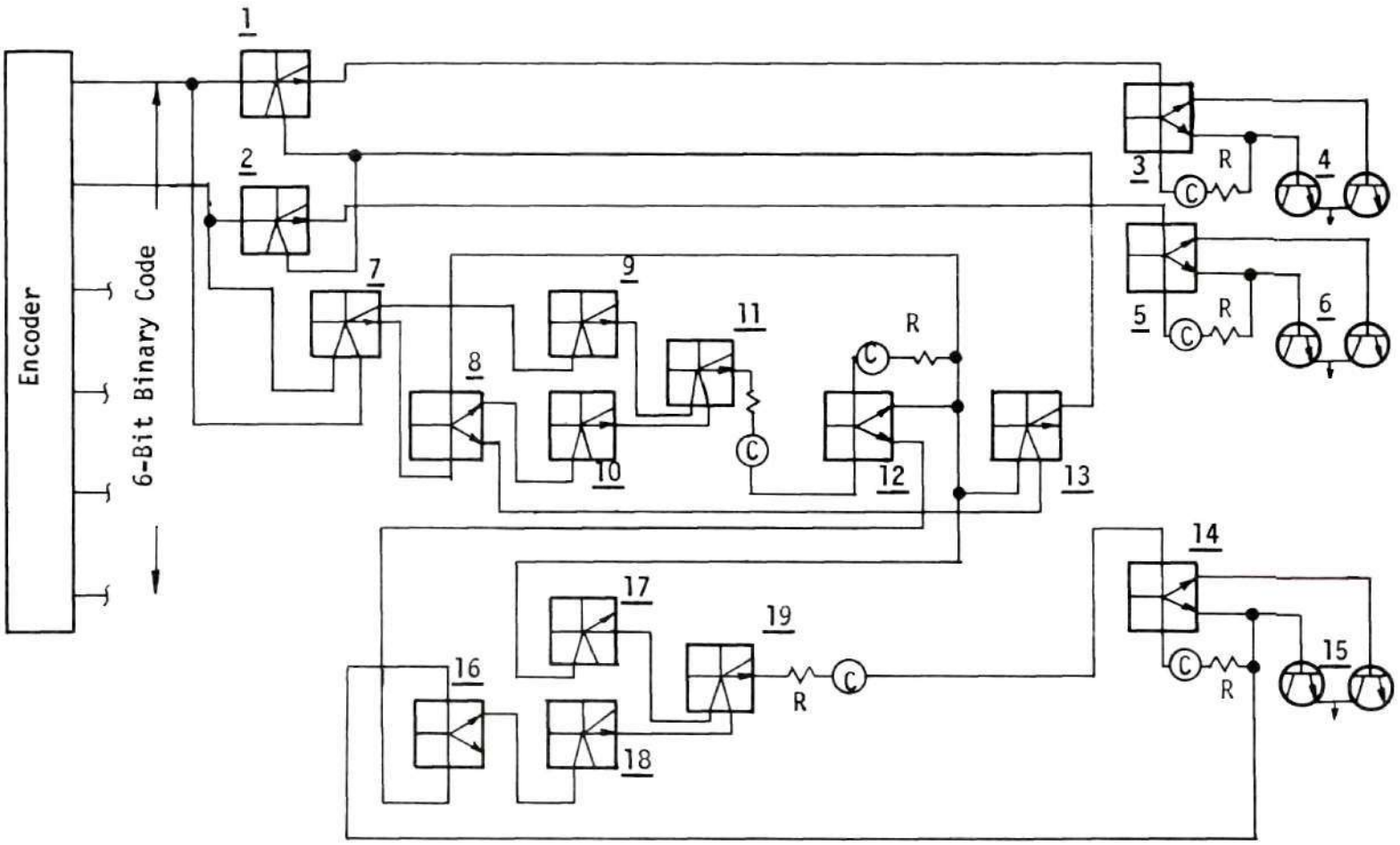

Figure 15. Control Circuit, Synchronous Mode

The diaphragm amplifiers are shown in Figure 15 as 4 and 6 for two bits, the other bits being identical but not shown, and their control pressure is supplied by fluidic flip-flops, 3 and 5. When a key is actuated and a code generated, this code is fed to the power ports of NOR gates 1 and 2, which then provide control signals to switch 3 and 5. When, for example, 3 is switched, the diaphragm amplifiers provide pressure to drive the binary actuator forward. The resistor-capacitor combination which is also connected to 3 as shown will, after a time determined by the RC time constant, reset the flip-flop to its normal or rest position. The net result is to provide a constant pressure pulse to the digital actuators whose length is set by the RC time constant. Thus, the elements 3 and 4 act as a one-shot multivibrator.

In order to insure that once a key has been actuated the operation of the digital actuators will position the corresponding character regardless of further key action, each bit passes through NOR gates such as 1 and 2. These are designated inhibit gates. A signal to the control ports of 1 and 2 effectively blocks, or inhibits, all six bits so that those bits which were zero in the code just generated may not be changed by further key action.

It is necessary, therefore, to generate an inhibit signal after the code has been generated and had time to propagate to the flip-flops 3 and 5. This signal should continue until either the key is released or until the cycle length is complete. This guarantees that the character corresponding to the key actuated will be printed once and only once, and no other keys actuated before release or before the end of a cycle will have any effect. In order to generate the inhibit signal

each bit of the code is fed to NOR gate 7 (which would require parallel operation of more than one physical gate unless six inputs were available). The output of 7 (OR or unbiased side) denotes actuation of any key. Note that before actuation of the key the output of 7 has set flip-flop 8 to drive NOR gate 10. The NOR gates 9, 10 and 11 comprise an AND gate which has an output only if both 9 and 10 have inputs. Assuming that these inputs exist, the output of 11 provides a control signal to flip-flop 12. The switching of 12 may be delayed by an RC time constant as shown if it is required for propagation of the code from 1 to 3. The flip-flop 12 and its RC time-constant feedback determine the minimum cycle length. When 12 switches it immediately causes NOR gate 13 to switch and provide the inhibit signal to 1 and 2 (and the other four bits, as well). The output of 12 is also fed back to flip-flop 8 causing it to be switched. This state of flip-flop 8 is an indication that a key has been actuated and the print cycle has been initiated. Now observe that if the signals 7 and 12 to 8 are reasonably well balanced then 8 will not switch to the other state if the key is let up before the end of the cycle (as indicated by the state of 12). However, at the end of the print cycle when 12 resets, the controls signals will be unbalanced on 8 and it will reset. Also observe that if the flip-flop 12 resets at the end of the cycle and the key is still down then the control signals on 8 are again balanced and it will continue to indicate a key actuated. The output of this state of 8 is fed to 13, whose output is from the OR side. Therefore, an inhibit signal is generated either during the cycle length (signal from 12) or while the key is down (signal from 8).

In summary then, the six-bit code may be transmitted to the actuators only when a key has a transition from up to down after the end of the last cycle and when no other keys are down.

As seen from Figure 14b, it is desired in this mode to begin the printing motion at the same time as the positioning motion. Therefore, the output of 12 also is fed to flip-flop 16. The operations of 16, 17, 18, 19 and 14 are the same, respectively, as 8, 9, 10, 11 and 3. That is, 17, 18 and 19 are an AND gate which has an output when both 16 and 12 have inputs to 17 and 18. Assume that 16 has an input to 18 and 12 is switched at the beginning of a cycle to provide an input to 17. The output generated at 19 is then fed to flip-flop 14 which switches to the proper state to cause printing motion by the action of the diaphragm amplifiers 15. When 14 switches, its output is fed back to 16 which also switches, removing the input from 18 and thus from 14. The flip-flop 14 remains in the same state for a period determined by the RC time constant which feeds back to its control port. The output to the print piston is thus essentially a constant pressure pulse of a given length. The beginning of the print motion may be delayed after the beginning of the position motion by use of the RC combination between 19 and 14 if other design considerations demand it. When flip-flop 12 resets at the end of the cycle, its output also resets 16 so that another print motion can occur. However, it will not occur until the key has been released, the print cycle has ended and another key depressed, since this is the only way to get 12 to switch and provide an input to 17. It may seem that 16, 17, 18 and 19 are superfluous until it is realized that if they are omitted and 12 connected directly

to 14, and design of the print mechanism dictates that the pressure pulse to 15 end before the end of the cycle (which is the likely case), then 14 will not reset to take pressure off 15, and thus off the print piston, because the control signals to 14 will be balanced. With the elements intervening between 12 and 14 this is not the case, and 14 delivers a pulse of length determined only by its own RC time constant.

The circuit of Figure 15 then provides the necessary control functions to carry out the operations of Figure 14b with the exception of the carriage motion. It is shown in a succeeding discussion on the carriage motion that this is best accomplished mechanically, and is therefore not considered here.

Asynchronous Mode

The circuit of Figure 16 comprises a method of achieving control on the basis of sensing the completion of the mechanical motions. The underlined numbers by each element are for reference. The control circuit accepts the six-bit output from the encoder which is applied to the power ports of the inhibit gates 1 and 2. Positioning circuitry is shown for two bits only, the others being identical. The output of 1 and 2, when the bit is a "1" (high pressure) causes the flip-flops 3 and 5 to be set to cause flow through the diaphragm amplifiers to the digital actuators and thus position the type head. This pressure to the actuators continues until the flip-flop resets as explained subsequently.

As in the synchronous mode, in order to allow completion of the print cycle without interruption from further key actuation the position code is inhibited immediately after the flip-flops 3 and 5 are set.

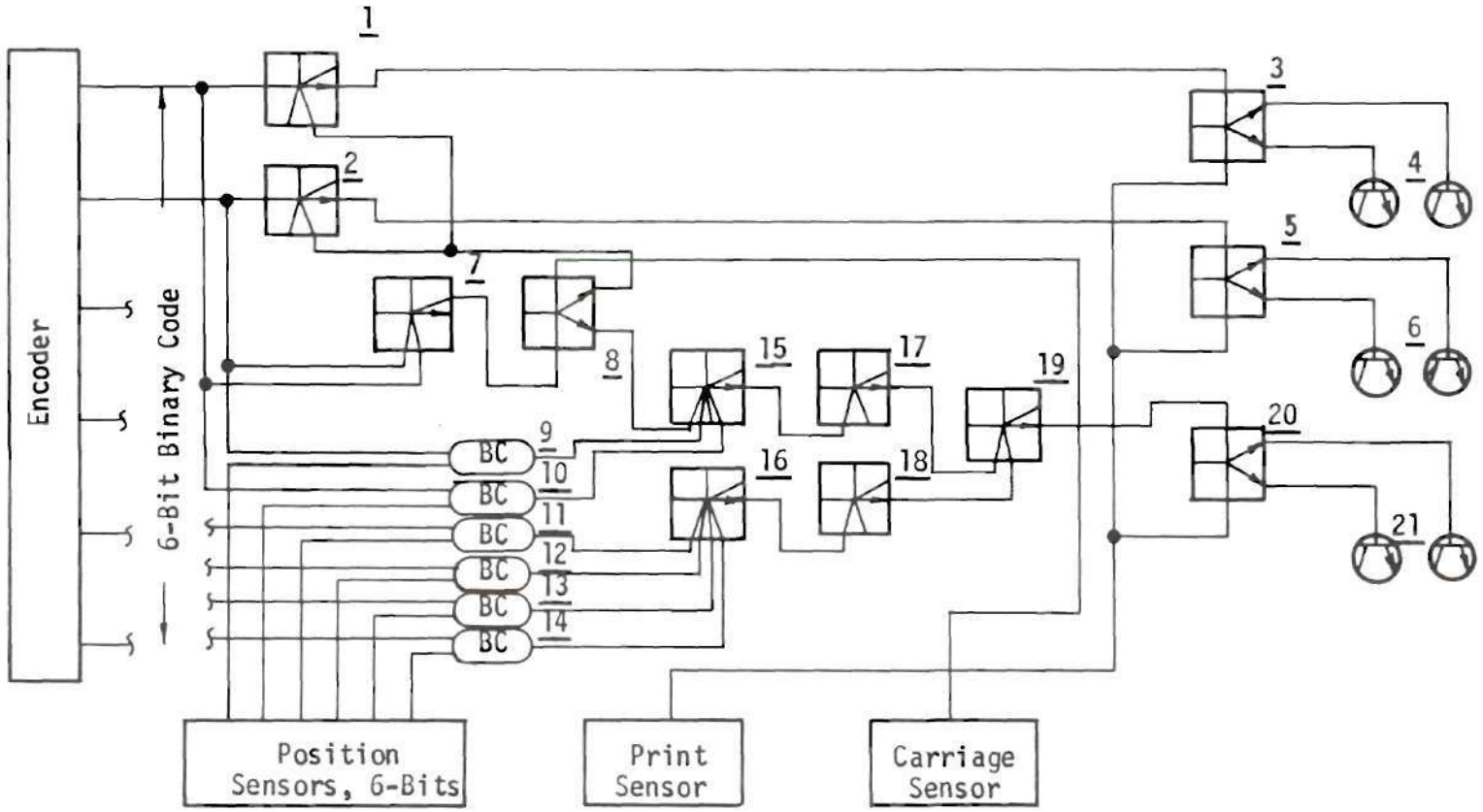

Figure 16. Control Circuit, Asynchronous Mode

This is accomplished by feeding the six-bit code to the OR gate 7 so that any generated code will set flip-flop 8, the output of which provides the control signal for the inhibit gates 1 and 2. Note that six inputs would be required for 7 so that it represents at least three physical four-input devices. Also observe that the circuit assumes that the signal propagation to 1 and 2 from 8 is slower than that through 1 to 3. If this should not be the case, a delay would have to be introduced at the output of 8.

This mode of operation requires that the final position of the type head be sensed. This is not simple since there are as many "final" positions as there are characters. In order to determine when the motion is complete, it is necessary to encode the final position and then compare with the code generated by the keys. This comparison is shown in Figure 16 where the position sensor (described subsequently) generates a six-bit code corresponding to the final position of the type head. When the final position is reached, the corresponding bits of the two codes will be the same (i.e., either 1 and 1 or 0 and 0). The agreement of individual bits is determined by the bit comparison (BC) blocks in Figure 16.

The bit comparison blocks are diagrammed in Figure 17a. Their operation can be explained if F_i is defined as indicating agreement (logically) in the i-th bit generated by the encoder and sensor. If M is the i-th bit from the encoder and N is the corresponding bit from the sensor, then

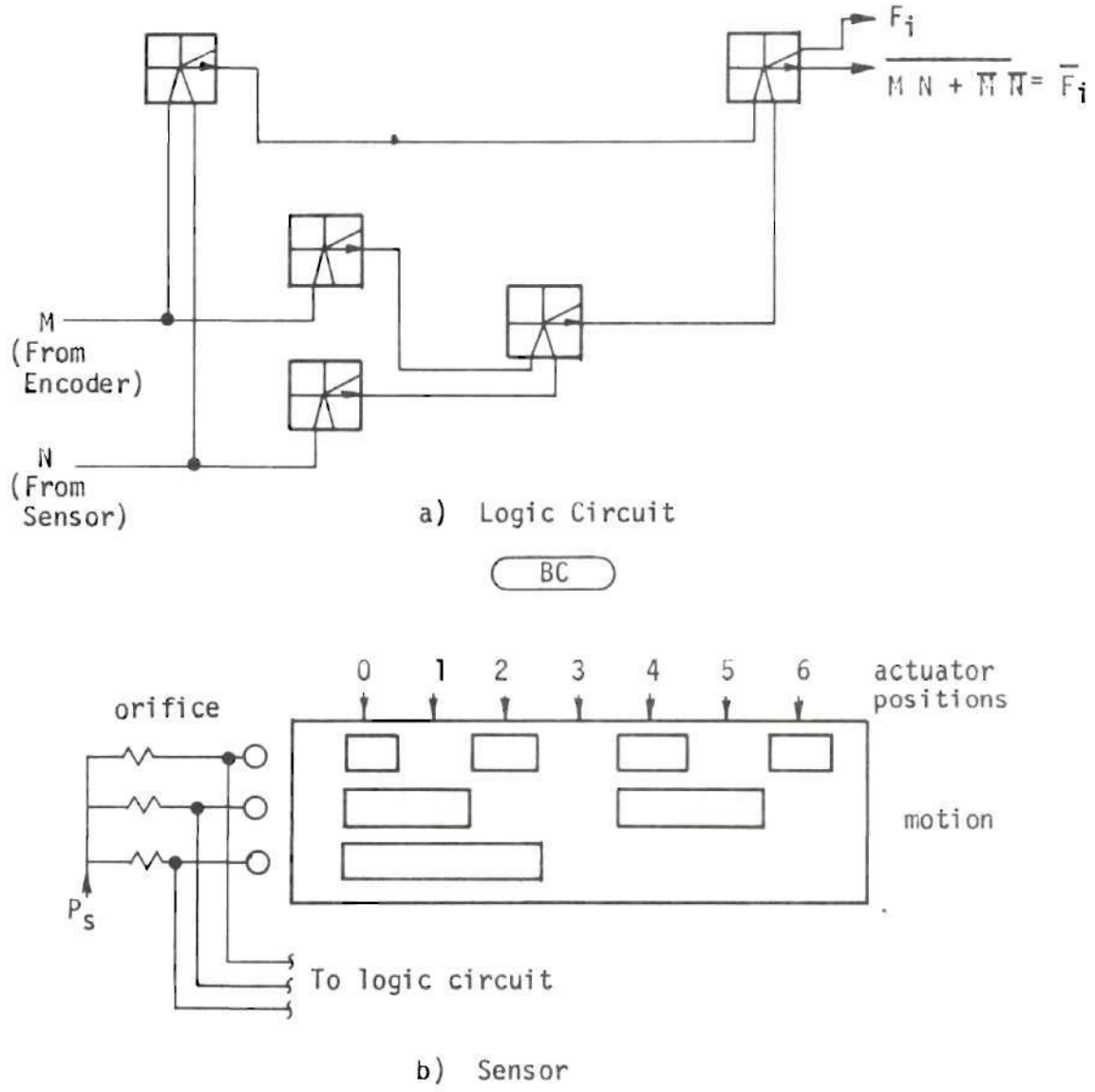

Figure 17. Bit Comparison

$$\overline{F_i} = MN + \overline{M}\,\overline{N} \tag{113}$$

is the Boolean equation for each bit. Figure 17a is an implementation of $\overline{F}_i$ using NOR gates. The output $\overline{F}_i$ is convenient since the final position, denoted as F, is given by the Boolean equation

$$F = F_1 \cdot F_2 \cdot F_3 \cdot F_4 \cdot F_5 \cdot F_6 \tag{114}$$

so that the F_i are inputs to an AND gate. Using NOR's to make up this AND gate would require the inputs to be inverted, and so fewer elements are needed if the negated output $\overline{F}_i$ is taken. The elements 15 through 19 then implement Equation (114) above and the output of 19 is F.

Figure 17b illustrates an absolute encoder which could be used to encode a linear motion of the positioning mechanism. A similar scheme can be used for rotary motion. The encoder consists of a moving vane with slots corresponding to the zeros of the binary code. The vane shown illustrates a three-bit encoder. The position is sensed with the back pressure on the three orifices supplied by a constant pressure. Note in Figure 16 that the six-bits sensed represent both motion axes and thus represents two separate encoders.

The output of 19, indicating that the type head has reached its final position, provides the control signal to set the flip-flop 20 which then drives the diaphragm amplifiers 21 of the print drive.

It can be seen that when no keys are actuated the six-bit encoder output and the position sensor output could agree bit by bit. This,

of course, is sufficient for beginning a print cycle which would print the character corresponding to this code repeatedly. This situation can be avoided by making the connection shown in Figure 16 from the output of 8 to the control port of 15. This makes it necessary to actuate a key to switch 8 and remove this signal to 15 in order to have an output at 19.

In the asynchronous mode, it is necessary to sense the end of the forward print stroke in order to allow return of the print piston and binary actuators. This sensor can be of the back pressure type similar to that of the position sensor where the orifice is blocked by the type head structure at the appropriate position. In Figure 16, the output of the print sensor is used to reset flip-flops 3, 5 and 20 allowing the positioning and printing mechanisms to reset.

As in the synchronous mode, it is assumed that the carriage motion can be mechanically interlocked so that fluidic actuation is not required. However, the asynchronous logic scheme requires sensing of its completed motion. The output of this sensor resets flip-flop 8 to release the inhibit gates and lock out the print subsystem with the input to 15.

Thus, the circuitry of Figure 16 is sufficient to sequence the major subsystems of the typewriter on an asynchronous basis.

Selection of Control Subsystem

Having discussed two possible methods of control which are rather different in their philosophy and implementation, it is necessary to compare them in the light of the overall objectives of the design.

The basic criterion is to minimize power consumption and maximize speed of typing. For this subsystem the implications of the criterion are that the number of fluidic elements should be minimized, since each one consumes power continuously, and the delays introduced by the control system should be minimized. These delays arise from the switching delays of the fluidic elements and transport times of the connecting lines. Maximum delay due to an amplifier will be shown to be on the order of one millisecond, which is negligibly small for 30 characters per second or less. Line delays are a function of physical location of elements and actuators, but are again on the order of one millisecond or less (the velocity of sound in air being about 1000 feet per second).

For comparison on the basis of power consumption it is only necessary to count the number of elements in implementation of each mode. The synchronous mode requires 26 elements if 7 is counted as three elements to account for all six bits as input to it. The asynchronous mode requires 52 elements if 7 is counted as three elements. It is reasonable to expect that the power consumption of the synchronous mode will be only half that of the asynchronous. Of course, the supplemental criteria of reliability, cost, ease of maintenance, noise generation, etc. are all better satisfied by the lower number of elements.

The delays introduced by the control system are not particularly serious for either mode. The six-bit code propagates through only two elements (e.g., 1 and 3) to begin the positioning of the type head, so this path is negligible. The synchronous mode allows compensation

for any other delay through the RC time constants. However, the generation of the inhibit signal in this mode traverses seven elements so that a delay of ten milliseconds might be expected. At typing speeds of ten characters per second this is no problem and is, in fact, useful since it gives a delay in the inhibit signal. At much higher speeds it would be a serious problem. However, these higher speeds would probably only be attained by automatic operation where the inhibit signal would probably not be needed. In the asynchronous mode, the only delay of significance is that in the circuitry for sensing the final position. This propagation path includes six fluidic elements and connecting lines, and an estimate of the delay could be six to ten milliseconds. At speeds of, say, ten characters per second this is only a small fraction of the cycle length and would not be detrimental. At speeds of 30 characters per second it would constitute about a third of the cycle length and would definitely be a factor.

From the discussion thus far it could be concluded that the synchronous mode has a definite advantage. One basic consideration remains. The synchronous mode assumes that the mechanical motions controlled by the fluidic circuit will perform their functions in a given time and with small deviations relative to their design actuation times. The asynchronous mode does not ostensively require this assumption since the completion of the mechanical motions is sensed. In a broader context, however, the asynchronous mode does require repeatability of the motions, at least to a small fraction of the cycle length corresponding to the fastest manual operation, since the typist cannot

take into account variations in response of the machine elements. Thus, the one basic advantage that the asynchronous mode might seem to have, that of guaranteeing completion of each mechanical motion in proper sequence, is really of small value.

On the basis of this comparison then, the synchronous mode would seem to meet the overall criteria best and will be used in the further design.

CHAPTER VI

KEYS AND ENCODER

Introduction

Input to the typewriter is from a standard keyboard consisting essentially of 44 keys and a shift key to give both upper and lower case alphabet, numerals 0 - 9 and certain marks of punctuation and special characters. The space bar and tab key are considered along with the carriage motion instead of in this chapter. The input from the keyboard is utilized to generate a digital code to select the character to be printed from the type head by means of linear, digital actuators. This is in accordance with the basic ground rules established in the beginning. It is also assumed here that the upper and lower case are arranged on the type head so that the shift key can provide the necessary signal to select the upper case character corresponding to any key. This can be accomplished in a variety of ways. One would be to put the lower case around one half the circumference of a cylindrical head and the upper case on the other half so that 180° turn due to the shift key will allow the same code to select the upper case characters. Another scheme would be to place upper and lower case characters of the same key adjacent to one another circumferentially so that the shift key would move the head one character space. The digital actuator would then cause a maximum of 360° rotation to select characters from either case. The first scheme above would only require

a 180° maximum rotation by the digital actuator. Similar variations on the axial motion could also be envisioned. Of course, another bit in addition to those required for one case could be added to one of the digital actuators. This would not require separate and independent mechanical coupling of the shift key signal to the type head as do the previous schemes. For the purposes of the present analysis it will be assumed that the shift key is separately coupled and that the digital actuators select one of 44 characters by the code generated. This then requires six bits which can encode 2^6 or 64 characters maximum.

Coding

If the problem of generating the six-bit code is considered from the Boolean logic standpoint, it is seen that any bit, α_i, has a Boolean equation

$$\alpha_i = \beta_1 + \beta_2 + \cdots + \beta_n \qquad i = 1, \cdots, 6 \tag{115}$$

where the β_j are keys of the keyboard, and n of them have $\alpha_i = 1$ in their code. That is, if any of the keys β_j is actuated, the bit α_i is a logical "1". The equation then shows that the encoder for a given bit is essentially a multi-input OR gate, as illustrated in Figure 18a. The number of inputs to the gate depends on which bit is encoded, the arrangement of the type head and the choice of a code. This can be illustrated as in Figure 18b. Suppose the type head has six rows and eight columns of characters on its surface which can be represented by

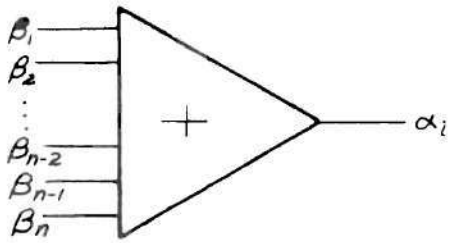

a) Single Bit Encoder

α_6	0	1	0	1	0	1	0	1
α_5	0	0	1	1	0	0	1	1
α_4	0	0	0	0	1	1	1	1
α_1 α_2 α_3								
0 0 0								
0 0 1	β_{17}	β_{18}	β_{19}	β_{20}	β_{21}	β_{22}	β_{23}	β_{24}
0 1 0	β_1	β_2	β_3	β_4	β_5	β_6	β_7	β_8
0 1 1	β_9	β_{10}	β_{11}	β_{12}	β_{13}	β_{14}	β_{15}	β_{16}
1 0 0								
1 0 1	β_{25}	β_{26}	β_{27}	β_{28}	β_{29}	β_{30}	β_{31}	β_{32}

b) Input Gate Lead Determination

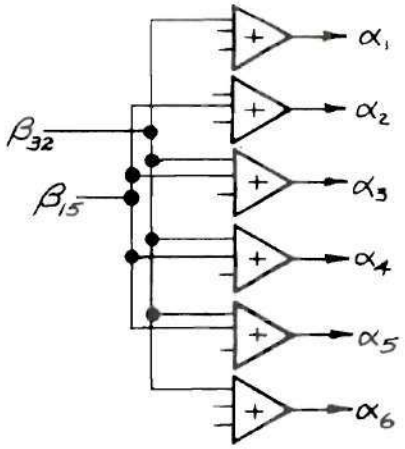

c) Key to Encoder Connections

Figure 18. Aspects of Coding Problem

the 6 X 8 matrix shown. Each character has a corresponding six-bit code with $\alpha_1\ \alpha_2\ \alpha_3$ representing the rows and $\alpha_4\ \alpha_5\ \alpha_6$ the columns. Note that for the bit α_2 there are 16 spaces in the matrix with a logical 1. These might be assigned the characters β_1 through β_{16} and the logical equation becomes

$$\alpha_2 = \beta_1 + \beta_2 + \cdots + \beta_{16} \tag{116}$$

Thus, the OR gate for α_2 would have 16 inputs for this particular type matrix and code assignment. If the α_3 bit is considered, it is seen that

$$\alpha_3 = \beta_9 + \beta_{10} + \cdots + \beta_{32} \tag{117}$$

and so a single key may connect to more than one gate (e.g. β_9 through β_{16}). The number of gates to which a single key provides input may be seen by simply noting which bits have logical 1 in the code for that matrix position. For example, β_{32} connects to five gates, as shown in Figure 18c. Also shown in Figure 18c are the connections for β_{15}. Observe that both keys connect to the input of α_3, but only β_{32} connects to α_1 and α_6. It is essential that the inputs to any encoder gate be isolated from one another, otherwise extraneous bits will appear in the code. That is, each gate lead must have an effective diode to prevent feedback to other leads. For instance, if β_{15} is actuated and there is no isolation, then all six bits may well have outputs. Fortunately, the construction of Coanda amplifier input ports

is such as to provide effective diode action, because there is essentially zero gauge pressure at the junction of the input ports.

Another aspect of the coding scheme is that not all the matrix positions are needed in most cases. There are only 44 keys, but the matrix of Figure 18b, for example, has 48 spaces. In order to minimize the gate leads, which tends to reduce the number of physical gates, those spaces having the largest number of bits in their code would not be used. In Figure 18b these would be those marked β_{16} and β_{32}, plus two others, say β_8 and β_{24}.

In Figure 18 the encoder for each bit is represented as a single logical OR gate. Due to physical design limitations, about which more will be said later, it is common to build OR gates with two control ports (gate leads) and it is possible to have as many as four control ports with present technology. In Figure 19 is illustrated the actual implementation of α_2 from Figure 18. This is shown for four-input OR gates only, and illustrates the fact that five OR gates are required if each has four control ports. If two-input OR's are used, then fifteen OR gates are required. Since the power consumption is about the same for two or four inputs, it is important which is used.

A further point for consideration is that, for some character matrices, the number of gate leads, and therefore number of amplifiers, can be reduced by using other than consecutive numbering of rows and columns. For example, if the columns of Figure 18b are numbered 0 through 8 (in binary) instead of 0 through 7 and the eighth column has no characters on the type head, then the total number of gate leads is reduced from 128 to 116. The number of amplifiers for this seven bit

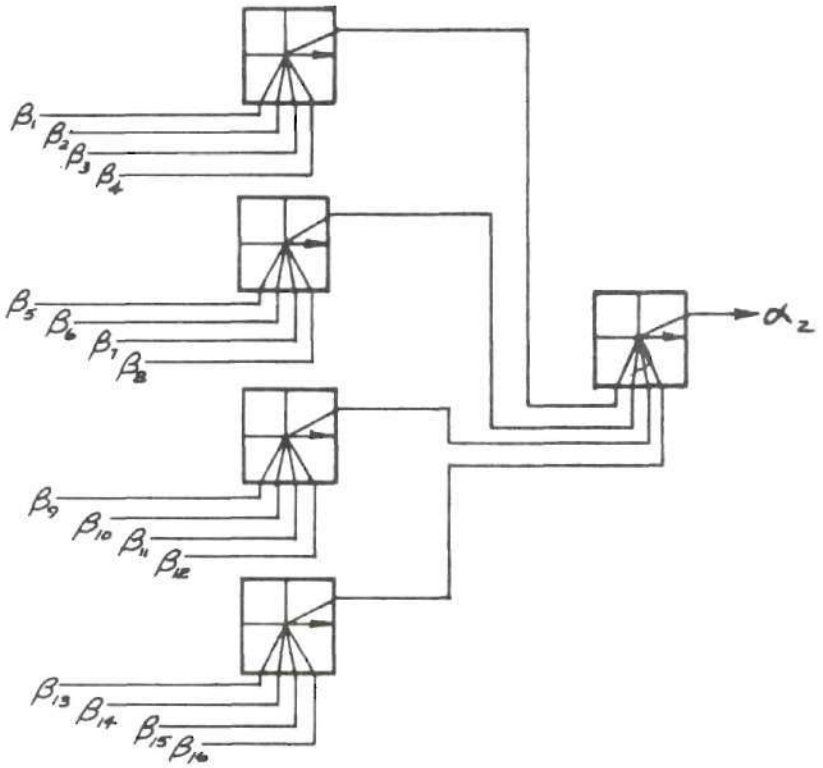

Figure 19. Implementation of Single Bit Encoder

encoder is 46, whereas the six-bit encoder using consecutive numbering as in Figure 18b required 49. This small reduction in the number of amplifiers is accompanied by the necessity for an additional piston in the binary actuator and a probable increase in the size of the type head due to the blank column. In order to determine whether or not there is any advantage in a particular matrix or coding scheme, it is useful to consider the likely possibilities and to quantify the difference in them. Table 2 is a comparison of five row and column combinations. It is necessary to have at least 44 spaces, so 7, 6, 5, 4 and 3 rows are considered with the necessary columns to give 44 spaces. Rows and

Table 2. Comparison of Type Matrices and Coding Schemes

	Matrix - Row x Column									
	7 X 7		6 X 8		5 X 9		4 X 11		3 X 15	
	C	MB	C	MB	C	MB	C	MB	C	MB
Column Bits	3	3	3	4	4	4	4	4	4	4
Row Bits	3	3	3	3	3	3	2	2	2	2
Total Gate Leads	106	106	110	100	105	101	112	108	110	110
Four-Input Gates	42	42	38	33	35	42	37	34	38	38
Levels, Four-Input	3	3	3	3	3	3	3	3	3	3
Two-Input Gates	98	98	102	90	95	91	106	102	102	102
Levels, Two-Input	5	5	5	5	5	5	5	5	5	5

C = Consecutive Numbering

MB = Minimum bits to reduce gate leads

columns are interchangeable in Table 2.

The manner in which Table 2 was developed is best described by taking the 6 X 8 matrix as an example. The columns labeled C and MB (which stands for "consecutive" and "minimum bits", respectively) refer to the previous discussion concerning the possible reduction of gate leads by using non-consecutive numbering of rows or columns. For the 6 X 8 matrix, consecutive numbering requires three row bits and three column bits, as shown in Table 2, and results in 110 total gate leads when the unnecessary four extra spaces are omitted from the 48 available. All the data in the table reflect omission of extra spaces. If one more bit is added to the column numbering, the MB scheme will result in 100 total gate leads, but this requires four column bits instead of three.

In order to determine the number of amplifiers needed, it is necessary to consider the number of leads for each bit out of the total shown. These are combined in the manner of Figure 19 to determine the total number of OR gates for each bit. The total for all bits are shown as 38 for consecutive numbering and 33 for minimum bits if four-input gates are used, and 102 and 90 if two input gates are used. All the data on number of amplifiers reflects the minimum possible number of gates for the necessary number of gate leads. For example, in Figure 18b the number of gate leads required for α_3 is 21 (discounting blank spaces). If these are simply combined in a straightforward manner as in Figure 20a, the result is nine four-input gates. This configuration has equal switching delay for all the keys. Since there is no advantage in equal delay, it is possible to eliminate two gates as shown

in Figure 20b. This has been done where possible in Table 2.

Table 2 also gives the number of logic levels in the longest propagation path for any bit of the encoder for both two- and four-input gates. This turns out to be three levels for four-input gates, as illustrated by Figure 20 and five levels for two-input gates. Thus, for either type gate the maximum switching delay is on the order of three to five milliseconds.

The coding scheme and type head design which best meet the design criteria could be selected from the information in Table 2, except for the fact that this choice also influences in a direct way other portions of the position drive subsystem. Since the space allowed on the type head for each character is more or less fixed, the dimensions of the head are determined by the row-column configuration; for example, for three rows and 15 columns, the distance moved to select the highest numbered column is much greater than to select the highest numbered row. However, the time allowable for the motion would be the same and so it is possible that one binary actuator would be much larger than the other. Intuitively this would seem to be a poor choice, but it must be considered in terms of the whole system. A more obvious point is that the weight and moment of inertia of the head itself, which forms part of the load in the position drive subsystem, are directly related to the choice of row-column configuration. A further point is that some of the matrices require a four-bit actuator which is more complex to design and build than a three-bit device. These considerations just mentioned do not allow a final choice of encoder configuration at this point. However, it is possible to draw some conclusions with respect

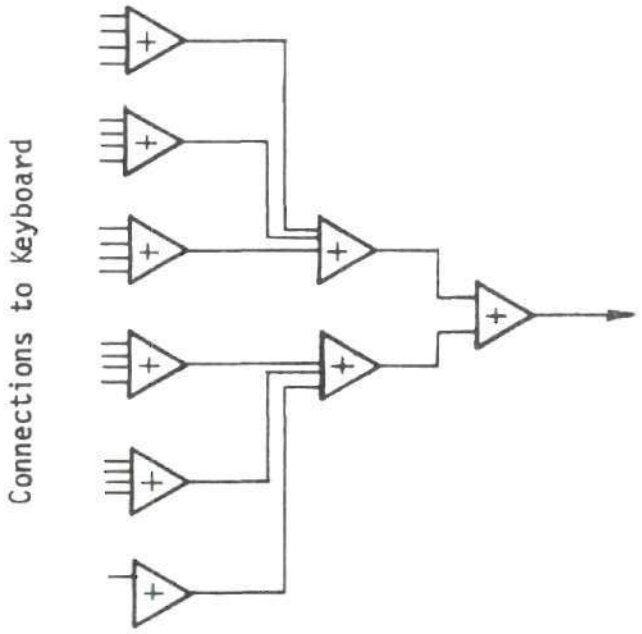

(a)

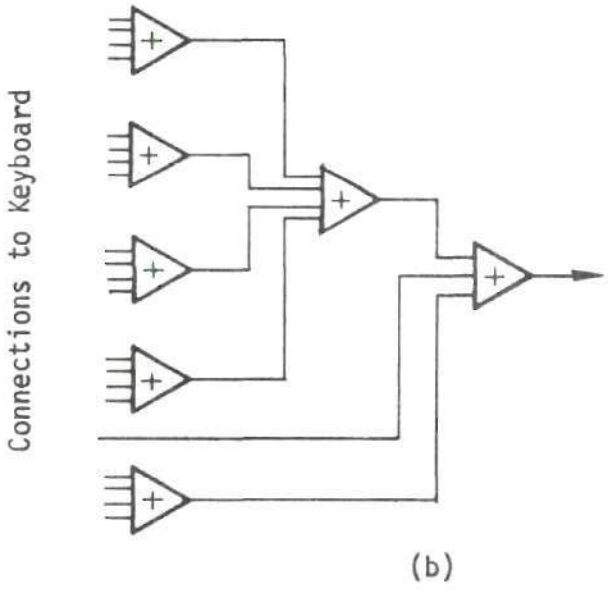

(b)

Figure 20. Minimization of the Number of Encoder OR Gates

to the design objectives of maximum speed and minimum power.

First, it is obvious that the number of OR gates is reduced by more than half if four-input gates can be used. It is very likely that this can be done since the demands on amplifier performance in terms of gain and pressure recovery are minimal, due to the fact that any amplifier drives only one other similar amplifier. As observed before, power consumption is about the same for both devices, so power is reduced with four-input gates. Secondly, speed tends to be higher for four-inputs since there are only three levels of gating, although this supposes equal switching times. This is a less important consideration, but supports use of four-input gates. As for type matrix choice, the decision is not clear cut. The 6 X 8 matrix with minimum bits has the lowest number of gates, 33, but requires four column bits. Other choices require up to 42 gates, or an increase of almost 25 per cent in the number of gates, but it remains to be seen whether or not this is significant for the overall machine.

Key Design

Input to the encoder is in the form of pressure signals from the keyboard. The use of fluidics in a typewriter offers several possibilities as to key construction which are unique. Some of these possibilities are similar to those already in the patent literature [4]. Figure 21 shows four possibilities which could be used, and they will be discussed as to their relative merits.

Since each key might have to supply as many as six amplifiers, it is conceivable that some amplification might be desirable. If the

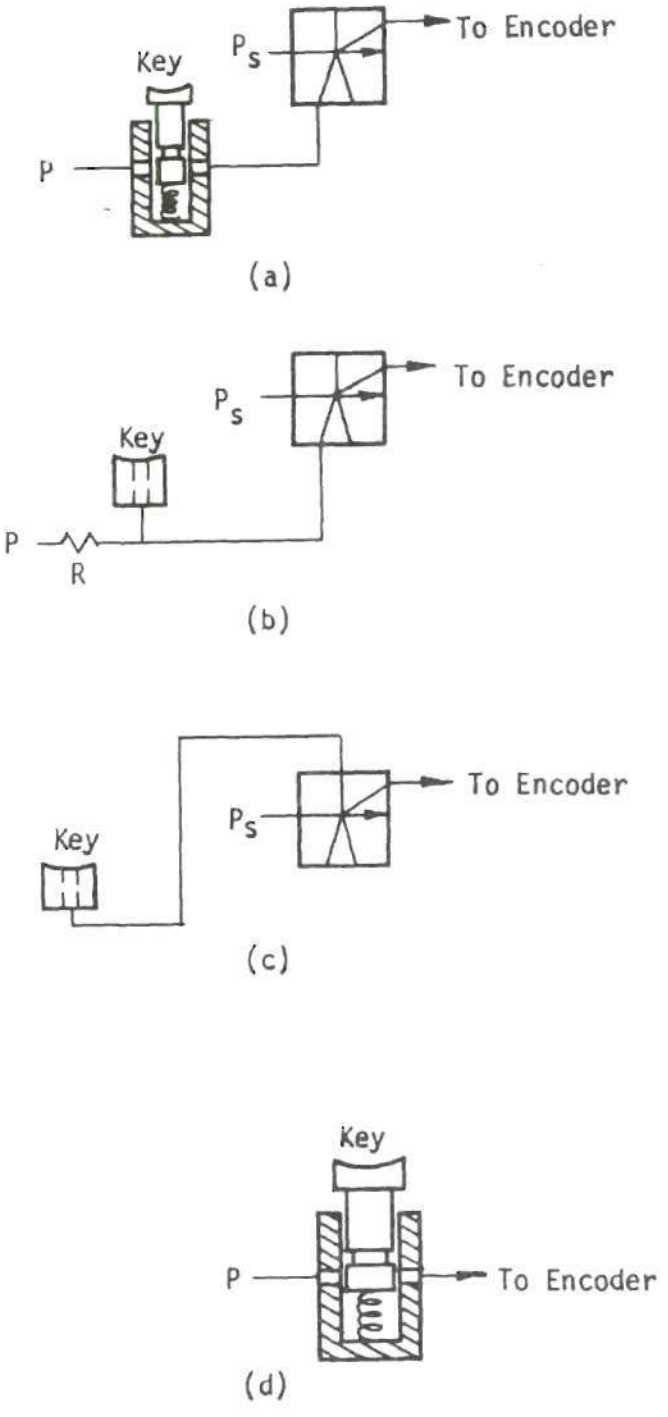

Figure 21. Key Configurations

configuration of 21a were used, where the key consists of a valve having some mechanical mechanism such as a sliding rod covering a port to which air pressure was supplied, it might be useful to limit the flow in order to reduce the size of these mechanical parts. Such size limitations might be useful due to necessity for close key spacing or for improvement of dynamic response of the moving parts when manually actuated.

Fluidics offers the unique possibility of keys which do not need to move in order to type a character. In Figure 21b is shown a key which consists simply of an orifice in a suitable shaped depression. The orifice serves as a vent for the pressure supplied from a source P. With the key uncovered the pressure at the control port of the NOR gate would be too low to cause switching. Covering the key with the finger tip would raise the pressure and switch the gate to generate a character code. The resistance R would be necessary since otherwise the large number of other keys connected to P would prevent an effective change in control pressure. While this scheme is unusual, it would require considerable power since flow exhausts continually through the keys and the NOR gates consume power continuously. Also, it would have to be determined whether or not the air flow on the typists fingers would be objectionable.

A means of providing a non-moving key which does not have flow out the key or consume power at the key is shown in Figure 21c. The bias of a NOR gate is due both to its internal geometry and to the interaction region vent. If this vent is blocked, the gate will switch

and remain until the vent is opened. The key in this case would consist of an orifice in a suitably shaped depression which would be covered with the finger tip. A major difficulty, in the practical sense, with this arrangement is that the vent is normally under a slight vacuum due to the entrainment properties of the amplifier power jet. Thus, dust and foreign matter, such as eraser shavings, could easily be drawn into the system. It might be possible to filter these out, but it would be difficult without upsetting to proper operation of the gate because of the pressure drop through any effective filter.

The fourth possible key configuration is the obvious one of a simple valve supplying pressure directly to the encoder. This is quite feasible if the flow required to switch the encoder gates is small enough. The sliding stem returned by a spring shown in Figure 21d is one possibility, and there are no doubt other mechanical configurations which could be simpler and cheaper.

There is another general consideration relating to the choice of key configurations. The schemes shown in Figure 21a and 21d could both have an easily determined threshold for actuation of a print cycle. That is, a given distance must be traveled, and thus a given spring force reached before a port is uncovered and a character printed. Therefore, when the typist's fingers rest lightly on the keys during a pause in typing, no unwanted characters are typed. With the non-moving keys, especially Figure 21c, this threshold is not inherent and must be added. One means of doing so would be to add a moving cover for the orifice with a spring return to provide a threshold.

Although this might be simpler and more responsive than the valve-type keys, part of the advantage and novelty of the non-moving key is lost. Of course, it might be possible to achieve the threshold by proper shaping of a depression around the key orifice, but this would require considerable experimentation to achieve satisfactory results. It is conceivable that the non-moving key could have considerable effect on typing speed (from the manual operator standpoint). One would assume that speed would improve due to less force being applied by the fingers, but this would need to be investigated.

In conclusion, several key configurations are possible, both with and without fluidic amplification. The one shown in Figure 21d is certainly the simplest and would consume the least power, thus conforming to that overall design criteria. However, configurations (b) and (c) with no moving parts might well have the best response time and thus contribute better to the criteria of maximizing speed. The final decision will be left until some quantitative evaluation is made in conjunction with the overall model.

CHAPTER VII

COMPUTER MODEL

Introduction

One of the purposes of this investigation is to consider the typewriter as a complete system and to indicate a preferred design as determined from the overall design criteria of maximum speed and minimum power consumption. In the previous chapters, the major subsystems defined in Figure 3 (except the carriage and pneumatic power supply) have been considered and their preferred configurations defined. However, no information as to the numerical values of size, speed, power consumption or other parameters were defined for the overall system. Furthermore, some questions still remain as to the makeup of the keys, encoder, carriage, and power supply which will be determined by the consideration of the system as a whole.

It is the purpose of this chapter to develop a set of design calculations based on the previous discussions and some further choices as to the form of the mechanisms. These calculations will be used to evaluate the effect of the various parameters of the system in meeting the design criteria, and thus to define a preferred system. This procedure will also provide information from which to design the compressor and accumulator. The design calculations will be developed by considering each subsystem in turn, and relating its parameters mathematically to the overall criteria. These relations will be

combined into a computer program to facilitate evaluation of the various parameters.

Before proceeding with the design calculations, it is necessary to consider the problem of pressure levels and pressure matching in the overall machine. It is conceivable that the supply pressures to individual fluidic devices and actuators be allowed to take whatever value might be advantageous, and thus demand numerous pressure levels in the machine. Such a situation has basic disadvantages from the standpoint of pneumatic power supply. To supply a multiplicity of pressures requires either (1) multiple compressors, which is not feasible for this application, (2) a multistage compressor with bleeds at various stages, which could be done but would be complex and costly, or (3) a single compressor with pressure regulating and reducing valves, which would be both costly and inefficient. All of which says that it is very desirable to limit to as few as possible the number of different supply pressure levels.

It has been determined in the previous chapters that the overall system would utilize both Coanda pure-fluidic devices and diaphragm amplifiers as the final drive amplifiers. If only one or the other were used it is possible that only one pressure level would be needed, but it has been shown that a very significant power reduction is made by using diaphragm amplifiers, and this design aspect will be retained. If all the amplifiers were of the diaphragm type, a great many more amplifiers would be required. For example, Jensen [16] shows a NOR gate using diaphragm elements which would require six complete physical

elements for a four-input NOR, and four is the largest fan-in successfully used. Thus, an encoder of 40 gates would require 240 diaphragm elements. Such complexity is hard to justify, if there are not great disadvantages in Coanda devices.

One disadvantage to Coanda devices is the pressure recovery of only about 25 to 40 per cent in most commercially available devices. Restriction of the power jet to less than sonic velocity implies a maximum supply pressure of approximately 12 psig, which produces three to five psig output pressures. Use of all diaphragm elements might permit higher pressures, but it is not clear that this follows since this means higher stresses on the thin plastic diaphragms, which could be damaged over a long period. Maximum operating pressure for the diaphragms would have to be experimentally determined.

Based on the foregoing considerations, it is reasonable to accept circuitry of both Coanda and diaphragm devices as shown in Figures 15 and 19. To determine the number of supply pressures necessary, reference is made to Figure 15. If, for example, a nominal 25 per cent pressure recovery for Coanda amplifiers is assumed, consideration of the position-drive amplifiers 3 and 4 shows that the maximum control pressure to the diaphragms is about three psig, assuming sonic velocity in the Coanda supply jet. This means that the maximum supply pressure to the diaphragm device is also three psig. Further, it requires two supply pressures of approximately three and 12 psig. If it is also assumed that the pressure gain of the Coanda devices is about four, then the control pressure for 3 would be 0.75 psig. Since this pressure

is supplied from the inhibit gate 1, whose supply is the output of the encoder final stage, the assumptions concerning gain and recovery dictate that the encoder final stage supply pressure also be 12 psig. It can be shown that the other Coanda devices can all be operated from three psig, so that the final result is that two supply pressures, P_s and $4P_s$ are required for the general circuit configurations developed so far. The value of P_s is yet to be determined. Subsequent work in this chapter will reflect this result.

Key Interface

In Chapter VI, several possibilities for keys and means of driving the encoder were discussed and shown in Figure 21. In order to select one of these configurations on the basis of the design criteria it is necessary to determine power consumption for the associated amplifier interface. If these amplifier are used, they must drive from one to six amplifiers on the first stage of the encoder. The energy per cycle for a given interface amplifier is

$$w = P_s Q_s T_r \tag{118}$$

It is assumed here that the cycle length is identical with T_r, the total motion time for the actuators. It can be seen that this is true from Figure 14b, if it is assumed that no time tolerance is required in designing the mechanical actuators.

If the control pressure and flow for an encoder first stage amplifier is assumed to have a linear output characteristic as in

Figure 22, then by superimposing the encoder amplifier input characteristic, the size of the interface device can be determined. From Figure 22

$$p = p_m - \frac{p_m}{q_m} q \tag{119}$$

Since

$$p_m = \sigma P_s \qquad q_m = Q_s \tag{120}$$

which assumes incompressible flow downstream of the power nozzle, and

$$Q_s = \rho v \eta d^2 / \rho_s \tag{121}$$

by substituting Equations (120) and (121) into (119) and solving for d, the power nozzle characteristic dimension is given by

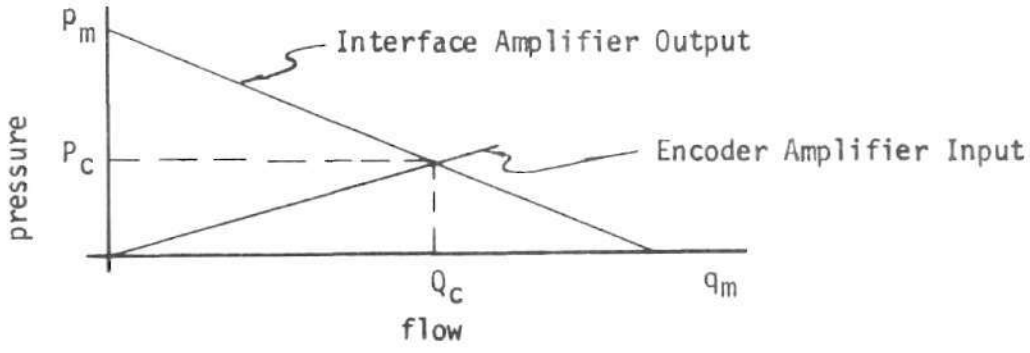

Figure 22. Interface Amplifier Matching Conditions

$$d = \left[\frac{6 Q_c \sigma P_s \rho_s}{\sigma P_s - P_c \nu \eta \rho}\right]^{0.5} \tag{122}$$

For given supply conditions P_s and T_s, it is possible to compute the velocity and density at the nozzle throat if atmospheric pressure is assumed at the throat; see Shapiro [35].

It is also possible to get an estimate of the switching time delay or response time once v and d are known. Comparin [10] gives some information which relates the response time to size and nozzle velocity through the Strouhal number

$$N_{SL} = \frac{\text{response time}}{\text{transport time}} = \frac{v t_r}{\ell} \tag{123}$$

Since length ℓ is related to d for a fixed geometry, t_r can be determined for a given N_{SL}.

These calculations can be summarized by Figure 23, which shows the input quantities required, the computation equations and the output information in a block diagram form, which is a part of the total system design computation.

Encoder

In Chapter VI, some information was developed showing the number of fluidic devices necessary for the encoder and how this number might be minimized (Table 2). In order to best meet the minimum power criterion, it is also necessary to minimize the power consumption of each of the encoder gates when operating at the specified supply pressure, P_s. Small [26] and others have pointed out that there is

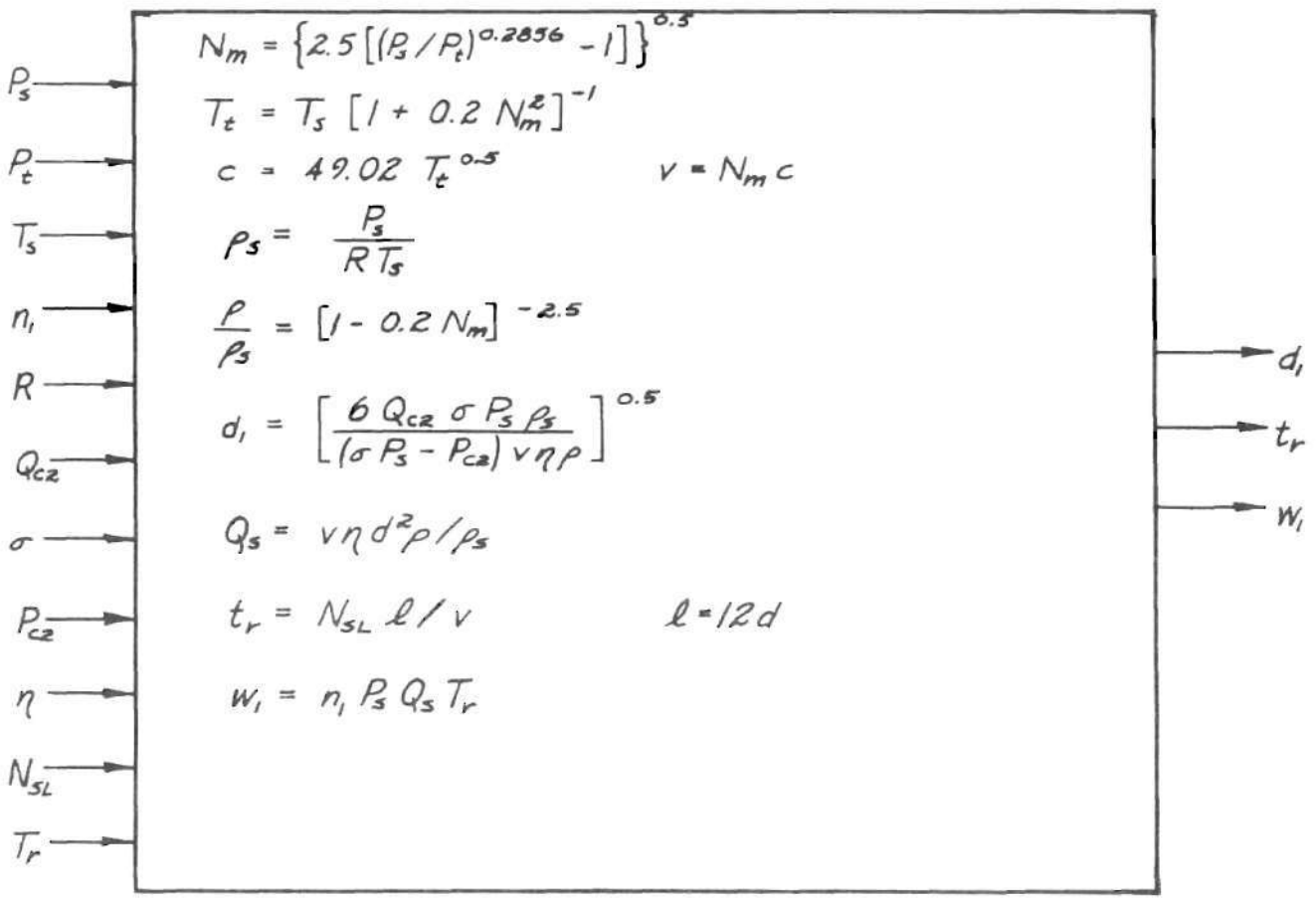

Figure 23. Key Interface Computation Block

a minimum Reynolds number at which Coanda devices operate properly, and that if minimum power consumption is desired the device should be operated at that minimum. Minimum Reynolds numbers are generally in the transition and turbulent region from approximately 1000 to 5000; see Comparin [10]. A later paper [11] by this author describes attachment at much lower Reynolds numbers; however, the geometry involved was quite different from that of more conventional amplifiers. For the purposes of this computation, it will be assumed that the size of the amplifiers is determined by the supply pressure and a Reynolds number in the range 1000 - 5000.

The energy per cycle for the encoder is given by

$$w_2 = n_2 P_s Q_s T_r + 6(4 P_s) Q'_s T_r \qquad (124)$$

In order to compute w_2 it is necessary to know the volume flows Q_s and Q'_s. These can be computed in much the same way as for the key interface. The throat velocity is computed from inlet conditions and throat pressure. The amplifier size can be computed from the definition of the Reynolds number, whose value is known, and the throat viscosity which is computed from Sutherland's formula, as given in Blackburn [36]. For the final stage amplifiers operating at $4P_s$, the calculations are exactly the same except that the inlet pressure is higher. The design Reynolds number is the same. In order to compute the key interface amplifier size in Figure 23, the encoder control flow and pressure are required. The pressure is computed from the amplifier pressure gain and recovery, and the flow by assuming that the control port size is the same as that

of the power jet. Throat velocity can then be computed in the same manner as the power jet velocity. The equations required for the encoder calculation are summarized in block diagram form in Figure 24.

Control Circuitry

The computations involved in computing the energy per cycle for the control circuitry

$$W_3 = 13 P_3 Q_3 T_r + 7(4 P_3) Q_3' T_r \tag{125}$$

are the same as for the encoder as shown in Figure 24, with the exceptions that the number of amplifiers is fixed and no calculations for control pressure and flow are required. The computation block of Figure 24 will not be repeated.

Type Head Rotary Position Drive

In Chapter III it was shown that the final drive configuration which best satisfied the overall design criterion was that shown in Figure 4f. In order to illustrate the effects on machine performance of this configuration which can perform the required task and is compatable with the other necessary typewriter functions. The mechanism used in the computations for this subsystem is shown in Figure 25. Similar schemes for this purpose have been used on commercially manufactured typewriters and teletypes.

The type head is shown mounted on a vertical shaft which is free to move both rotationally and axially in a carriage yoke. The rotation

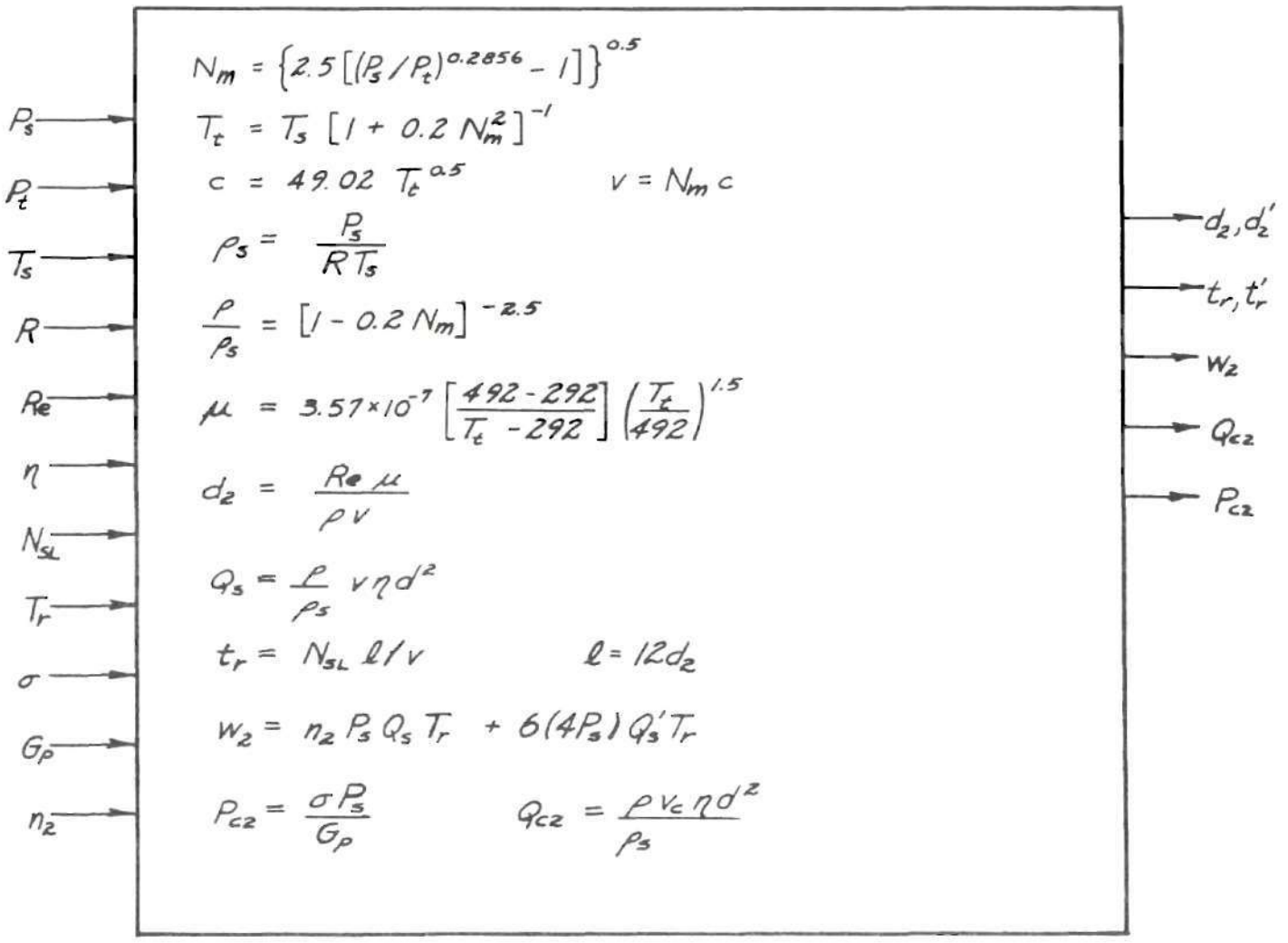

Figure 24. Encoder Computation Block

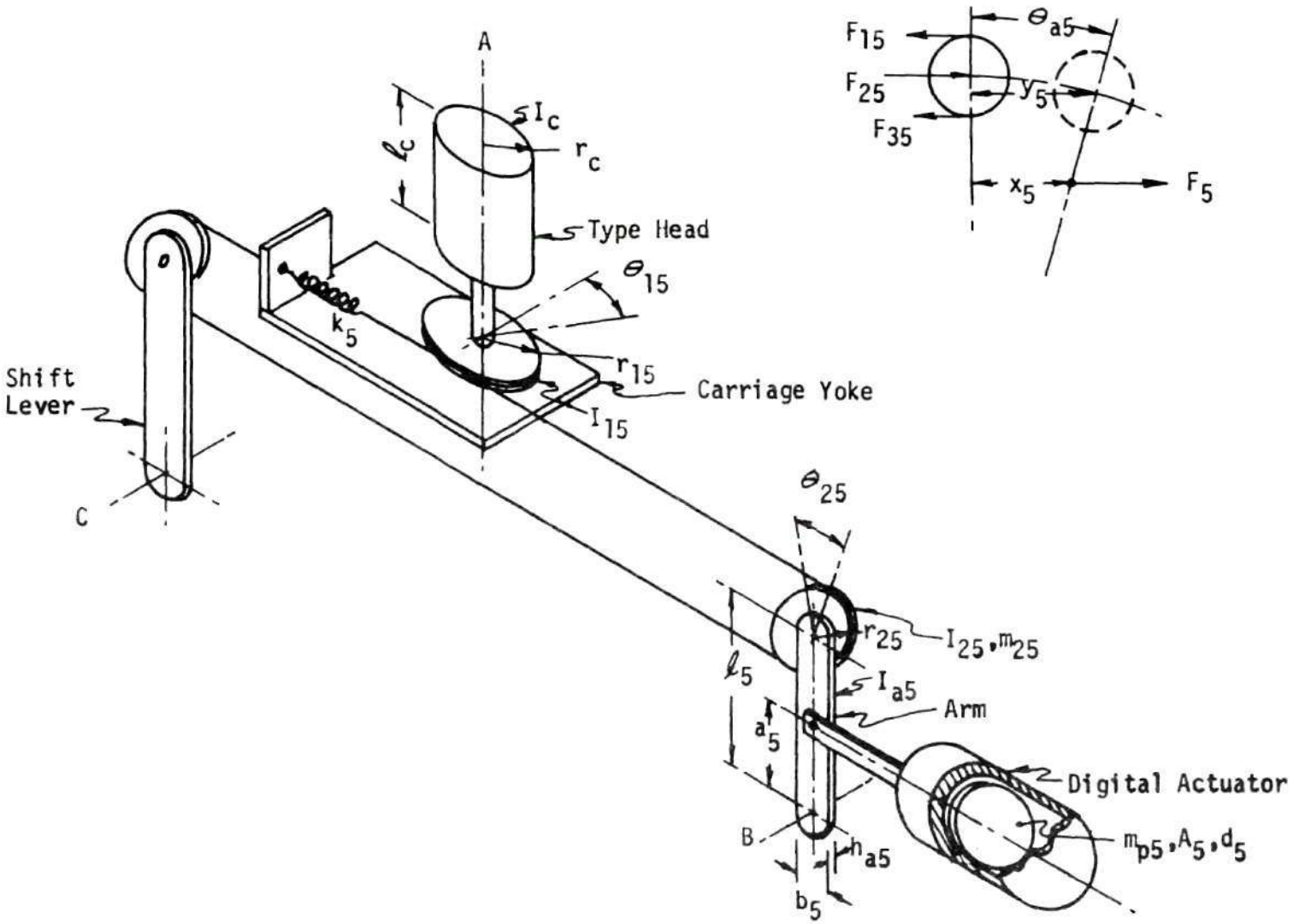

Figure 25. Rotary Drive for Type Head

of the head is due to the digital actuator motion which provides the force F_5 to pivot the arm about center B. The arm is connected to the type head by means of a flexible cable which wraps around the pulley. The spring on the end of the cable returns the head and actuator when pressure is released. Due to the pulleys on the arm and shift lever, tne carriage can be moved along the platen without rotating the head. When the carriage is locked at a print position, motion of the arm rotates the type head. Also shown is the shift lever which, when rotated about axis C by a driver which is not shown, will also rotate the type head in such a way that the digital actuator motion will select upper case characters. Printing is accomplished by rotating the carriage yoke about the cable center line to bring the type head against the platen. Several geometric parameters and forces are defined by Figure 25 for use in deriving an equation of motion for the subsystem.

The general equation of motion for the system of Figure 25 is Equation (79) where m and k are the equivalent mass and spring constant. The actual equation of motion gives expressions for m and k in terms of the parameters of Figure 25 is

$$F = \left[m_{ps} + \frac{\ell_5}{a_5 r_{25}} I_{25} + \left(\frac{2\ell_5}{a_5 r_{15}}\right)^2 (I_c + I_{15}) \right. \tag{126}$$
$$\left. + a_5^{-2}(I_{25} + I_{as} + m_{25}\ell_5^2 + 0.25\, m_{as}\ell_5^2) \right] \ddot{x}_5$$
$$+ \left(\frac{2\ell_5}{a_5}\right)^2 k_5\, x_5$$

This equation is derived from simple force and torque summations to compute force F which is provided by the actuator. It assumes that θ_{a5} is small and the cable is long, as well as that the arm can be treated as a long slender rod to compute I_{a5} about axis B. The bracketed multiplier of $\ddot{x}_5$ then becomes, by comparison with Equation (79), the equivalent mass m, and the bracketed multiplier of x_5 is the equivalent spring constant, k.

The energy per cycle for this subsystem is

$$W_5 = P_5 A_5 x_5(T_5) \tag{127}$$

It is necessary to have values for the three factors of this equation. The pressure, P_5, is arbitrary at present. The piston travel, x(T), is, for a worst-case design, that required to rotate the type head through a full set of characters. This can be found from the geometry as

$$x_5(T) = \frac{a_5 r_{15}}{2 \ell_5} \theta_{15}(T_5) \tag{128}$$

For a given τ and T_r, the time T can be found from Equation (18). Now observe that if the dimensions of the components of Figure 25 are known, then the equivalent mass, m, can be computed from the first term of Equation (126). Then k can be found from Equation (19). However, the mass, m, includes the piston mass, m_{P5}, which reflects the size of piston required to satisfy the forward stroke time, T, for the size components chosen. A more rational procedure would be to first assume the

piston massless and compute the system mass, m. Then from Equation (19), k can be determined. Having found k, the piston area can be found from Equation (80) as

$$A_5 = \frac{x_5(T_5)\,k}{P_s\,[1-\cos\phi]} \tag{129}$$

Then by assuming a geometry for the piston in order to compute the mass, m_{p5}, the system mass can be corrected to include m_{p5}. By iterating this procedure a consistant set of parameters can be found to define the subsystem geometry.

The piston geometry chosen was a cylindrical cup (one end open) with the diameter equal to the length, and wall and end thickness equal.

Having found the proper k, the actual spring constant can be found by combining second term of Equation (126) with Equation (19) to get

$$k_5 = \frac{1}{4}\left[\frac{\pi a_5}{2(\tau-1)\ell_5}\right]^2 \frac{m}{T_5^2} \tag{130}$$

In order to size the diaphragm elements which drive the digital actuator, it is desirable to know the flow through the element. If incompressible flow is assumed, Equation (3) can be combined with the derivative of Equation (80) to give

$$Q_5(T_5) = \frac{P_s A_5^2}{(mk)^{0.5}} \sin\left[\frac{\pi}{2(\tau-1)}\right] \tag{131}$$

which would be the maximum flow for $\tau \geq 2$.

These calculations are summarized as Figure 26, in which the calculations for moments of inertia are omitted but are a necessary first step in the procedure. Two other decisions were necessary with regard to the calculation of m. First, it was assumed that the type head was a hollow cylinder with both ends closed and constant wall thickness. Second, the computed piston mass was multiplied by three to account for the three pistons in the actuator. More about this will be said with regard to the actual computations.

Type Head Axial Position Drive

The general scheme for the axial motion mechanism is very similar to that of the rotary motion. Axial motion is achieved by having circular rack teeth cut on the end of the type head shaft. This rack engages a toothed sector which is rotated to drive the shaft upward. Figure 27 illustrates this mechanism. The toothed sector is rigidly connected to a cable as shown. Motion of the digital actuator rotates the arm about its pivot. Since the cable end is fastened to the carriage yoke, which is held at the print position, the arm motion rotates the sectors and drives the type head. Due to the two cable pulleys, the carriage can be moved along the cable to a new print position. Printing motion would be accomplished by rotating the carriage yoke about the cable center line. This means that the cables causing axial and rotary motion must be approximately colinear. Figures 25 and 27 do not show this relationship explicitly for the sake of clarity in the illustrations, but it is possible to build the mechanisms in this way.

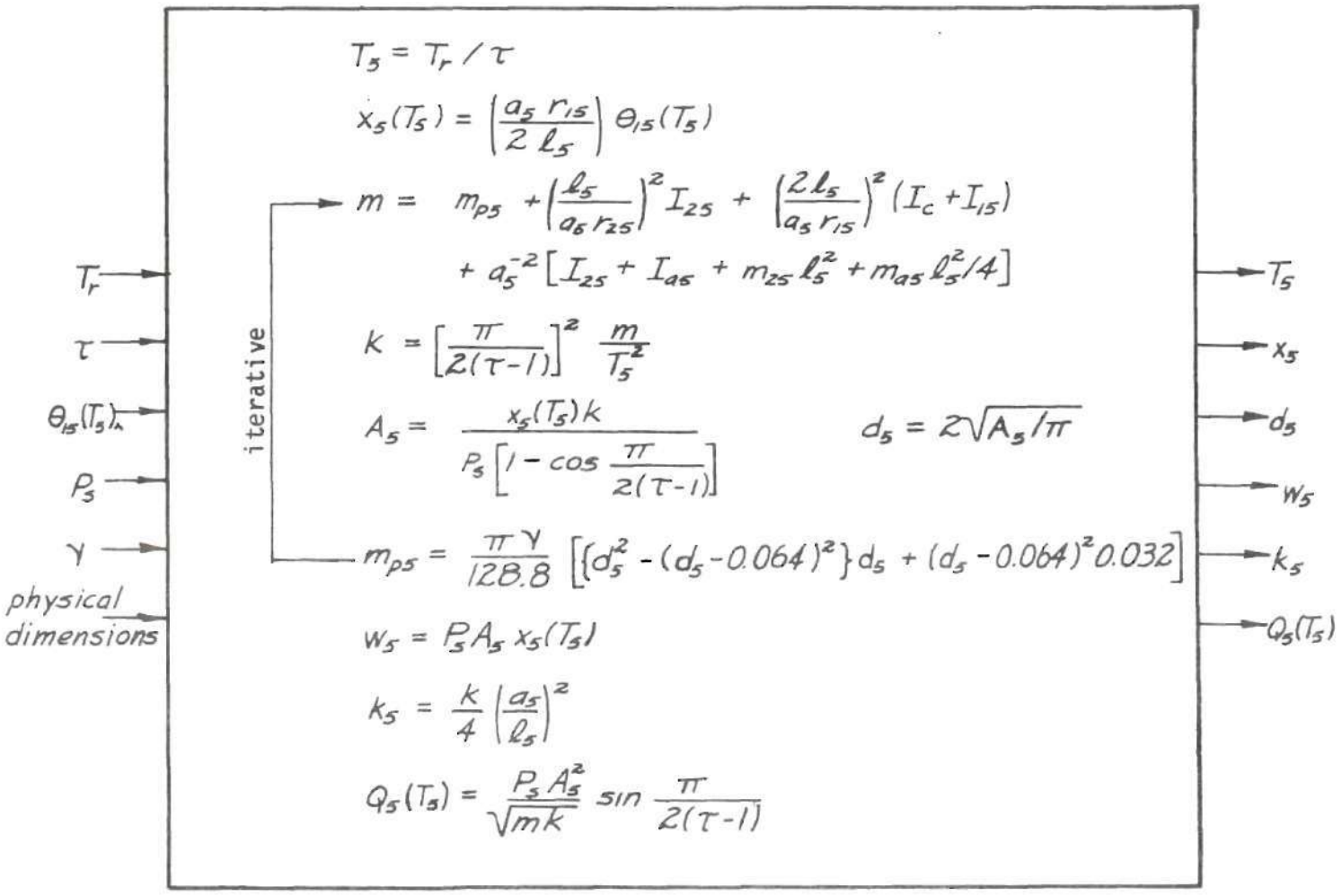

Figure 26. Type Head Rotary Drive Computation Block

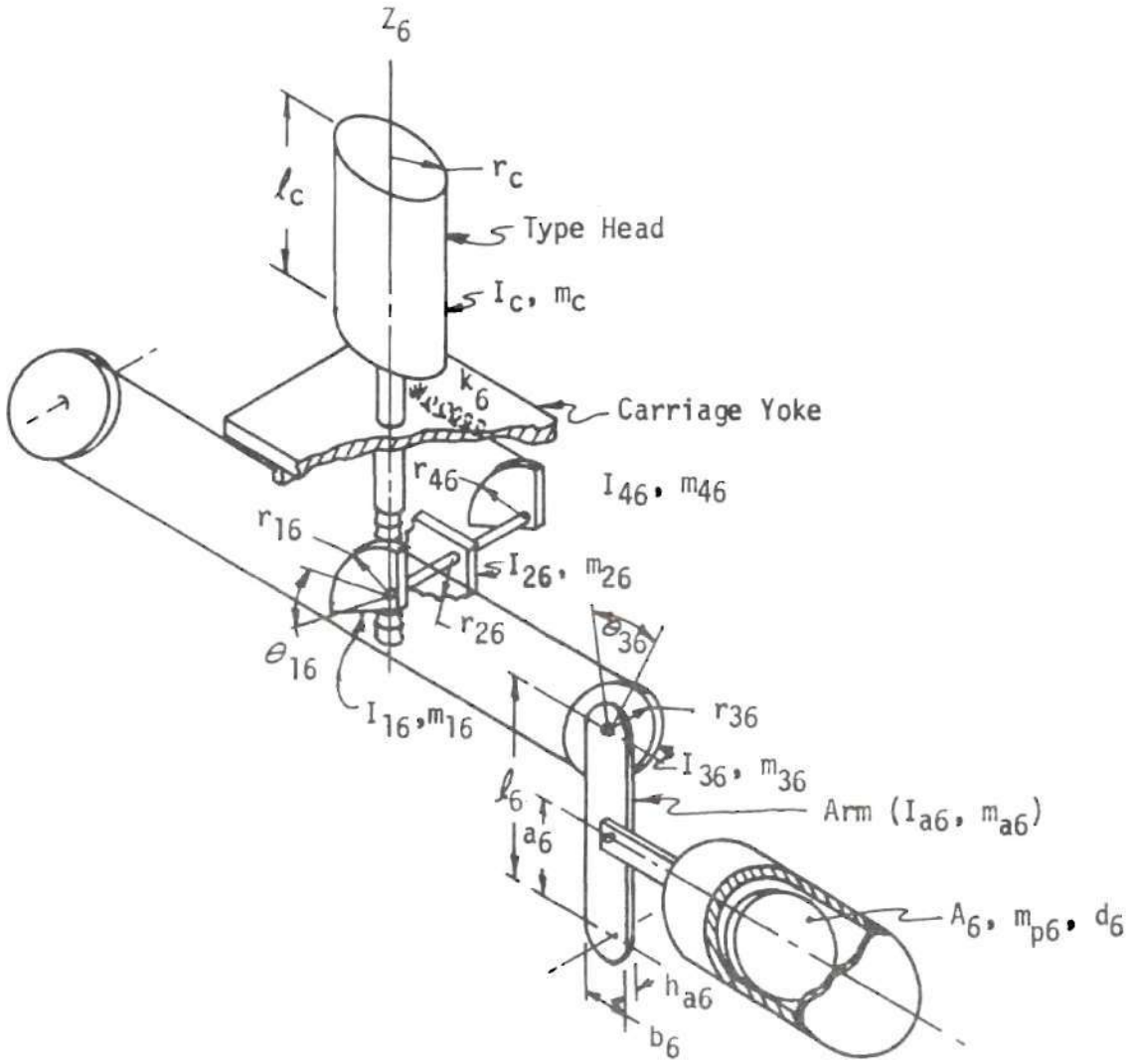

Figure 27. Axial Drive for Type Head

The return motion of the type head and actuator is due to the spring connected by a short cable to the sector assembly and anchored to the carriage yoke.

The development of the computational block for the axial motion follows exactly that for the rotary motion. The resulting equations, with the exception of those for moments of inertia, are given as Figure 28.

Print Drive

A print drive mechanism to accomplish printing which is compatible in function with the rotary and axial type head drives is shown in Figure 29. The carriage supports the type head with its bearings, the rotary motion pulley, and the axial drive cable and gear tooth sectors. The yoke is pivoted about the type head motion cables on a carriage body, which is not shown. The yoke is also supported by the link connected to the collar on the actuator shaft. Printing is accomplished when the piston drives the arm to rotate the actuator shaft. This motion is transmitted to the link and yoke, driving the type head to the platen. The carriage moves to a new print position when the carriage body is driven along the platen. The collar on the actuator shaft is keyed or splined to the shaft to permit axial motion and still provide driving force to the yoke.

Since the carriage yoke serves to combine the actions of the axial and rotary type head drives and the print drive, it is apparent from Figures 25, 27 and 29, that some of the components of these three subsystems, which mount on the yoke, must be dimensionally compatible.

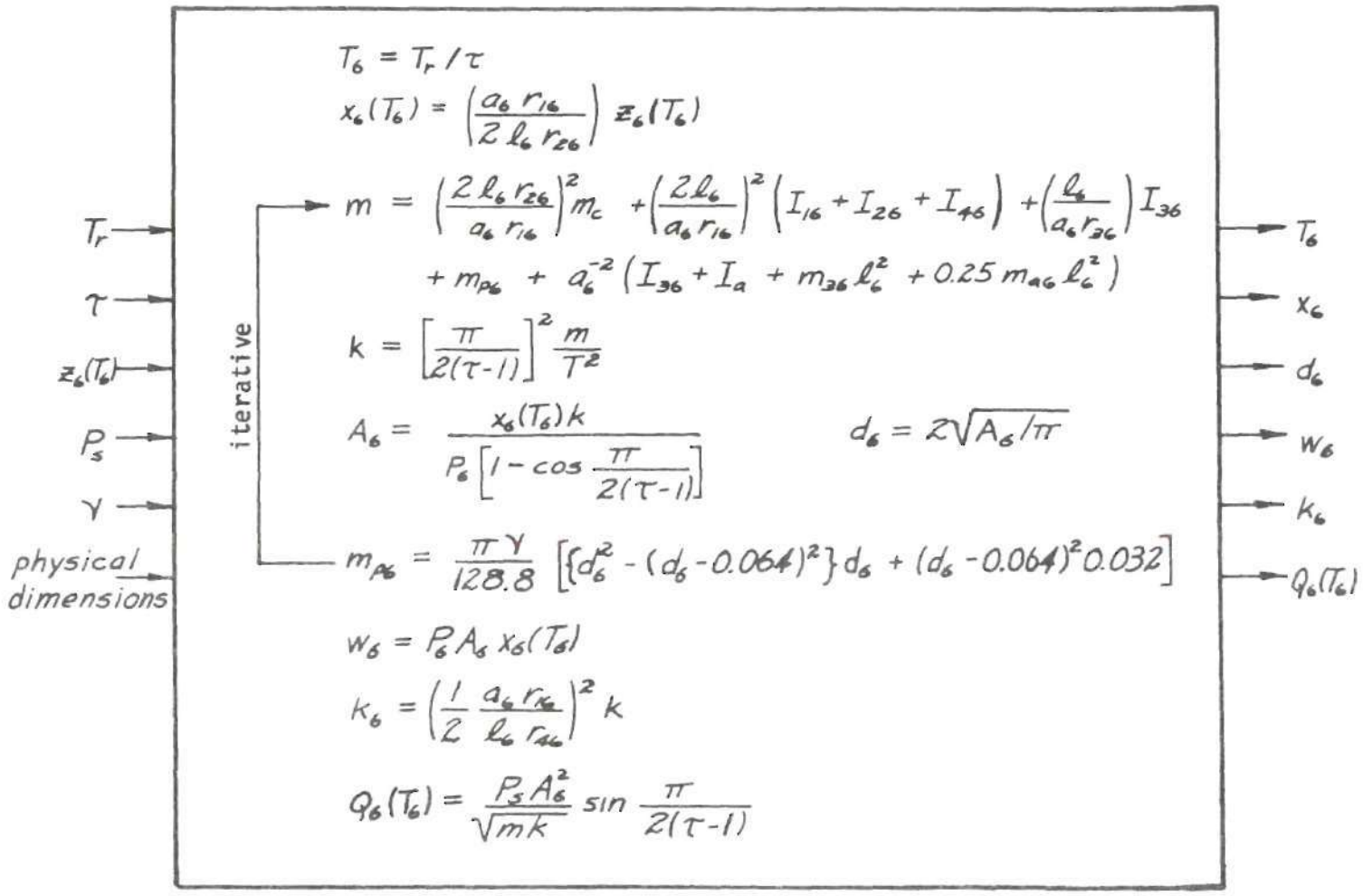

Figure 28. Type Head Axial Drive Computation Block

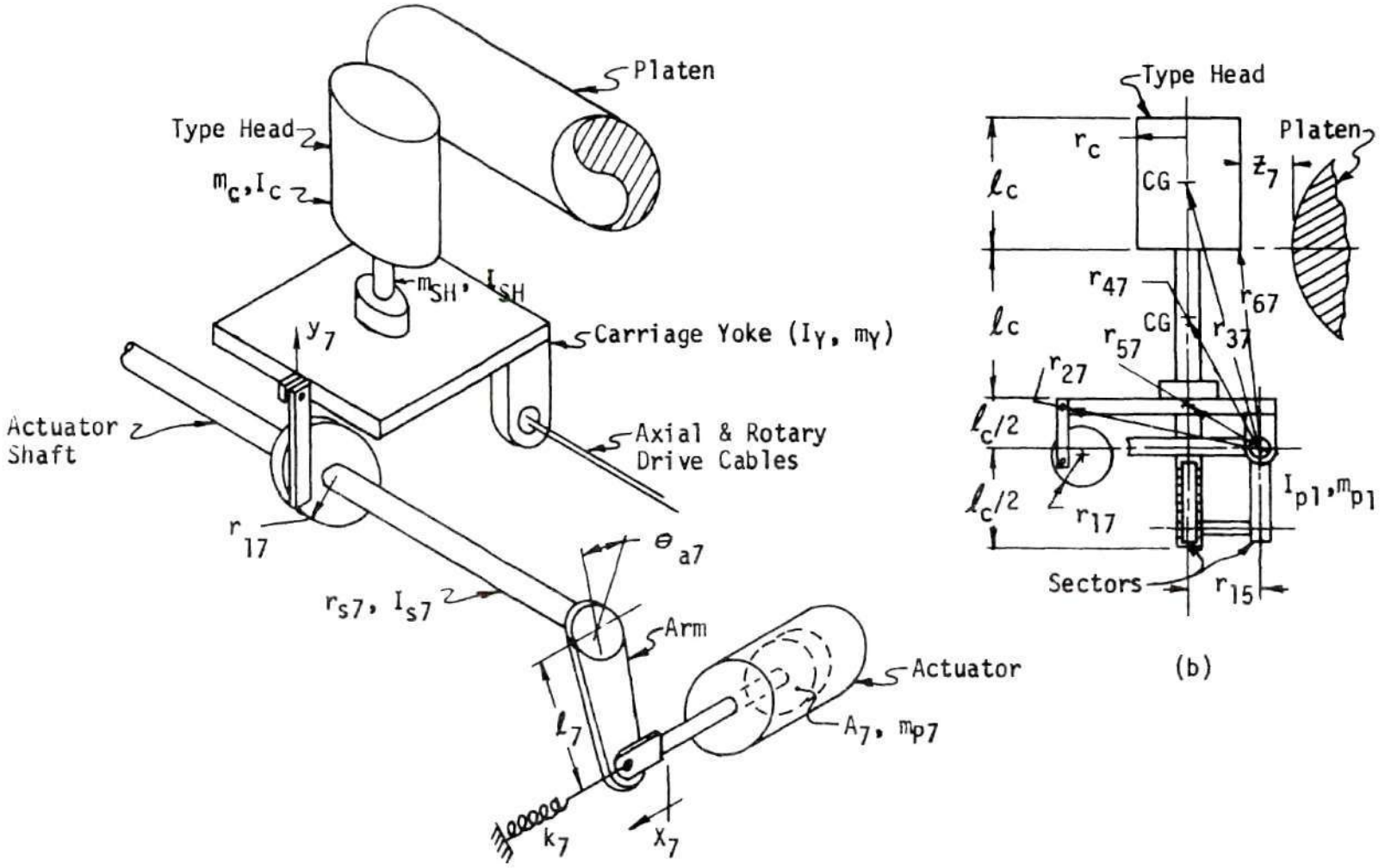

Figure 29. Print Drive Mechanism and Nomenclature

To begin with, the distance from the print head centerline to the yoke pivot line must be r_{15} to prevent changing the type head position by the printing motion. This is seen in the side view of Figure 29b. Also, the cable sector for the axial motion must be tangent to this yoke pivot line and the toothed sector must be mounted on the head centerline. In Figure 29b, the type head is shown in the position of maximum axial motion which results in the maximum moment of inertia for printing. Since this requires a stroke of approximately ℓ_c, the distance from the type head to the yoke is also ℓ_c. Some sketching to approximately the expected dimensions will show that the two vertical distances shown as $\ell_c/2$ are reasonable choices.

In order to compute the moments of inertia required for the equation of motion, it is necessary to determine the radii shown in Figure 29b. It can be seen that with the exceptions of r_{17} and r_{27} these can be computed as functions of r_{15} and ℓ_c, which is simpler than specifying each individual dimension of the component parts, and which also relates the type head dimensions to the radii shown. As a matter of record the relations used in the computations of this chapter are shown in Table 3. In addition to these, it is assumed that x_7 and y_7 are small so that the angles of rotation are small.

As a further preliminary to the equation of motion, note that the moments of inertia required for those components on the yoke are about the cable (pivot) centerline of the yoke. For most of the components this is simply a matter of using readily available formulas and the transfer axis theorem. For the type head itself a formula for the

Table 3. Geometric Relations for Print Drive Subsystem

No.	Dimension	Defining Relation
1.	r_{27}	$2.5r_{15}$
2.	r_{37}	$[r_{15}^2 + (2.5\ell_c)^2]^{1/2}$
3.	r_{47}	$[r_{15}^2 + \ell_c^2]^{1/2}$
4.	r_{57}	$[r_{15}^2 + \ell_c^2/4]^{1/2}$
5.	r_{67}	$[(r_{15} - r_2)^2 + (1.5\ell_c)^2]^{1/2}$
6.	z_7	$\frac{r_{67}r_{17}x_7}{r_{27}\ell_7}$

moment of inertia through a thin shell about an axis through the center of gravity and perpendicular to the axis of symmetry is required. A brief derivation is given in Appendix C.

Having established a geometric basis for the computations, it will be remembered that the energy per cycle for the print subsystem was determined in Equation (84) as

$$w_7 = [\epsilon(T)]^2 \frac{1-\cos\phi}{\sin^2\phi}$$

where $\epsilon(T)$ is a known constant. Since for a given τ, ϕ is known, w_7 is fixed for this subsystem by τ. It remains to determine the size actuator needed, the spring constant, and the value of $Z_7(T)$, which cannot be chosen independently since the final velocity of the type head at impact is fixed.

By writing the equation of motion, the equivalent mass is determined as

$$m = \left(\frac{r_{17}}{2.5\ell_7 r_{15}}\right)^2 I_c + m_c r_{37}^2 + I_{SH} + m_{SH} r_{47}^2 + I_Y + m_Y r_{57}^2 \qquad (132)$$
$$+ I_{pl} + m_{pl} r_{15}^2 + \ell_7^{-2}\left(I_s + I_a + 0.25 m_a \ell_7^2\right) + m_{p7}$$

This derivation neglects the effect of the axial motion sectors which are light in weight and close to the axis of rotation. The equivalent spring constant determined from the equation of motion is

$$k = k_7 \qquad (133)$$

In order to compute a consistent set of parameters, an iteration for m_{p7} can be carried out as in the rotary and axial drives. This requires determination of the actuator piston size. The actual equation of motion from which (132) and (133) are found has the form

$$m\ddot{x} + kx = P_s A - m'g\frac{r_{17}}{2.5\ell_7} \qquad (134)$$

where

$$m' = m_c + m_{SH} + m_Y + m_{pl} \qquad (135)$$

This additional force due to the weight of the components on the yoke has the effect of increasing the piston size, as can be seen by comparing the area determined by the solution of Equation (134)

$$A = \frac{x_7(T_7)\,k_7}{P_s(1-\cos\phi)} + \frac{m'g\,r_{17}}{2.5\,\ell_7 P_s} \tag{136}$$

with that determined from the solution of the general Equation (79), which results in the form of Equation (129). However, in this subsystem $x_7(T_7)$ is not an input and A_7 is computed by combining Equation (136) with

$$w_7 = \left[P_s A_7 - \frac{m'g\,r_{17}}{2.5\,\ell_7}\right] x_7(T_7) \tag{137}$$

and solving for A_7. This results in a quadratic in A and the result is

$$A_7 = \frac{m'g\,r_{17}}{2.5 P_s \ell_7} + \left[\frac{w_7 k}{P_s^2(1-\cos\phi)}\right]^{0.5} \tag{138}$$

The equivalent spring constant is determined by

$$k = \phi^2 m T^{-2} \tag{139}$$

which then allows Equation (136) to be solved for A and the piston diameter. Using the same piston geometry as in the rotary and axial motions the piston mass m_{p7} can be found. Then having found a consistent set of parameters, the distance $x_7(T_7)$ can be found by

rearranging Equation (136), and from this value and the geometrical relations of Table 3, Z_7 can be found.

If it is desirable to drive the carriage yoke over only a part of the print stroke, then an adjustment in $\epsilon(T)$ is required. This mode of operation might be helpful in providing uniformity of printing since the type head would strike the platen in "free flight" and be able to rebound with less interference. In such a case the kinetic energy achieved at impact would be

$$KE'(T_7) = 0.5 I' [\dot{\theta}_Y(T_7)]^2 \tag{140}$$

where I' is the term in brackets in Equation (132) and represents the yoke and components mounted on it. Considering Equations (132) and (7), it can be shown that

$$KE(T_7) = KE'(T_7) \frac{m}{\left(\frac{r_{17}}{2.5 \ell_7 r_{15}}\right)^2 I'} \tag{141}$$

and from Equation (10)

$$\epsilon(T_7) = \left[2KE'(T_7) \frac{m}{\left(\frac{r_{17}}{2.5 \ell_7 r_{15}}\right)^2 I'} \right]^{0.5} \tag{142}$$

The value of $KE'(T_7)$ is the previously specified 10^5 ergs.

The computations, then, which represent the print subsystem are

shown in Figure 30, and are in addition to Table 3 and the moment of inertia calculations.

Diaphragm Amplifiers

The original assumption with respect to the diaphragm amplifiers for the final drive to the actuator pistons was that they had neglible pressure drop over the ridge. In order to determine an approximate size to meet this condition it is necessary to know the flow rate. For a worst-case design, the maximum flow rate for each of the axial, rotary and print actuators was determined. The largest of these three flows then determines the size if the amplifiers are standardized to a single size.

The operating characteristics of the diaphragm devices have been described mathematically by Jensen [17]. If an amplifier with a round cavity and straight ridge is chosen, then Jensen shows that

$$R_o = \sqrt{\frac{\rho}{2}}\ \frac{3N_o}{P_s r_o^3 C}\left[1 - \frac{\xi}{r_o^2}\right]^{-3/2} \tag{143}$$

where R_0 is the ridge resistance defined by

$$R_o = \frac{1}{CA}\sqrt{\frac{\rho}{2}} = \frac{\Delta P^{0.5}}{Q} \tag{144}$$

at zero control pressure. The quantity N_0 is the initial tension in the diaphragm. Jensen found that 0.1 lb/in. was a reasonable value for N_0 when using 0.002 inch thick polyurethane film as a diaphragm. The quantity ξ is a geometric parameter determined from the ridge

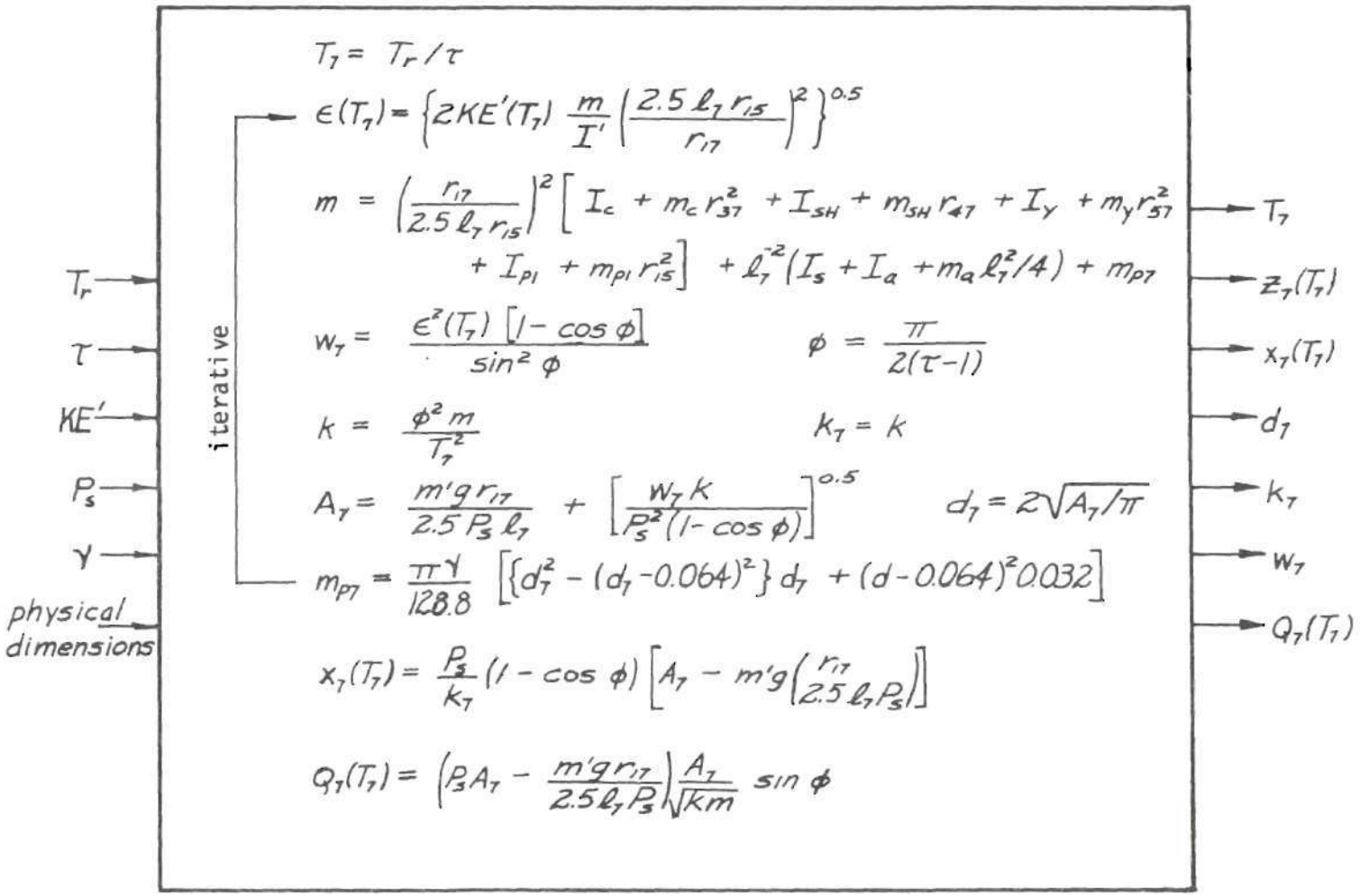

Figure 30. Print Drive Computational Block

position. If the switch-open point of the amplifier occurs at a control pressure of $P_s/3$, the value of ξ is approximately $0.259r_d$. In order to determine a value for R_o, it was assumed that the pressure drop in Equation (144) was one per cent of P_s and Q was the maximum for any subsystem actuator. Equation (143) can then be solved for r_d, which is the basic amplifier dimension.

Carriage Motion

The function of the carriage is to position the type head at predetermined print positions along the platen. Carriage movement takes place when any character is typed, when the space bar is depressed, when the tab key or back-space key is actuated, or when the carriage must be returned to the beginning of a line. The position of the carriage in most typewriters is determined by a rack and pinion arrangement in conjunction with an escapement mechanism. Because of the required accuracy and long total travel of the carriage, this general arrangement or an adaptation of it will be retained.

Energy to move the carriage can be supplied in several ways. The common way is to drive the carriage forward after each print stroke, or for tabulation, with a spiral power spring or constant force Negator* spring. Return power is provided manually or electrically. Conversely, it would be possible to drive the carriage forward to space or tab by pneumatic power (in the case of fluidic typewriters) and return and

---

*Hunter Spring Company

back space with spring energy. From a power minimization standpoint there is no difference. It would also be possible to eliminate the spring and use pneumatic power in both directions. This latter means has some disadvantage in that an additional pneumatic actuator is required which is probably more costly than the spring. Of the former two, there is no difference in components or complexity and the more common power-return was chosen.

In the previous sections describing the type head motion drives and printing drive, it is obvious that the carriage would consist only of a moving frame, the yoke and type head along with the associated drive components (see Figures 25, 27, 29), and the escapement mechanism (not shown). In actuality, this may not be true since it is possible to mount the pneumatic actuators and diaphragm amplifiers on the carriage body and connect with flexible control tubing. This will depend on their size as required for dynamic performance and the dynamic performance required of the carriage. The mechanisms shown in Figures 25, 27, and 29 allow consideration of the possibility that the actuators must be mounted off-carriage. Mounting on the carriage would then be a simplification, mechanically and computationally, which is easy to formulate.

A workable scheme for driving the carriage in both directions is shown in Figure 31. If it is assumed that the carriage moves with neglible friction and the spring is of the constant force type, then the equation of motion is

$$m\ddot{x}_B = F_k \tag{145}$$

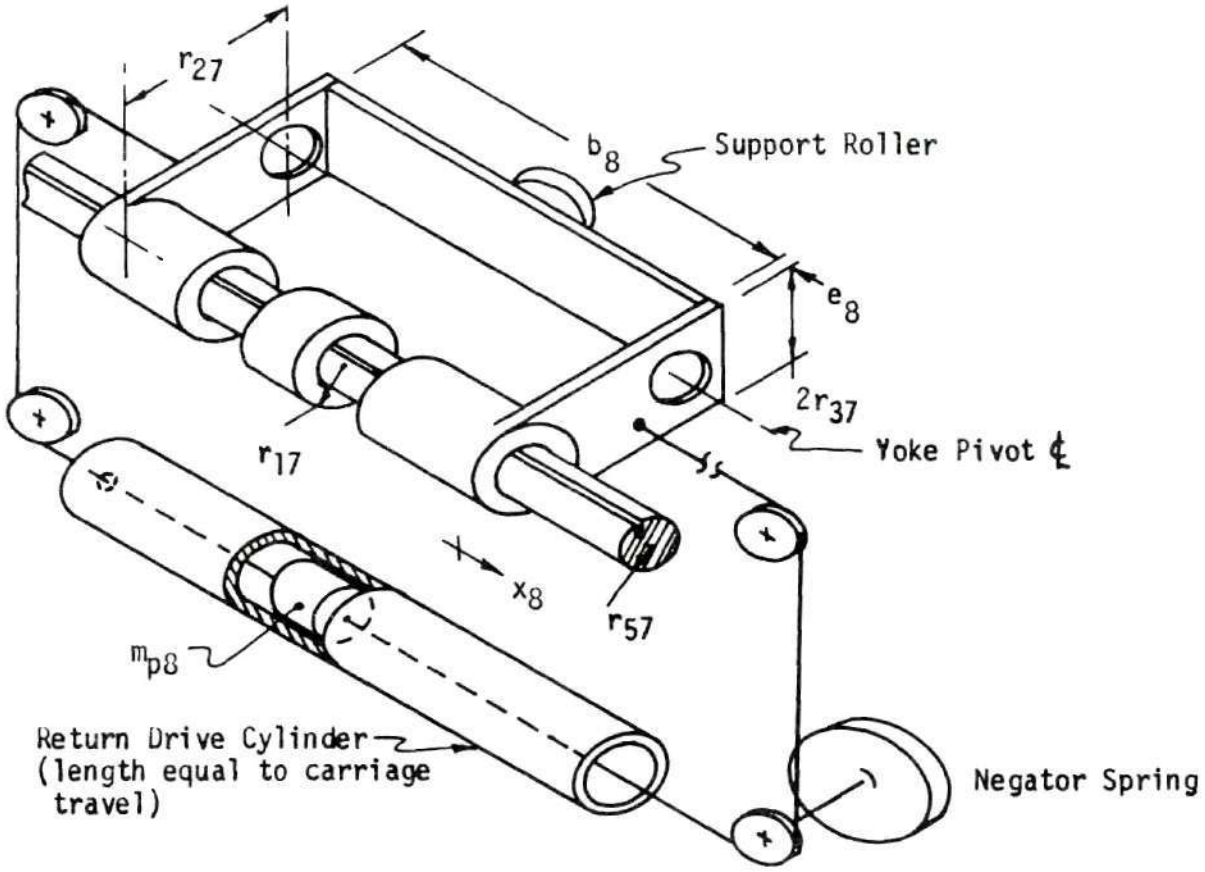

Figure 31. Carriage Drive Mechanism

where F_k is the spring force. The solution can be written ($t = T_8$)

$$F_k = \frac{2m}{T_8^2} x_8(T_8) \tag{146}$$

Since this describes the forward motion for each space after printing, the value of $x_8(T_8)$ is one print space. A common value is 0.1 inch (10 characters per inch). The value of T_8 is the same as T_r for the other subsystems if the time required to actuate the escapement is neglected. The remaining quantity needed to determine the spring force is the equivalent mass, m. This includes the carriage body, the yoke and all parts mounted on it, and the return piston (the moment of inertia of the pulleys is neglected.) If the type head motion digital actuators or print actuator are placed on the carriage, their mass would be included. To be consistent with the previous subsystem definitions, these are assumed not to be on the carriage until some numerical data has been generated.

On the carriage return let the equation of motion be

$$P_s A_8 = F_k + m\ddot{y}_8 \tag{147}$$

where y is the motion co-ordinate. If this equation is solved and substitution made from (146) for F_k, the result is

$$y_8(T_{CR}) = \left[\frac{P_s A_8}{2m} - \frac{x_8(T_8)}{T_8^2}\right] T_{CR}^2 \tag{148}$$

Since for a worst case design $y_8(T_{CR})$ is the maximum printed line length (e.g., 10 inches), the only unknowns in Equation (148) are A_8 and m. Since m is a function of A_8 through the piston mass, the same iterative procedure as before will yield a consistent set of values.

The criterion of minimum power consumption is not applicable to this subsystem in quite the same way as for the others since the forward motion in printing is due to a spring in which energy was previously stored. It is desirable to reduce power consumption for the carriage mechanism, but this can only be done by reducing the mass and increasing return time, both of which have limitations. Moreover, this subsystem uses power when the other output devices are not being used, so that as long as it does not increase the required power over that already available, its power level need not be minimized. However, the amount of power or energy used by the carriage motion per print cycle can be computed. For the energy per cycle the equation is

$$w_8 = F_K x_8(T_8) \tag{149}$$

Computation of w_8 allows including the effect of carriage power in the overall system.

The equations used in the computations for this subsystem are summarized in Figure 32.

Total System Power

In order to have a measure of the total system power consumption for selection of one set of design values over another, the power

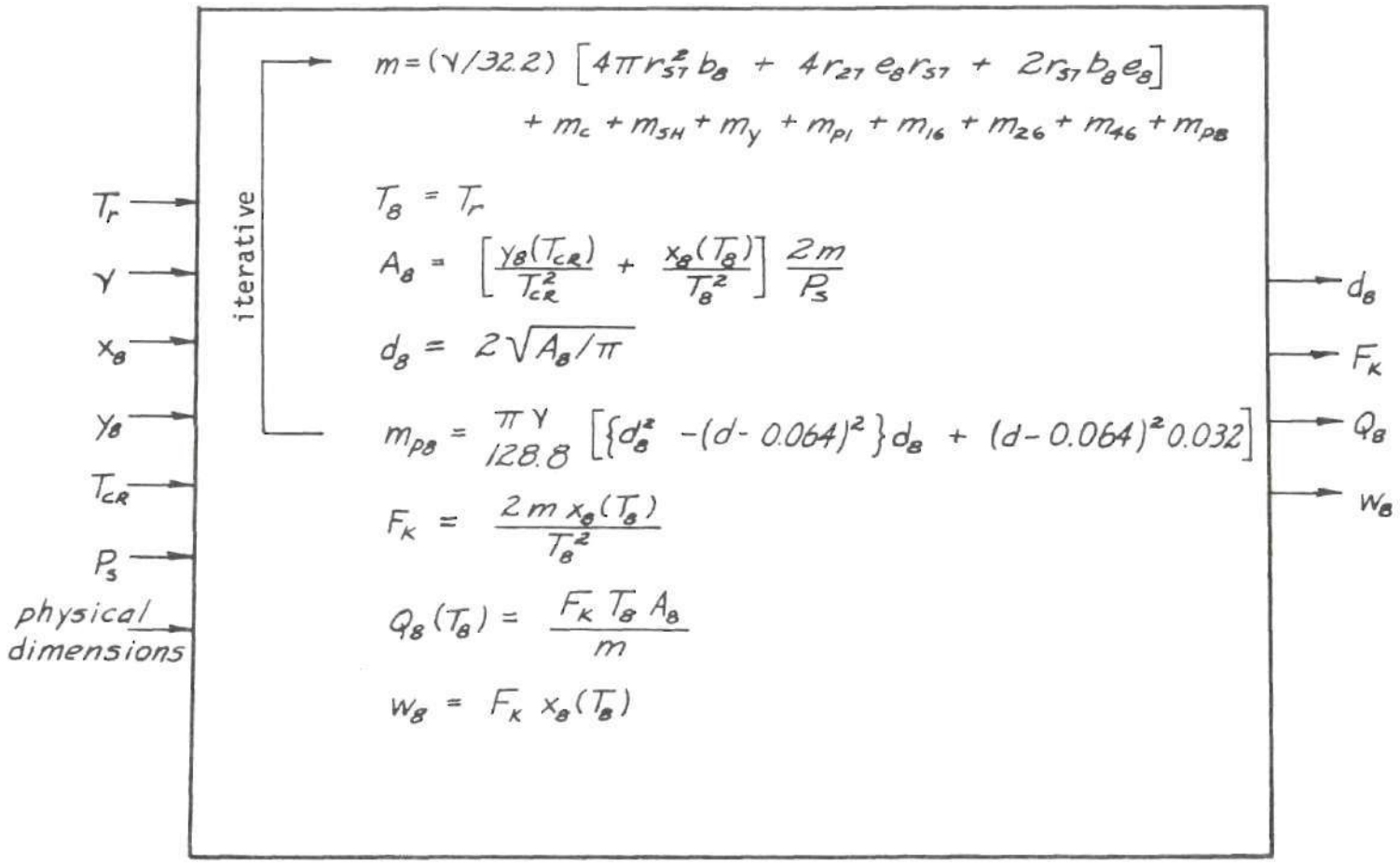

Figure 32. Carriage Drive Computational Block

consumption was computed from

$$\dot{W} = T_r^{-1} \sum_{i}^{8} W_i \qquad (150)$$

This is the average power level which is indicative of the load on the pneumatic power supply.

Overall System Design

The calculations denoted by the equations of the computational blocks of the previous sections, along with individual component mass and moment of inertia computations, were combined into a computer program to facilitate evaluation of various parameter combinations in terms of the overall design criteria of maximum speed and minimum power consumption. The actual program will not be given since it is straightforward and simply incorporates the computational blocks. A flow diagram for the program is given in Figure 33. In this flow diagram the iterative calculations for piston size within the blocks are not shown. Since the operating pressure and typing speed (characters/second) have an effect on the overall machine in terms of amplifier power consumption and actuator size and power, they were chosen as the basic variables for iteration in the program. The effect of other parameters was studied by changing the data input. The dashed lines of Figure 33 simply illustrate the dependence of the diaphragm amplifiers and carriage motion on previous subsystems and do not represent program flow. The outputs of the program were the quantities shown as outputs of the computational blocks. In addition the system power level,

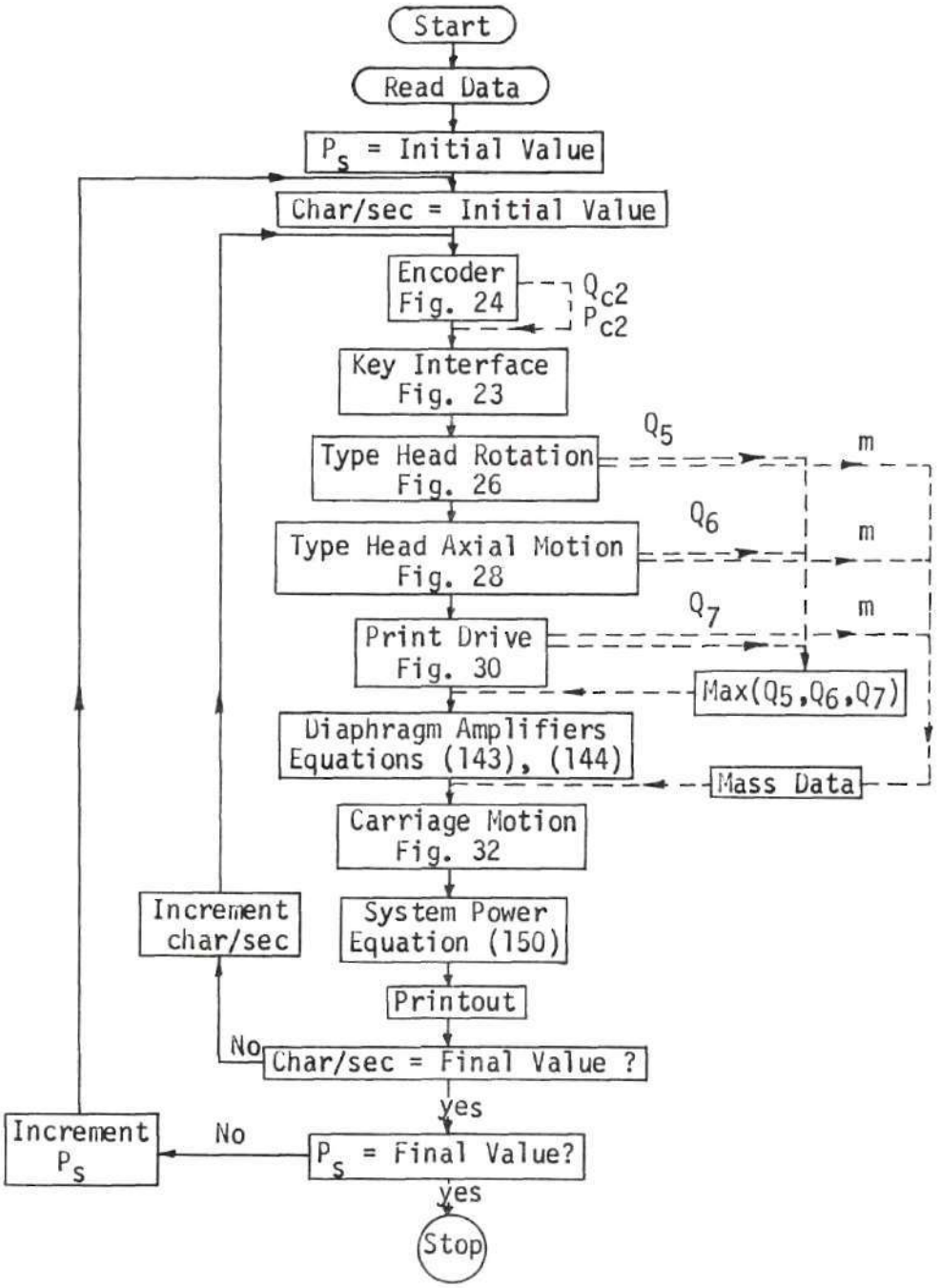

Figure 33. Computer Program Flow Diagram

Equation (150), certain maximum flow rates, and the values of each term in the equivalent mass equations of the rotary, axial, print and carriage subsystems were printed out. These latter values allowed insight into means of improving performance or reducing power consumption.

In order to use the program an initial set of input parameters was chosen and then modified in accordance with the results of the computation in an attempt to either improve performance or reduce size. The initial set of input dimensions was chosen so that the components could conceivably be put in a volume approaching a commercial office typewriter and would have sufficient structural strength.

The type head dimensions were based on a 7 X 7 matrix allowing a 0.2 inch square space for each character. Other parameters are chosen to satisfy relationships which have been discussed previously in the developments of the various subsystems. The initial parameters are listed in Table 4. Complete sets of parameters will not be listed hereafter, but rather changes in the set will be noted.

The fluid amplifier size for the encoder and control circuit as characterized by the power nozzle throat width, d, varies with supply pressure and Reynolds number. Key interface amplifier size is determined from load requirements. Figure 34 shows the range of sizes for various values of P_s and Re. The range of size shown from 0.001 inch to 0.035 inch or more covers many commercially available devices, the smaller sizes (0.010") being close to the limit of practical fabrication. Size decreases with Re, and amplifiers corresponding to

Table 4. Initial Input Data to Computer Program

Overall System:

Recovery = σ = 0.25	Strouhal No. = N_{SL} = 15
Aspect ratio = η = 1.0	Supply flow temp = T_s = 70°F
Reynolds No. = Re = 2500	Supply pressure = P_s = 1.0 psig
Characters/sec. = $\frac{1}{T_r}$ = 5	Specific wt. = γ = 0.25 lb/in^3

Interface: Number of amplifiers = n_1 = 49

Encoder: Number of amplifiers = n_2 = 34

Type Head:

Outside radius = r_c = .450"	End thickness = 0.125"
Inside radius = r_i = .325"	Shaft radius = 0.125"
Length = ℓ_c = 1.400"	Shaft length = 3.4"

Rotation:

Pulley radius = r_{15} = 0.5"	Arm length = ℓ_5 = 3.0"
Pulley radius = r_{25} = 0.5"	Arm distance = a_5 = 2.0"
Pulley thickness = 0.125"	Arm width = b_5 = 0.5"
Max. angle = $\theta_{15}(T_5)$ = 2.69 rad.	Arm thickness = h_{a5} = 0.125"
Time ratio = τ_5 = 3.0	

Axial:

Sector radius = r_{16} = 1.0"	Arm width = b_6 = 0.5"
Sector radius = r_{26} = 1.0"	Arm thickness = h_{a6} = 0.125"
Sector radius = r_{46} = 0.5"	Max. axial motion = $z_6(T_6)$ = 1.2"
Sector thickness = 0.125	Time Ratio = τ_6 = 3.0

Table 4. Continued

Arm length = ℓ_6 = 3.0"	
Arm distance = a_6 = 2.0"	
Print:	
Yoke length = b_8 = 2.5"	Kinetic energy = KE = 0.088 in.lb.
Yoke width = 0.75"	Collar radius = r_{17} = 0.25"
Yoke thickness = 0.125"	Time ratio = τ_7 = 2.5
Arm length = ℓ_7 = 3.0"	Actuator shaft length = 12"
Arm width = 0.5"	Actuator shaft radius = r_{57} = 0.25"
Arm thickness = 0.125"	
Diaphragm amplifiers:	
Flow coefficient = C = 0.8	Initial tension = N_o = 0.1 lb/in.
Carriage:	
Return time = T_{cr} = 1 sec.	Support thickness = e_8 = 0.125"

Re = 1000 lie in a range of difficult fabrication. Size also decreases with pressure. The curves show sizes above P_s = 3 psig although this is the approximate limiting pressure if the final stages operate at $4P_s$. Note that sizes for the final stages are plotted versus P_s and not $4P_s$, which is their supply pressure.

Power consumption and amplifier response time for a range of design Reynolds numbers and two pressure levels are shown in Figure 35. These data are for the encoder only. Both power consumption and response time increase with Reynolds number. Response time increases because the increasing Reynolds number forces a larger d and the fixed amplifier

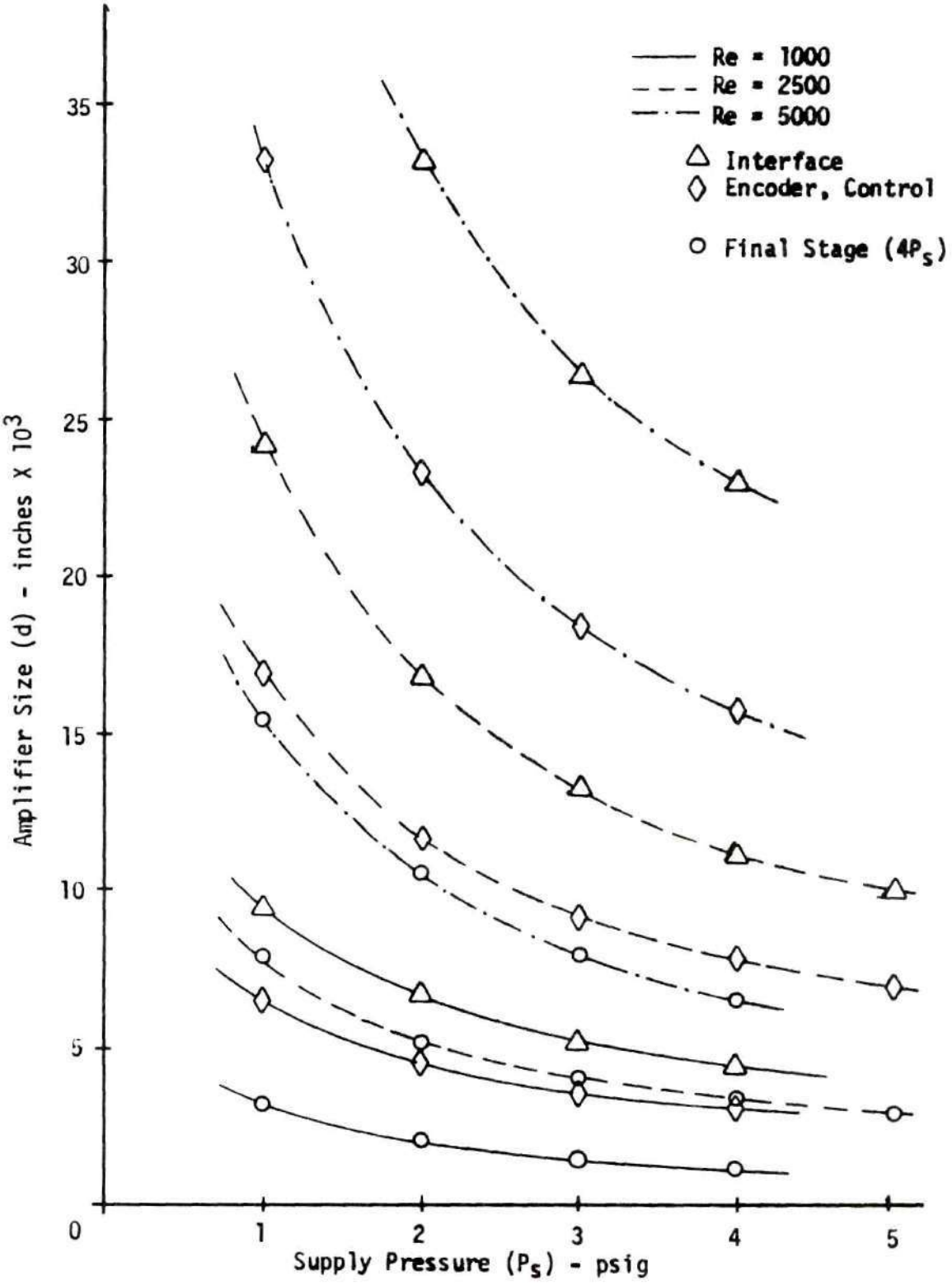

Figure 34. Amplifier Size

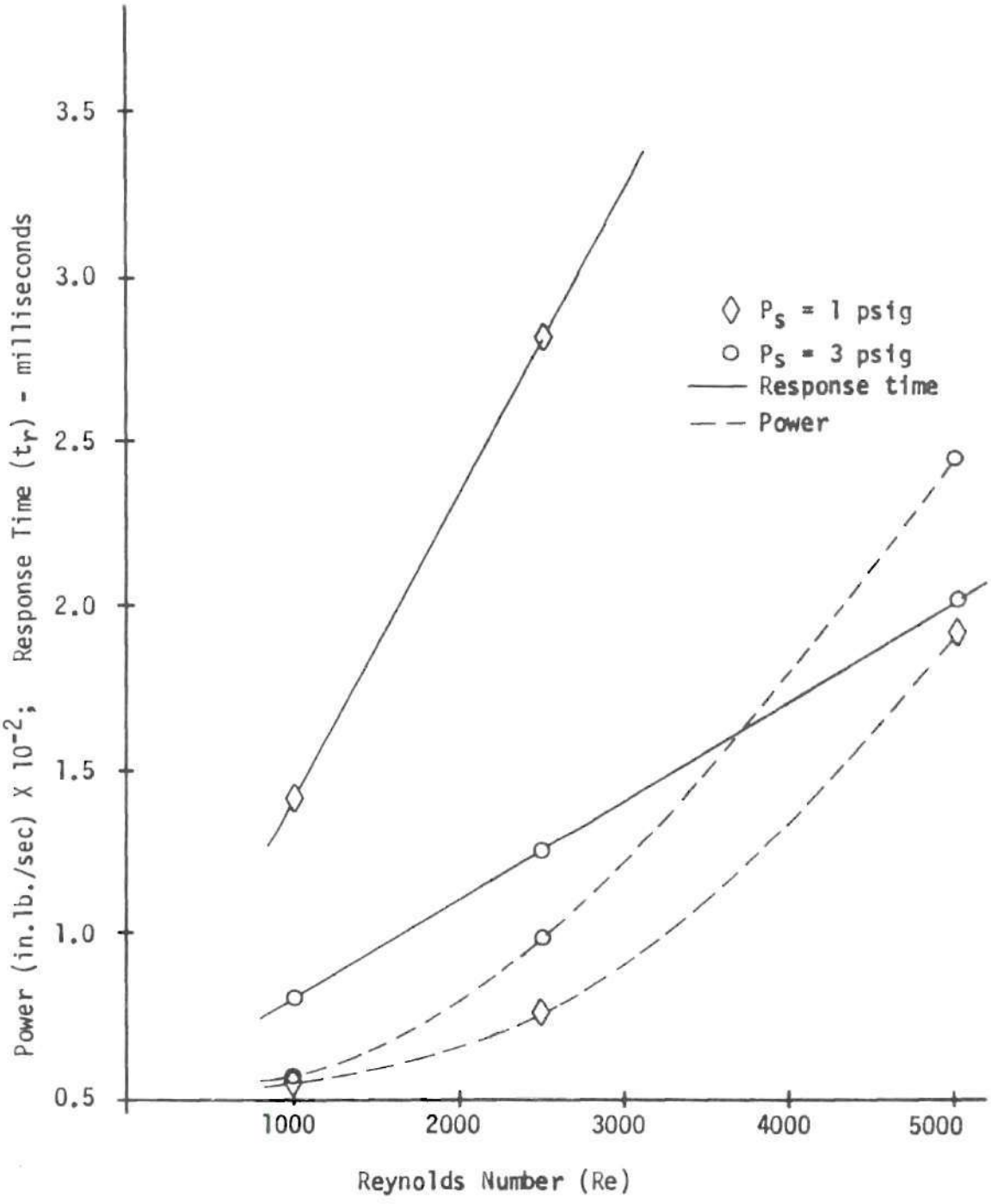

Figure 35. Amplifier Power and Response Time for Encoder Elements

geometry then requires a longer transmission path. Response time decreases with pressure because of the higher nozzle velocity. At low supply pressures (≤1 psig) and high Re the response time becomes significant (>3 msec). Power consumption is shown to increase with both Reynolds number and supply pressure.

Continuing to use the initial input data of Table 4, the overall system power consumption for various pressures and typing speeds is shown in Figure 36. As expected, the power increases with increasing typing speed due to the power required by the actuators. The variation of power with pressure depends on the typing speed. At low speeds, the power rises as pressure increases, but at higher speed the power consumption decreases. This is explained by the fact that the power consumption of the fluidic amplifiers increases with increasing pressure (Figure 35) and is not a function of typing speed, whereas the actuator power consumption decreases with increasing pressure. The curve for 15 characters/second actually shows a minimum. Note that the power consumption is relatively small, being on the order of 0.1 horsepower at 20 characters per second. The steep rise in the curves at lower pressure is indicative of the fact that iteration for piston size did not converge for some cases of low pressure and high typing speeds.

The specific weight, γ , used in computing Figure 36 was 0.25 (Table 4). This corresponds roughly to steels and zinc casting alloys which might be used. Since some of the power is used to accelerate the moving parts, the reduction of γ should reduce the power. A value of γ = 0.1 corresponds to aluminum alloys and is a rough approximation to some lighter metals and composites. The curves of Figure 37 show

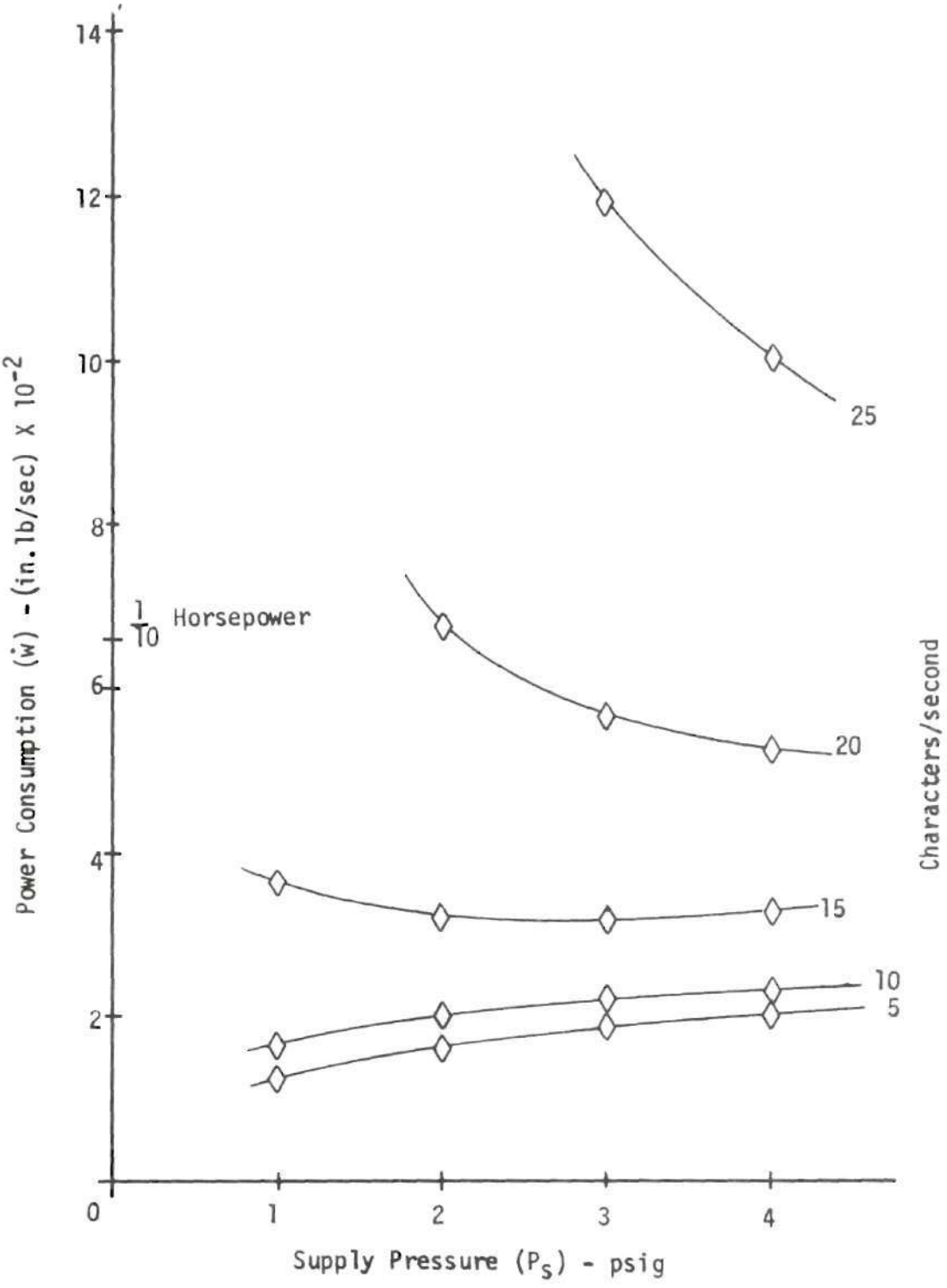

Figure 36. System Power Consumption, $\gamma = 0.25$

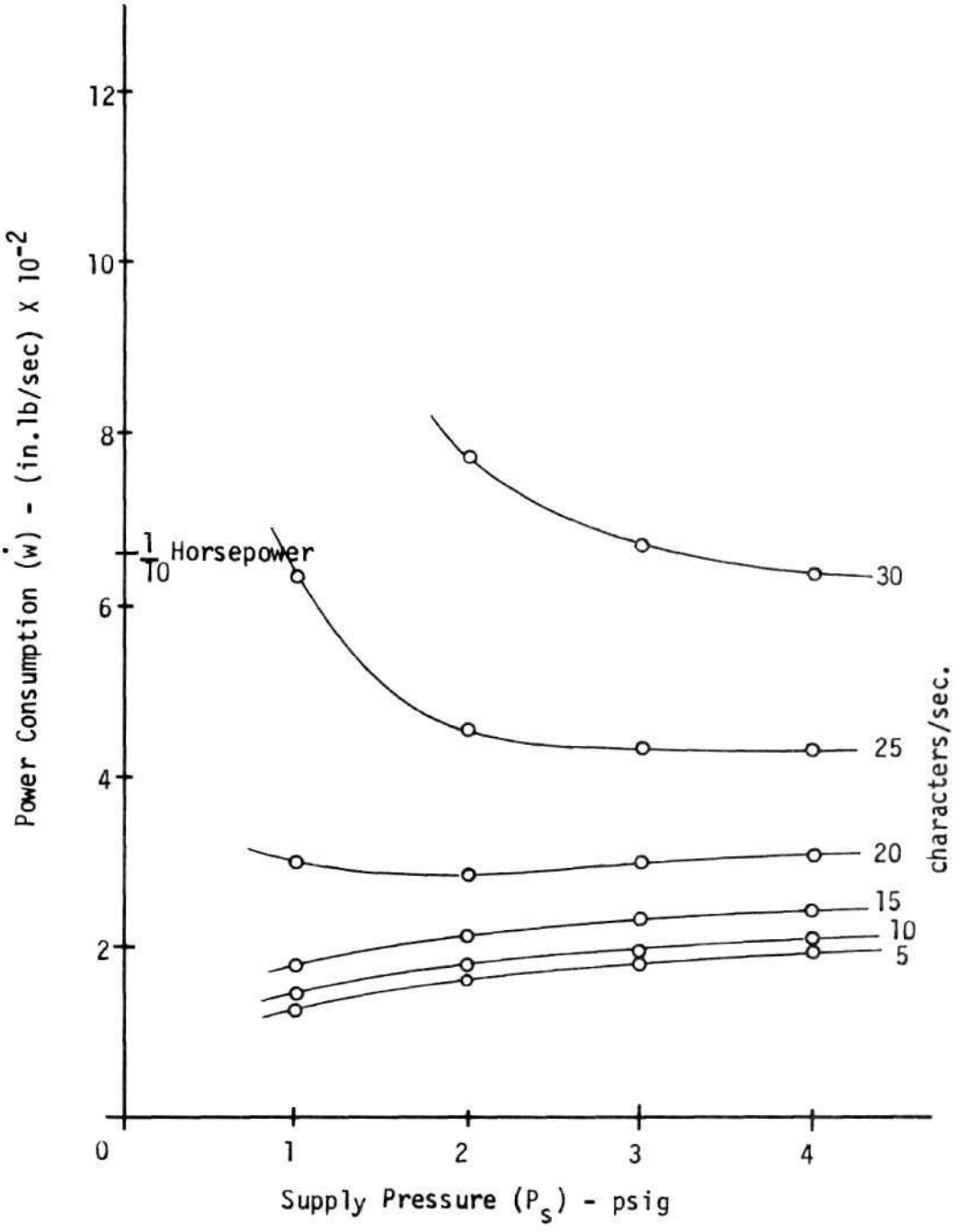

Figure 37. System Power Consumption, $\gamma = 0.1$

a reduction in power of about 40 per cent at 20 characters per second. The reduction is greater at higher speeds and very slight at five or ten characters per second. This points out that materials of construction are important for high speeds.

A more quantitative picture of the energy distribution among the various subsystems which improves understanding of Figures 36 and 37 is given in Figure 38. Energy per print cycle is shown for each subsystem for typing speeds from five to thirty characters per second. For the fluidic portions, the power is constant, and so the energy per cycle decreases with speed. For the positioning subsystems, the energy increases with increasing speed since the mass driven is constant or increasing slightly and the acceleration increases with increasing speed. The increase in energy per cycle for the printing subsystem is almost constant since it is designed on the basis of final kinetic energy.

It is of interest to observe the magnitudes of the energy for each subsystem. At low speeds, the fluidic devices use the largest part of the energy, half or more. At high speed, the positioning subsystems require half or more of the total. In either case, the printing energy is less than 10 per cent and that attributable to the carriage motion is neglibible. The key interface amplifiers account for a large fraction at any speed (16 - 60 per cent). It would be expected, then, that further reductions in power consumption would most likely have to come from the rotation or axial position drives or from eliminating the interface amplifiers. It can also be seen that, depending on the size of the pneumatic actuators, the carriage configuration might include the

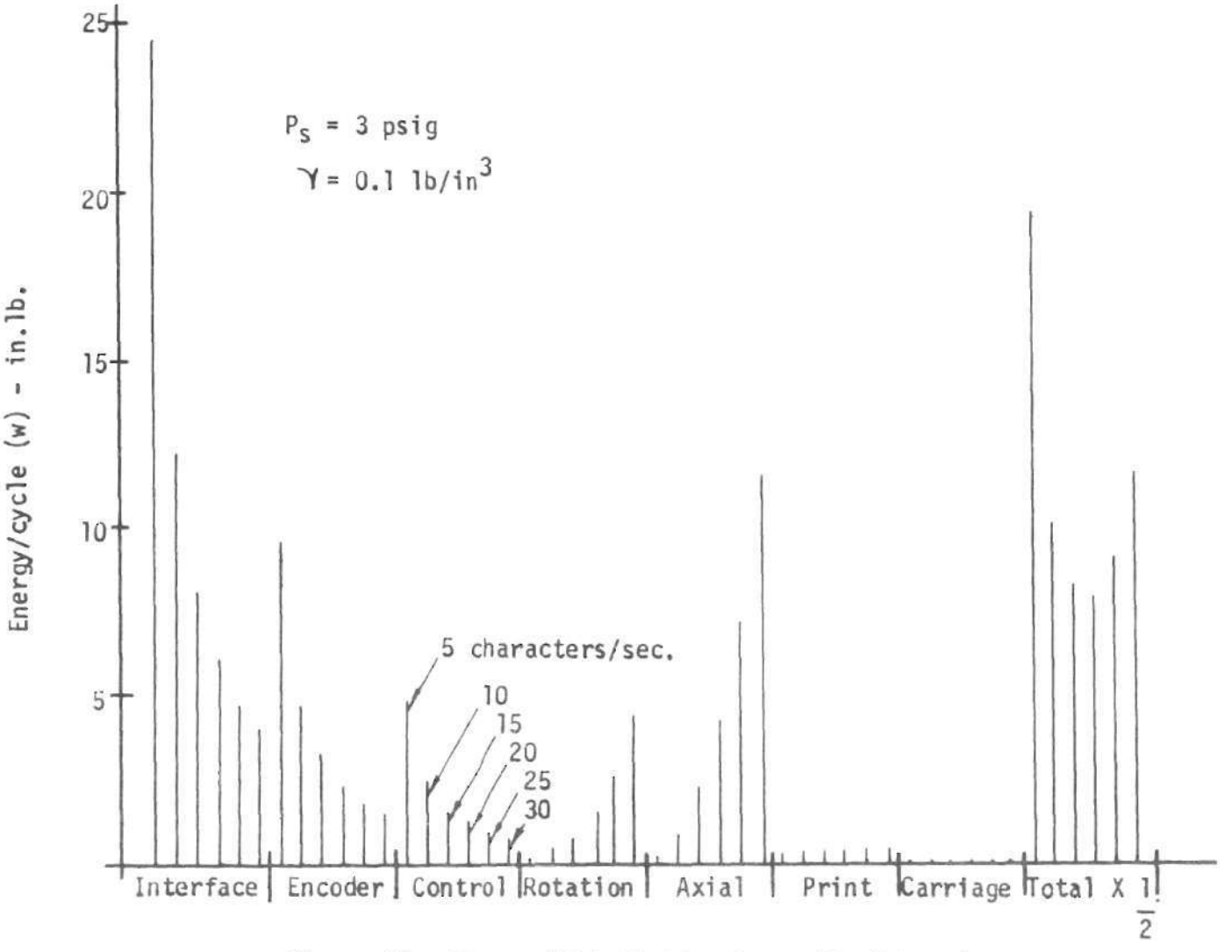

Figure 38. Energy Distribution Among the Subsystems

actuators since carriage power requirement is very low with the actuators off the carriage.

The size of the actuators required is shown in Figure 39. In general, size increases the typing speed and decreases with pressure. The smallest diameters required are for printing, and they are, for the most part, less than one-half inch. Pistons for type head rotation range from one-half inch to more than three inches at 30 characters per second. The largest pistons required are for the axial motion, which range from one to more than three inches. In addition to diameters, the stroke lengths of the actuators are shown by the solid symbols. Strokes for the rotary and axial motions are approximately one-half inch and are constant with pressure and speed since they are determined entirely by geometry. The print actuator stroke varies with speed, decreasing with increasing speed. This is due to the fixed final kinetic energy. It is easy to see that the positioning piston sizes are larger than would be practical for the higher speeds, and that the low speed print strokes are much too long. Some consideration of the diameter-stroke relationships is in order.

The piston diameter for the rotary and axial motions is essentially determined by the system mass reflected to the actuator. The equations for equivalent mass, m, given in Figures 26 and 28 show that one means of varying m is to vary the arm ratio ℓ/a. The results of varying ℓ/a for both subsystems is shown in Figure 40. Since the subsystems are independent, the curves show the variation of stroke and diameter for the rotary mechanism with the axial ratio, ℓ_6/a_6, fixed

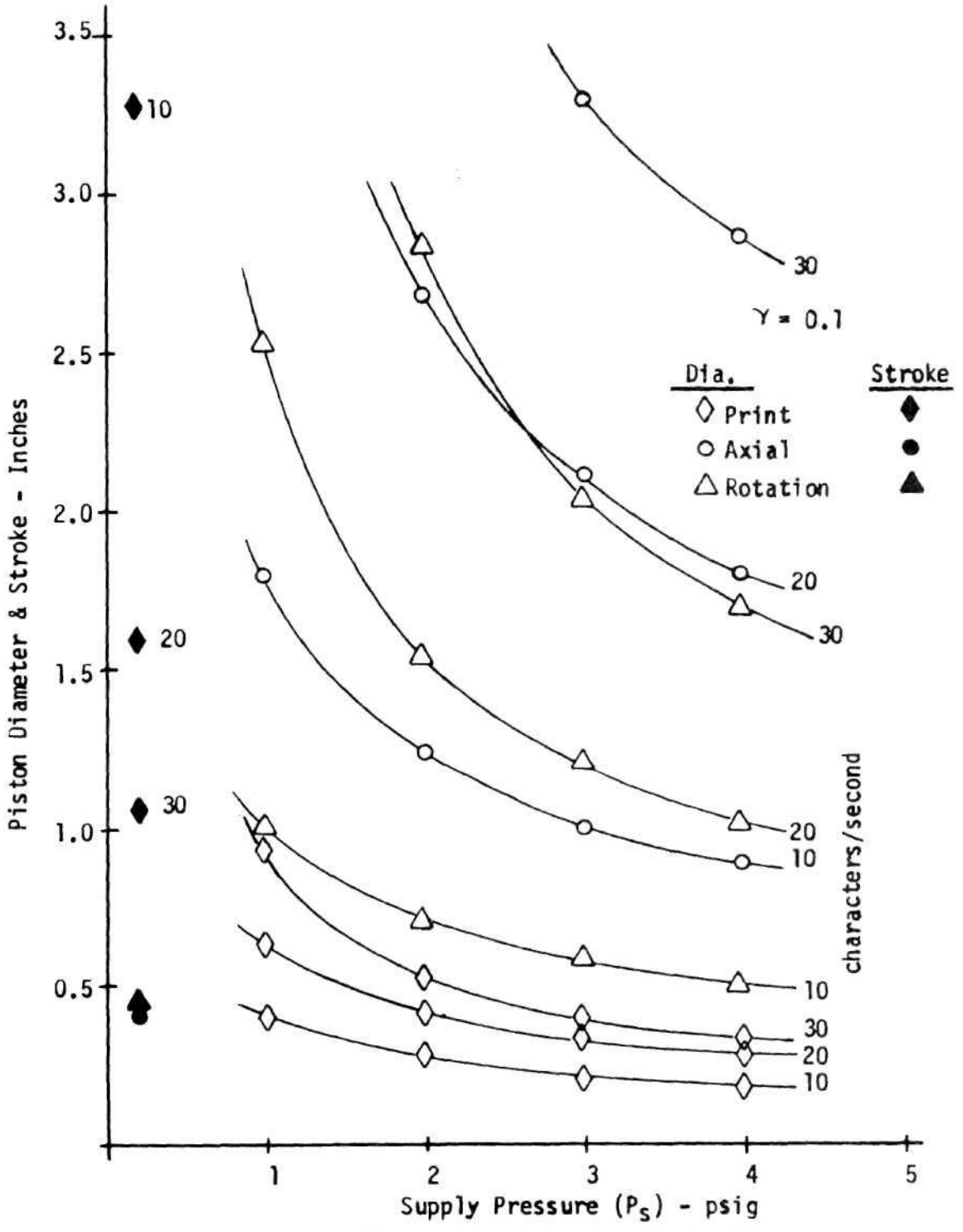

Figure 39. Actuator Piston Size

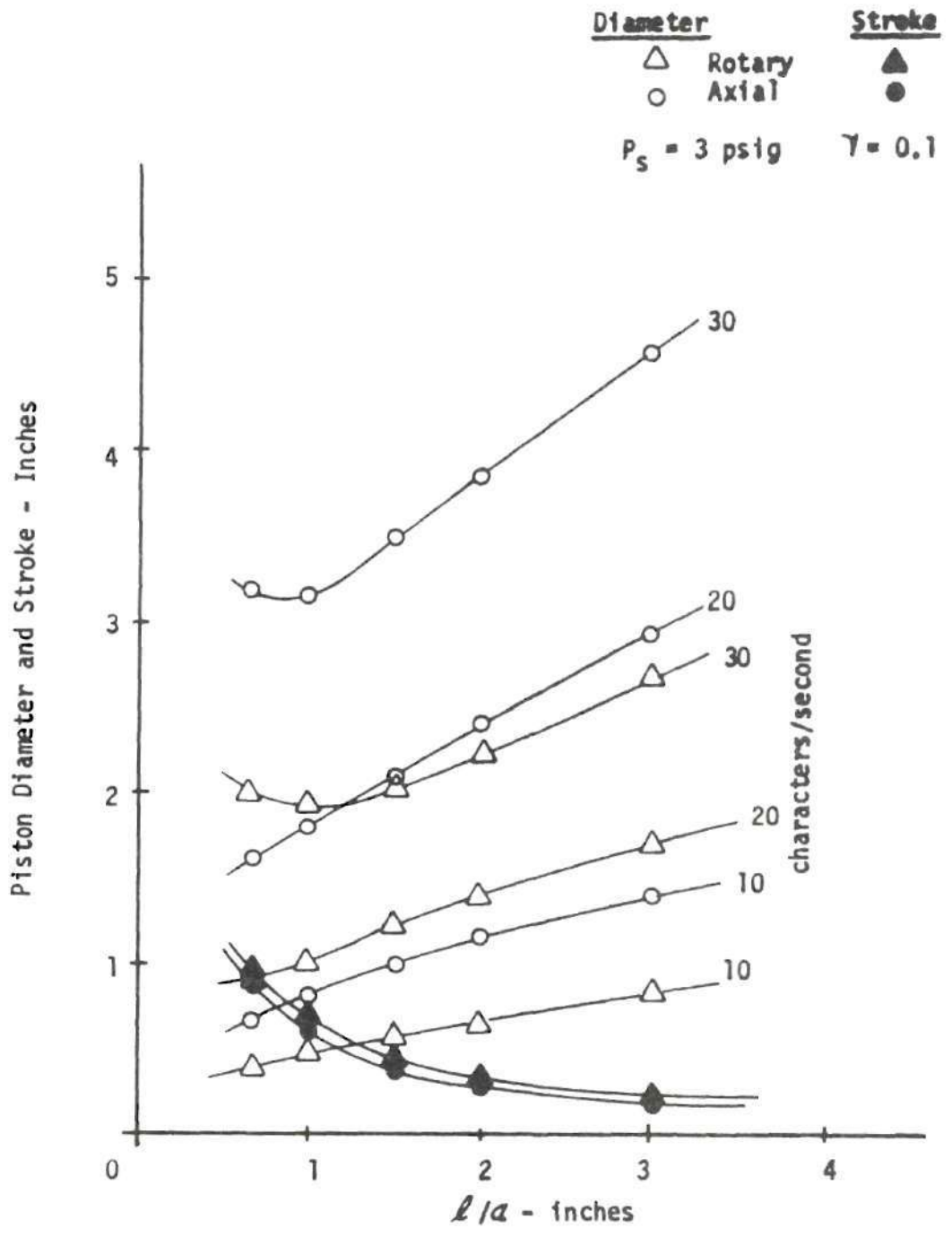

Figure 40. Positioning Piston Diameter and Stroke

at 1.5, and vice versa. Stroke decreases with ℓ/a increasing and diameter decreases or has a minimum. Despite the fact that these results are for P_s = 3 psig, the axial pistons are quite large (2" - 3") for more than ten characters per second. It would be possible to consider cylinder volume here, but for pistons too large to be practical, it would be of little consequence. As far as power consumption is concerned, it was found to be essentially constant with ℓ/a except for an increase at low ℓ/a (≤ 1.0) and high speed (>25 characters per second). The value of $\ell/a = 1.5$ seems to be a reasonably good compromise since it corresponds to the smaller diameters at high speed and to relatively short strokes.

As discussed in Chapter VI, the type head matrix and spacing of characters on the head determine the head dimensions, which is reflected in the mass, m. The computer program showed that the mass associated with the type head was a significant part of the total. In order to reduce the piston diameters further, the weight of the head was reduced by reducing wall thickness to 0.065 inch instead of the 0.125 inch used in Table 4. Also, the character space was reduced from a 0.2 inch square to a 0.15 inch square, which further reduced the type head size. Then the effect of the various relative dimensions as determined by the type matrix was computed. The results are given in Figure 41, which shows that the actuator piston diameters have been reduced to approximately two inches maximum. The 5 X 9 matrix gives the best balance of diameters, the maximum diameter (30 cps) being about 1.5 inch for both rotary and axial motion. The 5 X 9 matrix also results in reasonable

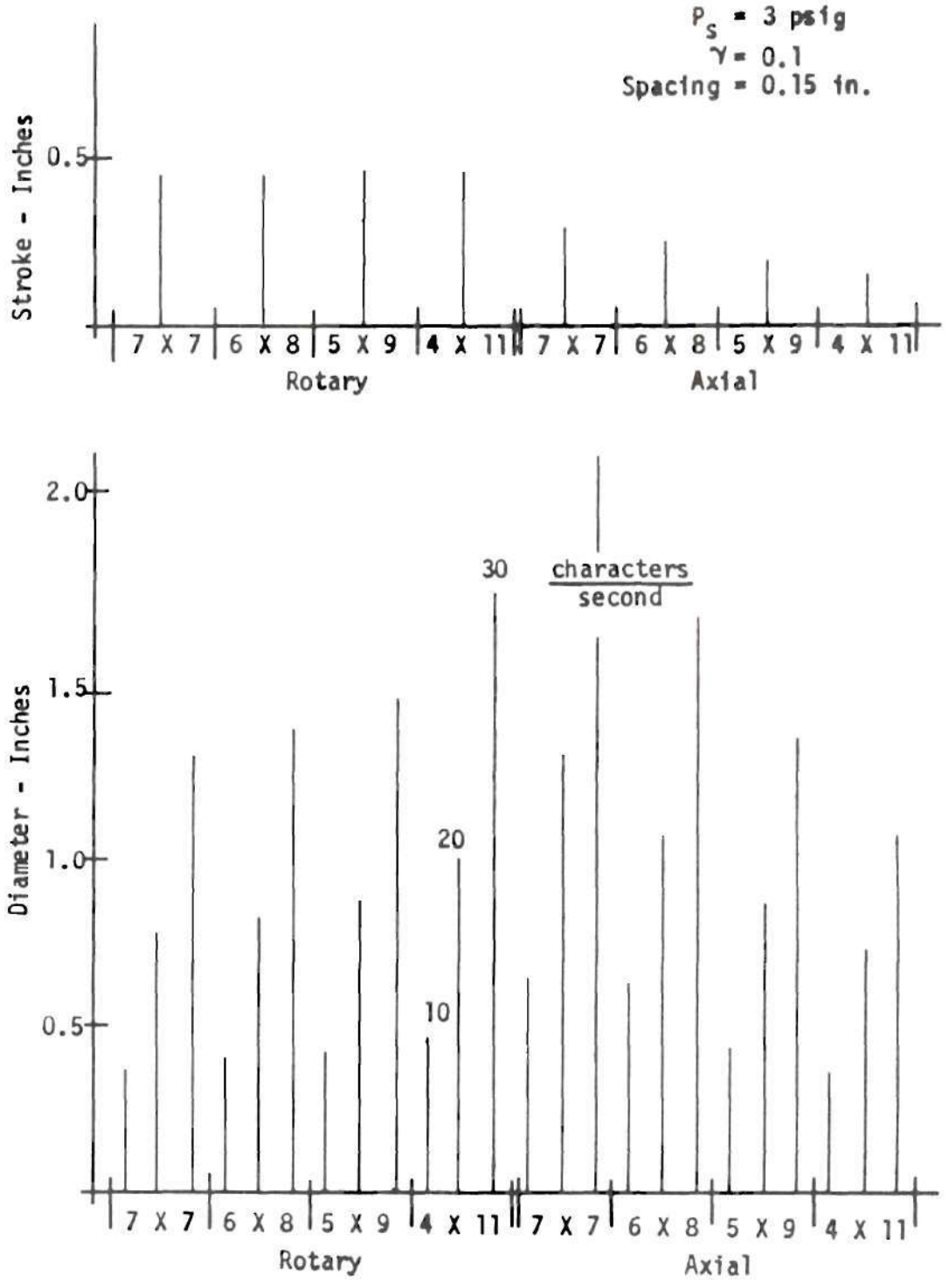

Figure 41. Position Actuator Dimension Variation with Type Matrix

strokes of less than 0.5 inch. Further reduction in piston diameter would be difficult to achieve.

Earlier in this section the excessively long stroke required of the print actuator piston was pointed out. The arm length, ℓ, is a factor in the required stroke, and Figure 42 shows the variation of piston diameter and stroke, as well as type head travel Z_7, with ℓ_7. It is obvious that the shorter ℓ_7 is, the smaller are both the diameter stroke. The type head travel remains relatively constant due to the constant final kinetic energy requirement. It would seem that while the output energy is constant, the input energy (force times stroke) is decreasing with ℓ_7. Consideration of the relative size of the terms in the mass equation shows that a very large portion of input energy goes into the arm and shaft at large values of ℓ_7 (this energy was not included in the printing energy) so that the energy for printing does not decrease, but the system does become more efficient. The power consumption of the overall system also decreases as ℓ_7 decreases for the same reason. Since very small values of ℓ_7 are not physically realizable, and the size of the print actuator is small, it becomes desirable to eliminate the arm and actuator shaft and place the print actuator on the carriage itself.

Placement of the print actuator on the carriage so that the arm and shaft mass are eliminated and the piston stroke, x_7, is made identical to y_7 (Figure 29) results in the actuator dimensions and the type head travel given in Figure 43. Diameters are generally less than 0.5 inch and strokes less than one inch. Type head travel is also less than

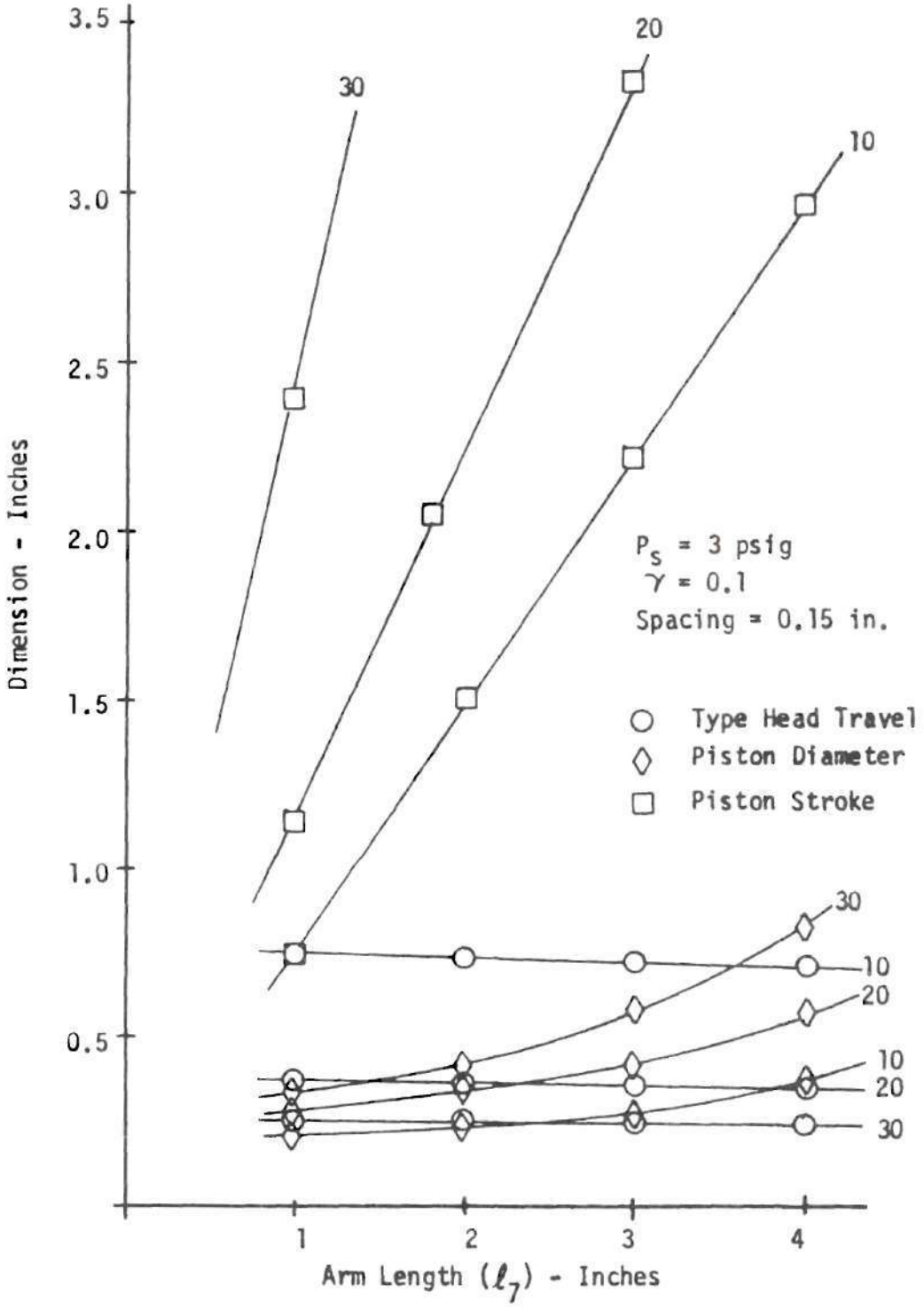

Figure 42. Print Subsystem Dimensions

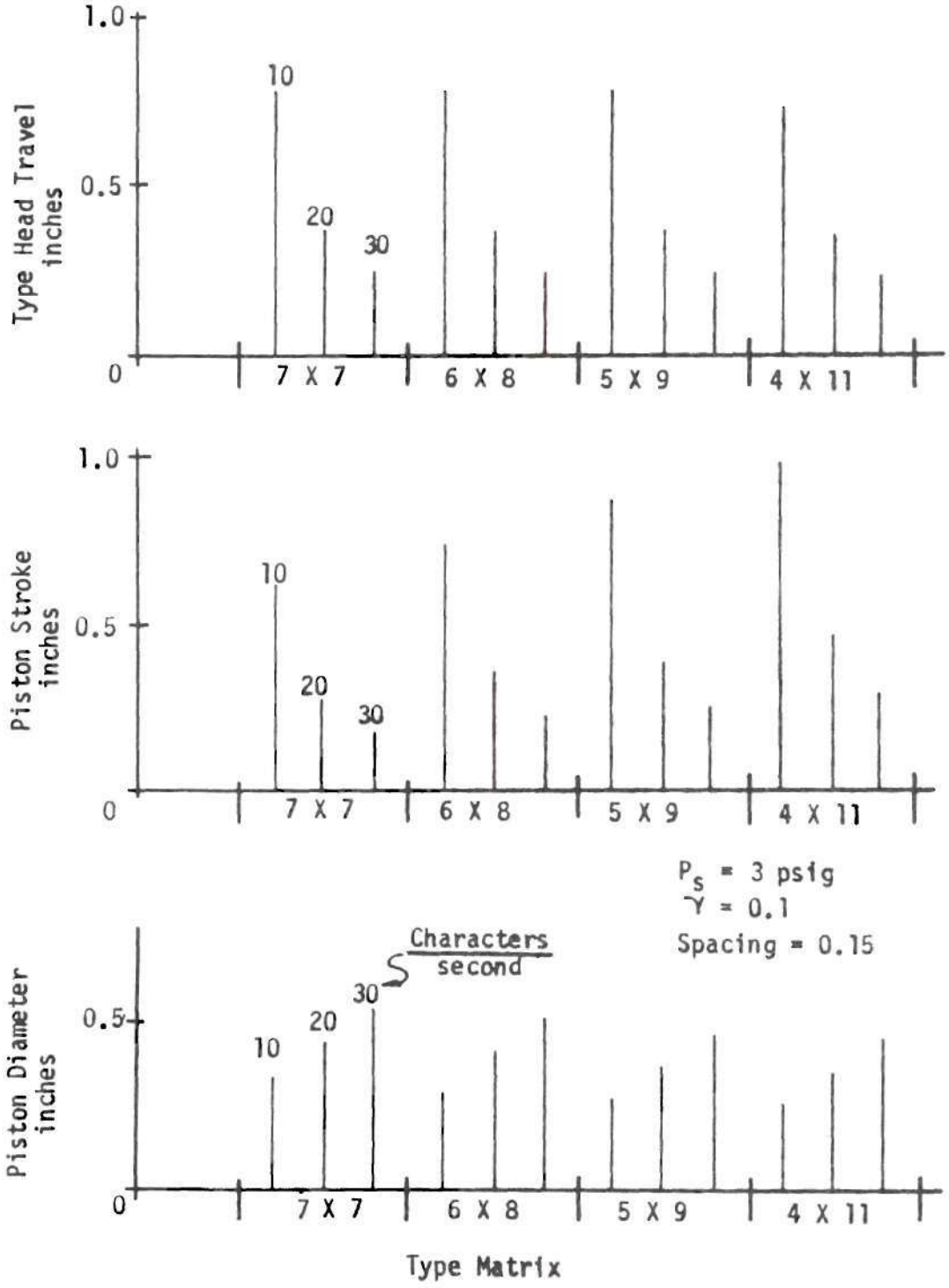

Figure 43. Print Subsystem Dimensions, Actuator on Carriage

one inch. These dimensions are similar to the previous mechanical arrangement except that the large piston strokes are eliminated.

Variation of system power requirements with different type matrices is not great, as shown by Figure 44. The 5 X 9 matrix does result in a minimum power consumption, which coincides with the previous choice of the 5 X 9 matrix for actuator size reasons. Figure 44 also compares total power consumption with the print actuator on and off the carriage for the 7 X 7 matrix, the on-carriage configuration having

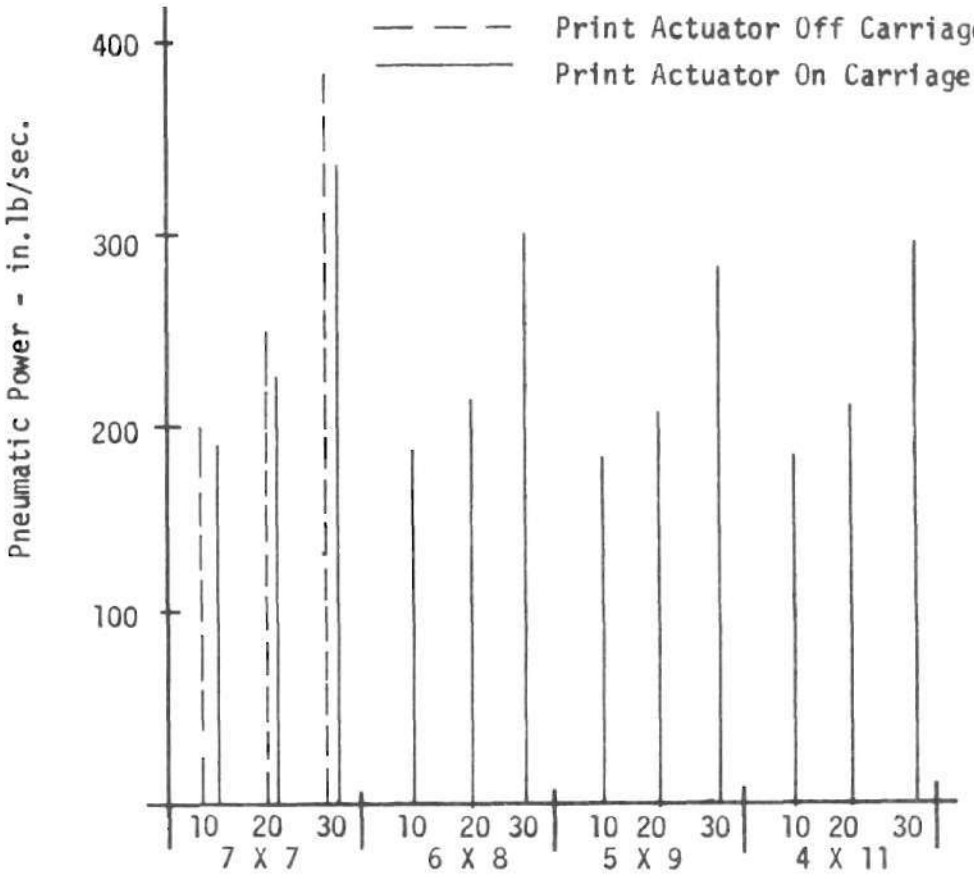

Figure 44. System Power Variation with Type Matrix

a slight advantage.

The derivations of Chapter III and IV relating to minimum power consumption assumed constant values of τ. (Figures 8 and 13). The calculations thus far in this chapter have all been based on τ_5 and τ_6 equal to three and τ_7 equal to 2.5. These values are in a range which give small variation of power with τ for the position and printing actuators. However, variation in τ affects the forward stroke time, T, and thus the force required, which determines piston size. The magnitude of this variation for τ between two and four for the print and position actuators is shown in Figure 45. The ratio of τ_7 to τ_5 in this calculation was constant at 5/6, and $\tau_5 = \tau_6$.

The curves of Figure 45 show that the position actuator diameters decrease with τ in the range covered. This is because T increases as τ decreases, giving more time to accomplish the motion. The effect is pronounced as speed increases. A minimum diameter at about $\tau = 3$ is shown for print piston size, though the total variation is small. The effect of τ on print stroke is to reduce the stroke as τ increases. This is due to the decreased time for forward motion requiring a higher velocity as τ increases.

Power consumption plotted as a function of τ_5 and computed for the same data as for Figure 45 is shown in Figure 46. The increase in power as τ increases for high speeds is due to increasing actuator piston size, as shown in Figure 45. These power curves may seem to contradict Figure 13, where power decreases as τ increases. However, in the present curves, the value of V (Equation 87) is not constant due to the manner in which the parameter values were chosen.

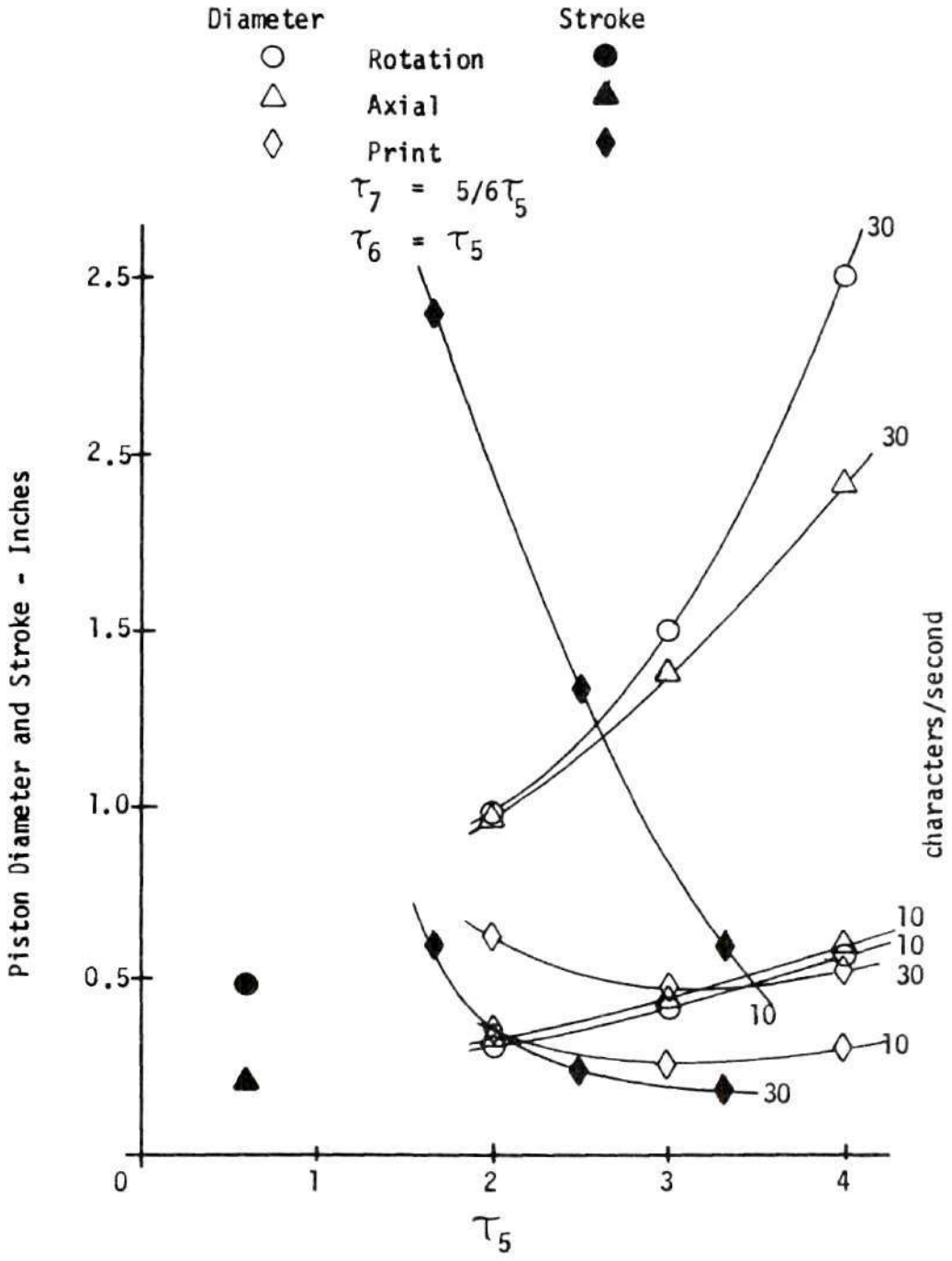

Figure 45. Effect of τ on Actuator Size

These last two curves would make it seem that a value of $\tau_5 = \tau_6 = 2.0$ and $\tau_7 = 1.67$ would be best if it were not for the large stroke print at low speed. This difficulty can be circumvented by designing at the lower values of τ, and, if a low speed design is desired, designing the printing subsystem for higher speed and delaying the start of its forward stroke sufficiently to coincide with the proper printing instant in the cycle. The power consumption level at 30 characters/second using the τ values just stated is approximately 0.036 horsepower.

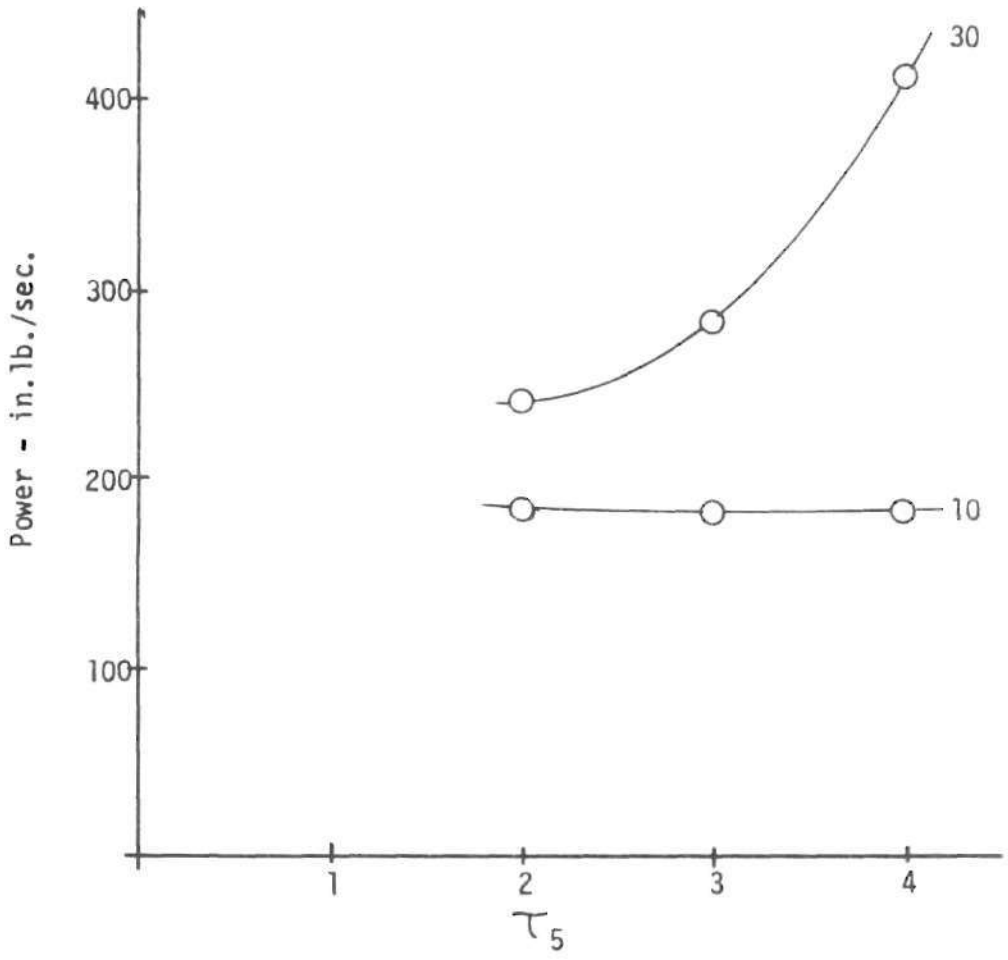

Figure 46. Power as a Function of τ

Summary

The parameter study carried out in the previous section is summarized in Table 5. The object of the study was to vary selected parameters which had an effect on the system power, fluidic amplifier size and performance and actuator size and performance. Those selected were the supply pressure, Reynolds number, typing speed, material of construction, type head dimensions and type matrix, position drive-arm ratio (ℓ/a), the print drive arm length, and the time ratio τ. The basic dimensions given in Table 4 served as a starting point and improvements in performance or size were made by varying the parameters mentioned above and listed in Table 5. From the study the following conclusions can be drawn.

1. Fluidic amplifier sizes are within the range of practical, commercial devices.
2. The supply pressure should be as high as possible ($P_s \simeq 3.0$ psig) to reduce actuator size.
3. A Reynolds number of 2500 gives feasible amplifier design.
4. The materials of construction for moving parts must be of low density, $\gamma \leq 0.1$ lb/in.^{3}.
5. The positioning subsystem arm ratio of $\ell/a \simeq 1.5$ is a reasonable choice.
6. The best choice for type matrix is 5 X 9 since it gives similarly sized actuators and lowest power consumption.
7. The print actuator should be mounted on the carriage.
8. Positioning actuators could be mounted on the carriage for

Table 5. Summary of Parameter Study

Data Input	Parameters	Output	Figure	Constant	Result
Table 4	P_s, Re	Amplifier Size	34		Range: 0.002" - 0.035"
Table 4	P_s, Re	Amplifier power	35		Typical variation
Table 4	P_s, Re	Amplifier Response	35		Less than 3 msec
Table 4	P_s, speed	System Power	36	Re = 2500	0.2 horsepower
Table 4 & $\gamma \rightarrow 0.1$	P_s, speed	System Power	37	Re = 2500	Up to 60% reduction at higher speeds
Table 4 & $\gamma \rightarrow 0.1$	Speed	Energy distribution by subsystem	38	above, plus $P_s = 3$ $\gamma = 0.1$	Depends on speed, actuators & interface large
Table 4 & $\gamma \rightarrow 0.1$	P_s, speed	Actuator Dimension		above, plus $P_s = 3$ $\gamma = 0.1$	Too large at high speed
Table 4 & $\gamma \rightarrow 0.1$	ℓ/a	position Actuator dimensions	40	above, plus $P_s = 3$ $\gamma = 0.1$	ℓ/a = 1.5 for axial & rotary
Table 4 & $\gamma \rightarrow 0.1$ $r_c - r_c \rightarrow 0.065"$ spacing $\rightarrow 0.15"$	Matrix, speed	Position actuator dimensions	41	above, plus $P_s = 3$ $\gamma = 0.1$	Size reduced, 5 X 9 matrix best choice

Table 5 - continued

Data Input	Parameters	Output	Figure	Constant	Result
Table 4 & $\gamma \rightarrow 0.1$ $r_c - r_c \rightarrow 0.065"$ spacing $\rightarrow 0.15"$	ℓ_7, speed	Print actuator dimensions	42	above, plus spacing = 0.15 $r_c - r_c = 0.065$	ℓ_7 short as possible, actuator on carriage
Table 4 revised print system	speed, matrix	Print actuator dimensions	43	above, plus spacing = 0.15 $r_c - r_c = 0.065$	stroke & diameter feasible
Table 4 revised print system	speed, matrix	System Power	44	above, plus spacing = 0.15 $r_c - r_c = 0.065$	$<$ 0.05 horsepower 5 X 9 matrix lowest
$2 < \tau < 4$	τ, speed	Actuator size	45	above, plus 5 X 9 matrix	Actuator size decrease
$2 < \tau < 4$	τ, speed	System power	46	above, plus 5 X 9 matrix	$\tau_5 = \tau_6 = 2$, $\tau_7 = 1.67$ power $\leq$ 0.036 horsepower

low speed designs. High speed designs would require further study.

9. System power consumption is low enough to be practical ($\simeq$ 0.04 horsepower) if the predicted level can be achieved.
10. The values of τ which give the lowest power consumption for the other parameters chosen are $\tau_5 = \tau_6 = 2.0$, $\tau_7 = 1.67$. For a low speed machine, this may require designing the print subsystem for higher speed.

The preferred design, then, consists of the mechanisms given in this chapter with the dimensions shown in Table 4, subject to the improvements summarized in Table 5 and in the conclusions above.

CHAPTER VIII

POWER SUPPLY

Subsystem Requirements and Model

In all of the preceding discussions it has been assumed that a source of compressed air was available at a constant pressure, P_s, for driving the final actuators and most of the fluidic circuitry. In addition, a source at a pressure of σP_s ($\sigma = 4$ in the previous discussions), but with a much lower flow was also required, as discussed in Chapter VII. The actuator designs all assumed a constant pressure throughout their stroke, and this constant pressure is likewise required for the fluidic devices. However, the demand on this pneumatic source has considerable variation. The Coanda devices have constant flow through the power nozzles, but the flow demand of the digital actuators and print actuator is intermittant and of varying flow depending on typing speed. The basic requirement of the pneumatic supply, then, is to provide two constant pressure sources with flow depending on design speed and varying during any one print cycle.

The required flow for the low pressure supply as a function of time for ten characters/second is shown in Figure 47. These flows correspond to a system with the final parameters described in the preceding chapter. Two ordinate scales are shown, one corresponding to inclusion of the key interface amplifiers in the system, and the other to their exclusion. The shape of the curves is approximate, but the

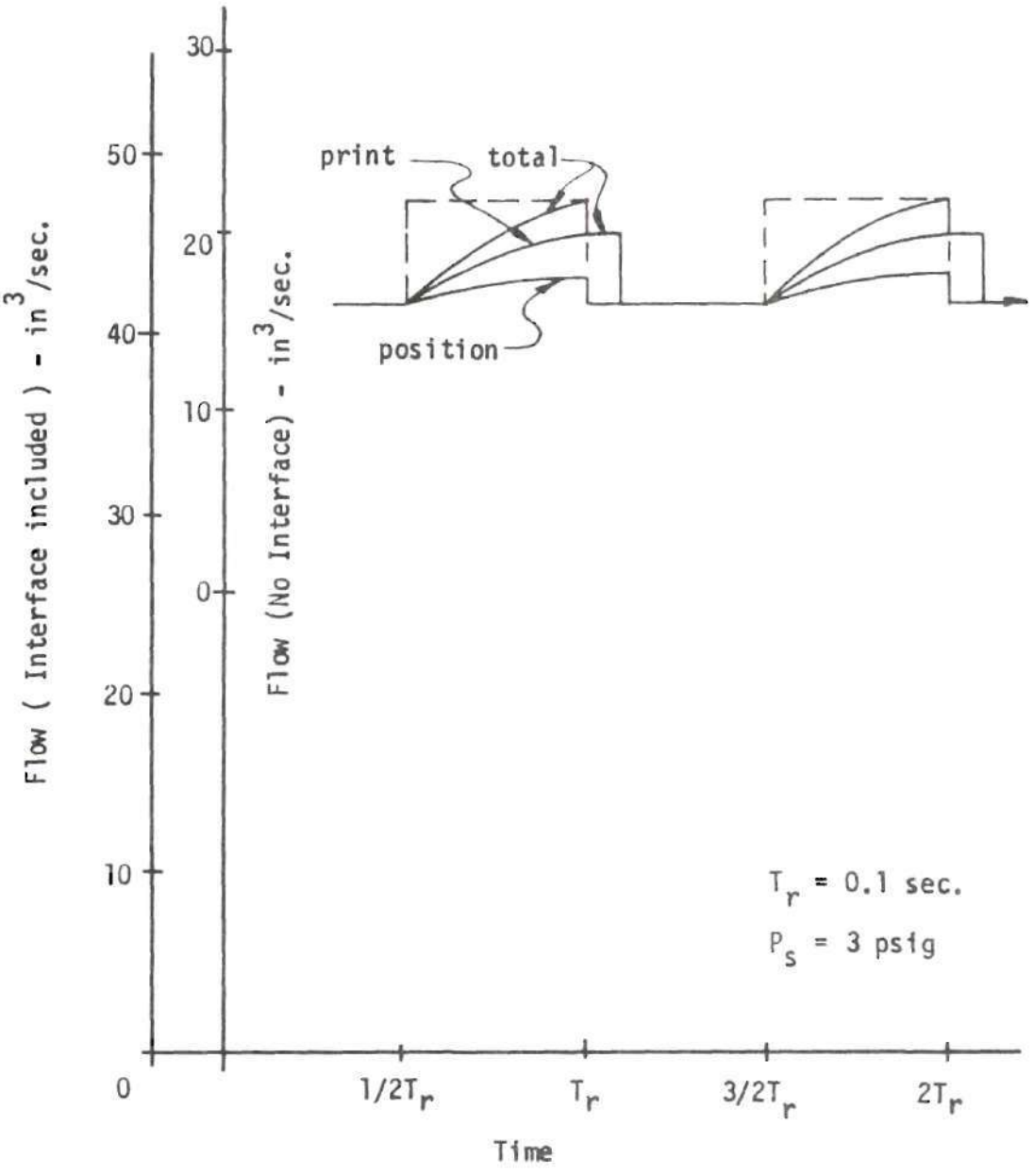

Figure 47. Flow Demand for Power Supply, 10 cps

maximum points are correct, as is the steady flow value. In order to simplify the further analysis of the power supply, the total flow curve is approximated by the dashed square-wave pulse train. An equivalent pulse train for 30 characters per second is shown in Figure 48.

The design of the supply could be based on these curves either with or without the flow due to the key interface amplifiers. In the subsequent discussion the interface flow will be omitted for two reasons. One, these amplifiers are not essential to the typewriter function, although they may be desirable for other reasons. Second, the intermittant component of flow is proportionately larger under these circumstances and presents a greater demand on the power supply ability to maintain constant pressure. In this sense, the choice represents a worst-case design.

In order to make some predictions as to the type and size of compressor required for the power supply, it will be assumed that the supply consists of a compressor with an accumulator on its output to assist in maintaining a constant pressure to the fluidics. It is further assumed that the output characteristic of the compressor near the operation point can be aprroximated by a straight line. In terms of an electrical analog, this characteristic can be modeled by a constant voltage source, P_c, and a resistance, R_c, as in Figure 49a. The accumulator analog is a capacitor for small pressure changes, and where the current in the circuit is analogous to weight flow rate and the voltage to pressure. For the square wave approximation to the flow curves, an analog with the same characteristics is given in Figure 49

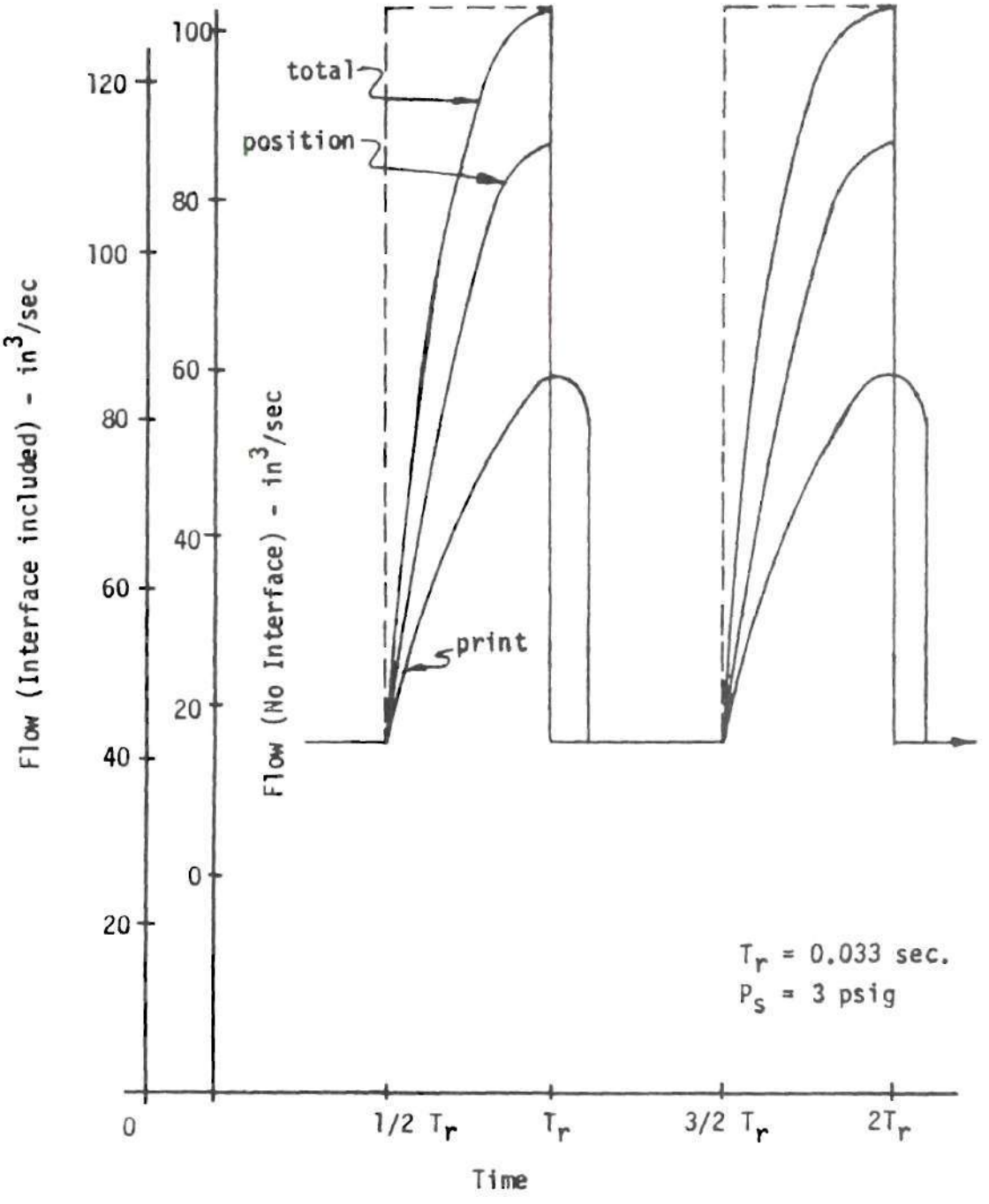

Figure 48. Flow Demand for Power Supply, 30 cps

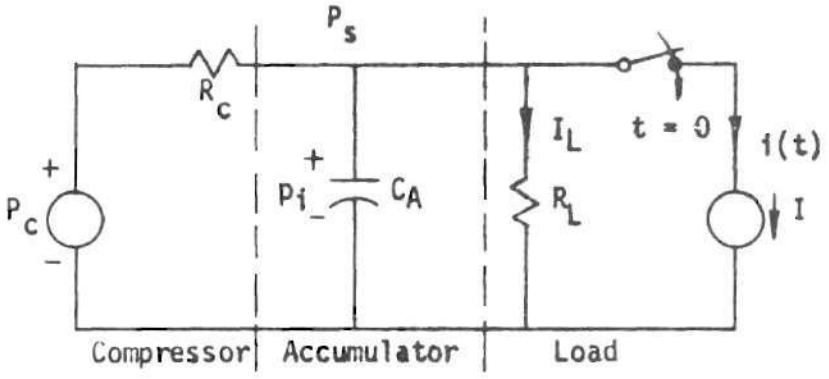

(a) Analog of Power Supply and Load

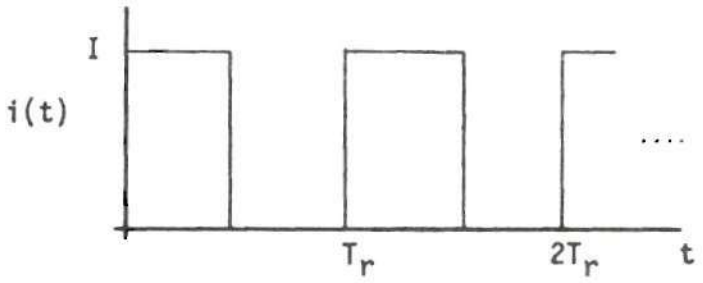

(b) Load Current Component Due to Actuators

Figure 49. Power Supply Analog

as a resistor, R_L, to provide a constant flow component and a switch and current source, I, to provide the intermittant flow component. The switch is assumed to operate in a repetitive manner corresponding to the typing rate.

By replacing the compressor analog with its Thevenin equivalent, it is easy to write the node voltage equation for P_s in Laplace form as

$$P_s(s) = \frac{P_c}{sR_cC_A(s + R_p^{-1}C_A^{-1})} + \frac{C_A p_i - i(s)}{C_A(s + R_p^{-1}C_A^{-1})} \qquad (151)$$

where

$$R_p = \frac{R_L R_c}{R_L + R_c} \qquad (152)$$

is the parallel combination of R_L and R_C. The quantity p_i is the initial value of P_s when the switch is closed at t = 0. It can be seen from the steady state with the switch open that

$$p_i = P_c R_p R_c^{-1} \qquad (153)$$

The inverse transformation of Equation (151) requires an expression of the Laplace transform of the fluctuating component of load current, I(s). Since the time domain function of this current is periodic, as in Figure 49b, with period T_r, the Laplace transform is given by

$$i(s) = \frac{I}{s[1 + \exp(-0.5T_r s)]}$$

Substituting this last expression into Equation (151) results in

$$P_s(s) = \frac{p_i}{s} - \frac{I R_p}{1 + \exp(0.5 T_r s)} \left[\frac{1}{s} - \frac{1}{s + R_p^{-1} C_A^{-1}} \right] \tag{154}$$

when simplified by partial fractions and Equation (153). Using a method shown by Wiley [37], the inverse transform of the periodic portion of the function of P_s is found to be

$$\frac{P_s(t)}{p_i} = 1 - \frac{I R_p}{p_i} \left[\frac{(-1)^n + 1}{2} - \frac{(-1)^n \exp(-v R_p^{-1} C_A^{-1})}{\exp(0.5 T_r R_p^{-1} C_A^{-1} + 1)} \right] \tag{155}$$

where

$$0.5 n T_r < t < 0.5(n+1) T_r \qquad -0.5 T_r < v < 0$$

and n is any positive integer. Since it is desired to predict the performance of the power supply after long-term repetitive operation of the keys, the transient portion of the solution is assumed to have decayed to zero and only the periodic portion is given in Equation (155).

The periodic response is shown in Figure 50. Pressure varies in an exponential fashion between the limits shown in the figure. It is obvious from this pressure response that $P_s(t)$ does not remain constant if the keys are operated repetitively. In fact, the peak pressure does not even return to p_i between key operations. Thus, the best that can be done with the system as postulated is to limit the lowest pressure at any time to some reasonable percentage of the design pressure, say 90 to 95 per cent. If the minimum pressure is defined by

$$\left.\frac{P_s(t)}{p_i}\right)_{min} = p_m \tag{156}$$

then from Figure 50

$$p_m = 1 - \frac{I R_p}{p_i}\left[\frac{\exp(0.5 T_r R_p^{-1} C_A^{-1})}{\exp(0.5 T_r R_p^{-1} C_A^{-1}) + 1)}\right] \tag{157}$$

Since I, p_i and T_r are known and p_m is to be a design parameter, the unknowns in this equation are R_p and C_A, which constitute the time constant of Figure 50. Solving for the exponent gives

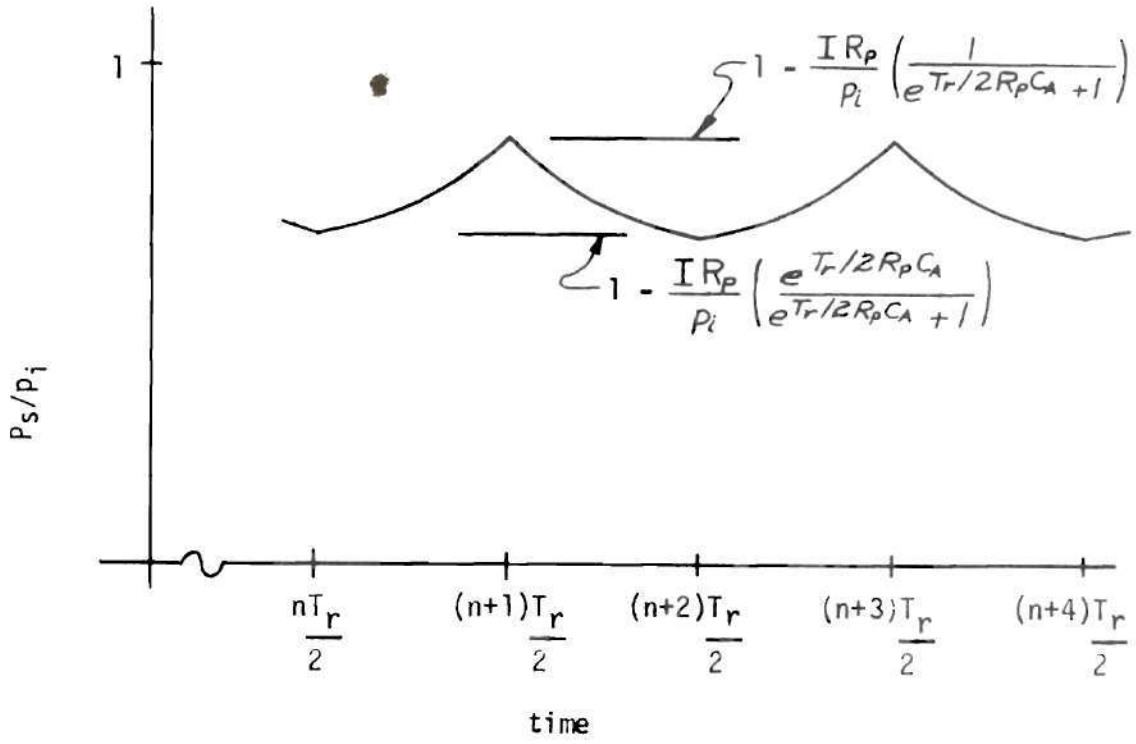

Figure 50. Supply Pressure Variation for Repetitive Operation

$$\frac{T_r}{2R_p C_A} = \ln\left[\frac{1-\rho_m}{IR_p\rho_i^{-1}+\rho_m-1}\right] \tag{158}$$

Since the left side is a positive number, the inequalities

$$1-\rho_m > IR_p\rho_i^{-1}+\rho_m-1$$

and

$$\rho_m-1+IR_p\rho_i^{-1} > 0$$

are required. From these it can be shown that

$$2(1-\rho_m)\rho_i I^{-1} > R_p > (1-\rho_m)\rho_i I^{-1} \tag{159}$$

Since R_2 in Equation (152) is known, it is possible to assume values of R_p in the range given by Equation (159) and solve for the corresponding C_A in Equation (158). Then R_c can be found from Equation (152).

Compressor Selection

Before computing numerical values for the components of the power supply, it is advisable to consider the type of compressor best suited to the application. One of the most widely used criteria for selecting the most satisfactory compressor is the specific speed, which is defined here as

$$S_N = \frac{SU^{0.5}}{E^{0.75}} \tag{160}$$

with dimensions as given in the Nomenclature. Shepard [38] shows the relationship of S_N to efficiency for various types of compressors, namely axial, centrifugal and rotary positive displacement. This relationship is summarized by Table 6. It is to be understood that the ranges given in Table 6 are not sharply defined and that there is some overlap in the specific speeds and efficiencies of the various compressors. Specific speed values for the typewriter can be developed from Figures 47 and 48. The compressor must be designed to supply the minimum flow shown in these curves, which is the flow I_L in Figure 49, at the design pressure, P_s. The peak flow must be supplied by the accumulator and the increase in compressor flow as the pressure drops to the value allowed by p_m. For any typing speed, specific speed is computed as

$$S_N = \frac{(3600\ rpm)(9.2\times10^{-3}\ ft^3/sec.)^{.95}}{(4810\ ft)^{0.75}} \simeq 0.6$$

at a compressor speed of 3600 rpm. From Table 6, it is obvious that this corresponds to a constant displacement machine. In order to design a centrifugal compressor for this application, the speed would have to be on the order of 5×10^5 rpm, which would require technology not consistent with the present application. The rotary, sliding-vane compressor used in many refrigeration appliance and small-horsepower air compressors could be a good choice from the standpoints of small size

Table 6. Specific Speed Range for Compressors

Compressor Type	Specific Speed	Efficiency
Axial	$S_N > 200$	0.75 - 0.90
Centrifugal	$200 > S_N > 50$	0.60 - 0.80
Rotary Positive Displacement	$50 > S_N > 10$	0.55 - 0.65

and reliability.

Low Pressure Compressor Size

Since a constant displacement compressor is to be used, it is advantageous to redraw Figure 49a with the Thevenin equivalent for the compressor. This is consistent with the original assumption of a linear output characteristic, but the physical interpretation of a constant displacement compressor with a bypass is intuitively more apparent.

Since the overall criterion in so far as the power supply is concerned is to minimize power consumption, it is advisable to have an expression for power in the circuit of Figure 51. The average power can be expressed as

$$\dot{w} = T_r^{-1} \int_{nT_r}^{(n+1)T_r} \frac{P_s^2(t)}{\rho R_p} \, dt \tag{161}$$

where $P_s(t)$ is given by Equation (155). Since the design must be such as to limit variation in P_s to a small percentage, an approximate

expression for $\dot{w}$ can be derived. During the switch-open portion of the period the energy expended is

$$w = \frac{P_s^2}{\rho R_p}\left(\frac{T_r}{2}\right) \tag{162}$$

During the switch-closed portion of the period the energy expended is

$$w = \frac{P_s^2}{\rho R_p}\left(\frac{T_r}{2}\right) + \frac{P_s I}{\rho}\left(\frac{T_r}{2}\right) \tag{163}$$

Let $P_s = p_i$ in Equation (162) and $P_s = p_m p_i$ in Equation (163). Then the approximate $\dot{w}$ is

$$\dot{w} = \frac{p_i^2}{2\rho R_p}\left[1 + p_m^2\right] + \frac{p_m p_i I}{2\rho} \tag{164}$$

Note that the average power, $\dot{w}$, is a function of R_p, so that the solution of Equations (158) and (152) for R_p, R_c and C_A also determines values of $\dot{w}$.

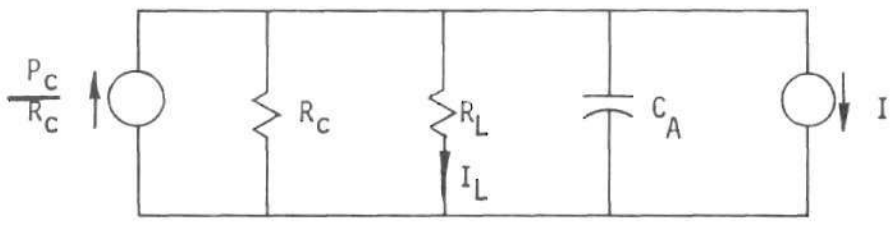

Figure 51. Equivalent Power Supply Analog

The results of computations of the values of C_A and $\dot{w}$ over the allowable range of R_p for p_m = 0.95 and 0.90 are shown in Figure 52 for ten characters per second, and in Figure 53 for 30 characters. There is obviously a trade-off between the power consumption and the accumulator size. Power is reduced with the larger accumulator since it stores energy between actuator strokes. At high typing speeds the large intermittant flow to the actuators requires a large bypass flow through R_c in order to limit variation in P_s. This is reflected in the lower values of R_p at the higher speed and in much larger power consumption and accumulator size. In view of the criteria of minimum power consumption and keeping size as low as practicable, a reasonable choice of parameters are those represented by the lower end of the knee of the C_A curve. The resulting parameters are summarized in Table 7. Note that the small variation in pressure required has increased the power consumption from the low value of 0.036 horsepower in Figure 46 to almost one-third horsepower in Table 7 (p_m = 0.95, 30 cps). This is due to the inefficiency created by the bypass loss in R_c. Some of this inefficiency could be eliminated by use of a quick-acting relief valve in place of the simple bypass R_c, but this situation will not be analyzed here.

The physical size of the compressor is of interest and some approximate calculations can be made. The displacement of a rotary sliding vane compression has been related to the geometry by Lehmkuhl [39]. The basic construction and definition of geometry for this compressor, adapted from Lehmkuhl's paper, are shown in Figure 54.

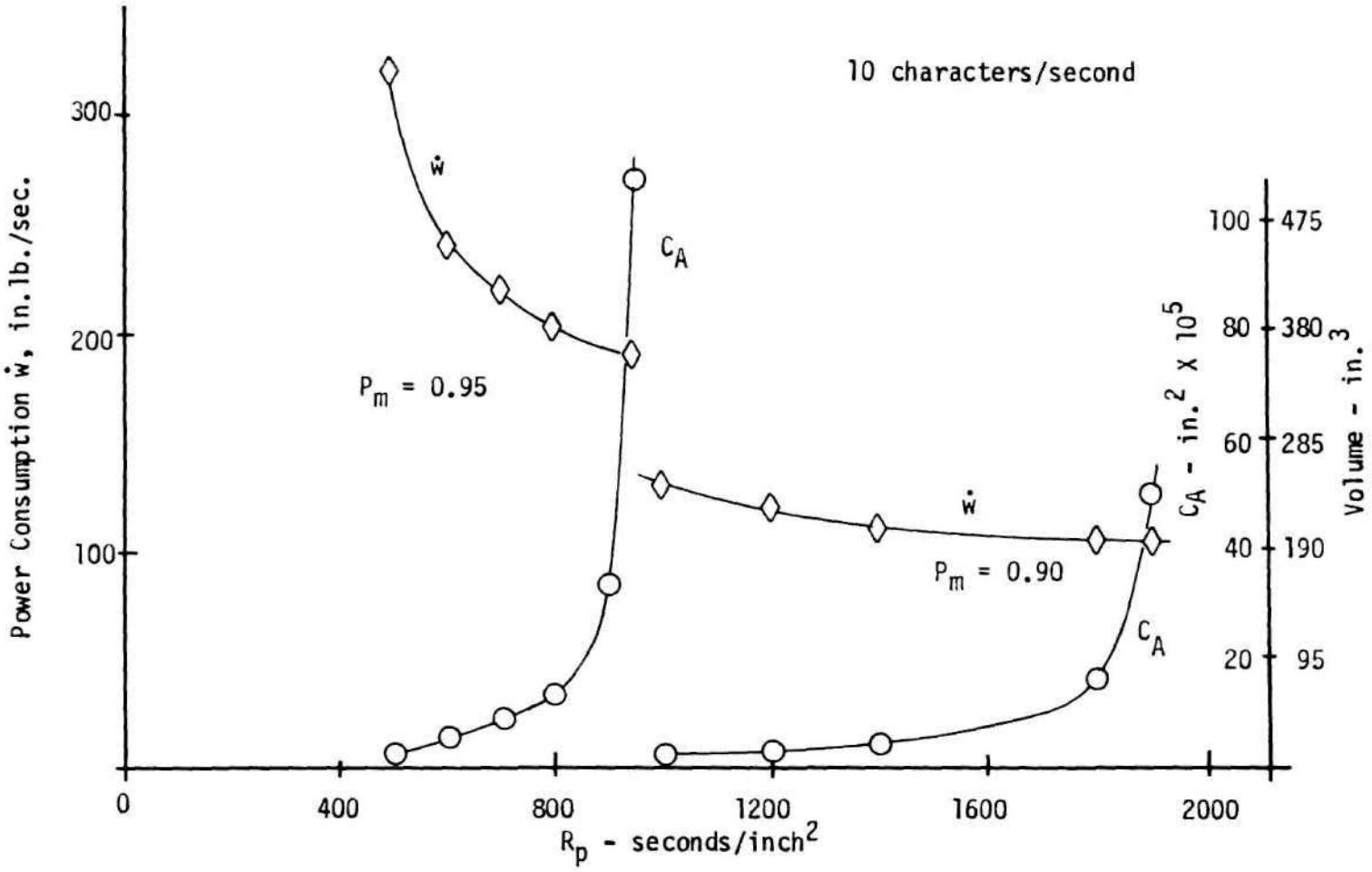

Figure 52. Compressor Power Consumption and Accumulator Size

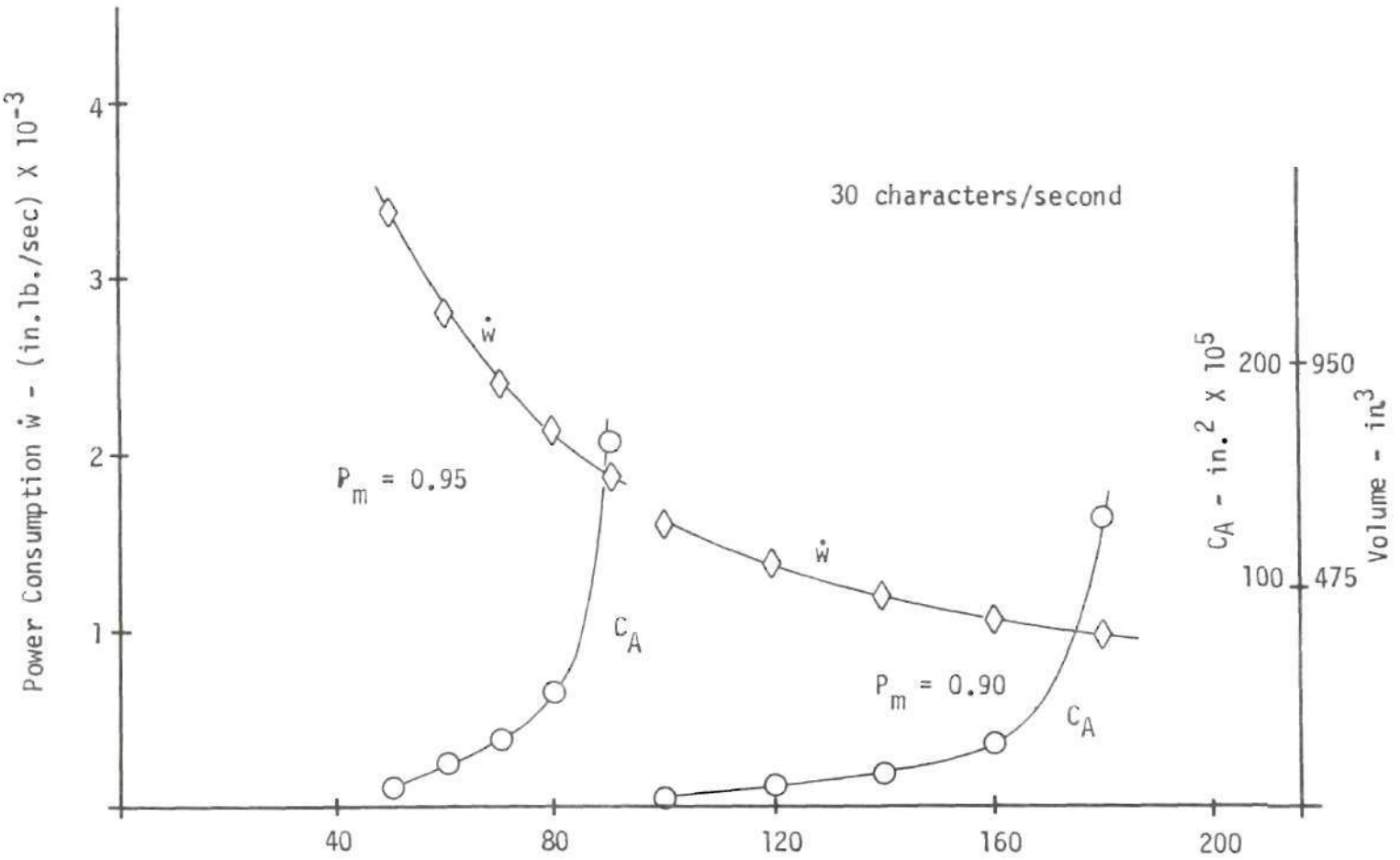

Figure 53. Compressor Power Consumption and Accumulator Size

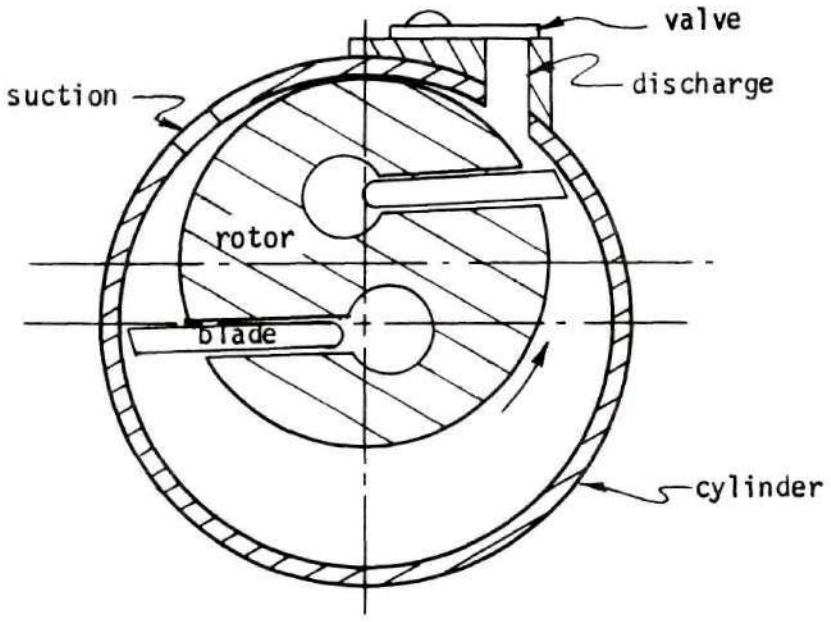

Compressor Construction

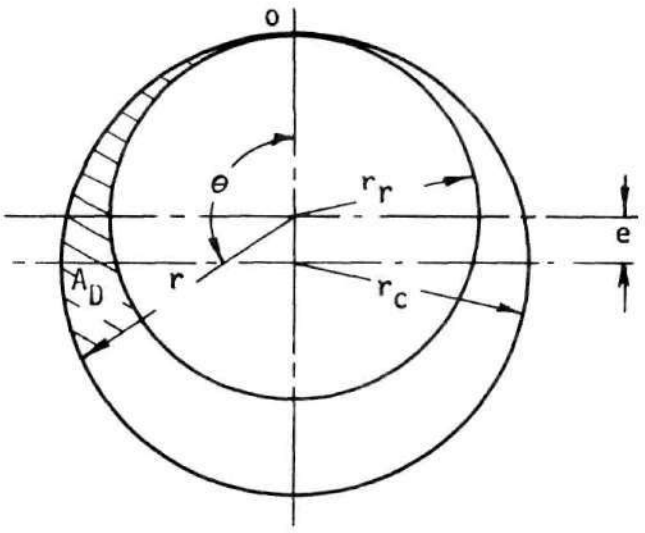

Displacement Nomenclature

Figure 54. Rotary Sliding Vane Compressor

Table 7. System Flow Parameters

p_m	0.90		0.95	
cps	10	30	10	30
$R_p \frac{sec}{in^2}$	1600	160	800	80
C_A in^2	7.04×10^{-5}	27.2×10^{-5}	14×10^{-5}	54.5×10^{-5}
$\dot{w} \frac{in.lb}{sec}$	105.9	1061	214.5	2145
$V_c in^3$	33.4	129	66.5	259
$R_c sec/in^2$	2860	167.5	1025	81.8
P_c lb/in^2	5.36	3.14	3.84	3.07
P_c/R_c lb/sec.	1.88×10^{-3}	1.87×10^{-2}	3.74×10^{-3}	3.75×10^{-2}
P_c/R_c $in^3/sec.$	2540	25,400	5070	50,700

The volume displacement per revolution of the rotor is

$$V_D = n A_D b \tag{165}$$

The approximate area A_D is given by

$$A_D = r_c^2 \left(1 - \frac{r_r}{r_c}\right)\left[\left(1 + \frac{r_r}{r_c}\right)\frac{\pi}{n} + 2\sin\frac{\pi}{n} + \frac{1}{2}\left(1 - \frac{r_r}{r_c}\right)\sin\frac{2\pi}{n}\right] \tag{166}$$

A typical valve for r_r/r_c for low pressure compressors is 1.25. If n is taken as four, the ratio A_D/R_c^2 can be computed as 2.3. Since the output flow is given by

$$V_o S = nA_o bS \tag{167}$$

and the product $V_b S$ is known from Table 7 (i.e., $P_c R_c$), then for a given speed, S, and blade width, b, A_D can be found, as well as r_r and r_c. These dimensions then define the compressor size, and they are given as Table 8 for two common motor speeds.

Compressor size for the low pressure supply is fairly small, as seen from Table 8. Depending on the choice of b, the cylinder diameter is 3.5 inches or less. Other combinations of b and r_c are possible, of course. Volumetic efficiency of this type compressor at this low pressure is very nearly unity, so that the driving motor efficiency is the only other efficiency consideration of any magnitude.

High Pressure Supply

Up to the present, nothing has been said of the means of obtaining the high pressure air supply for the control circuit as discussed in Chapter VII. This high pressure supply is not subject to the intermittant, high flow demand that is present in the low pressure supply. The flow is steady and therefore does not require the bypass arrangement to smooth out fluctuations. Coupled with the fact that the high pressure flow is only a small fraction of that actually going to the rest of the fluidic circuitry, this results in high pressure compressor output flow which is very small compared to the low pressure output flow. For example, the high pressure flow is 88 $in.^3/min.$, whereas the low pressure compressor output flow for 10 cps and $p_m = 0.95$ is 5070

Table 8. Sliding Vane Compressor Dimensions - Low Pressure (P_s)

Speed	1750				3450			
p_m	.90		.95		.90		.95	
cps	10	30	10	30	10	30	10	30
r_c in. b = 1 in.	0.79	2.51	1.12	3.55	0.57	1.79	0.80	2.53
r_c in. b = 0.5 in.	1.12	3.55	1.59	5.02	0.81	2.53	1.13	3.58

$in.^3/min.$ (Table 7). It can be safely said that the high pressure compressor is so small in size and power consumption that further consideration of it is of little importance, except to say that it should be of similar construction to the low pressure one, most likely an integral part of it and driven by the same motor.

CHAPTER IX

DEMONSTRATION MODEL

Purpose and Description

One of the objectives of the thesis was to construct a working model which would incorporate the basic features upon which the foregoing analysis was based. The purpose of the model was to show that the system proposed for a fluidic typewriter and the parameters chosen to define a preferred design did lead to an operable system with performance approaching that predicted. The model was not intended as a finished product, but as a breadboard demonstration of the basic mechanical and fluidic components.

The demonstration model is best described with reference to Figure 55, which is a general view and Figure 56, a plan view.

Printing was accomplished with a cylindrical type head from a teletypewriter impacting on a narrow paper tape. The type head was supported from a yoke pivoted on ball bearings, and the type head itself rotated on ball bearings. Printing motion was due to the cylinder mounted at the front of the yoke, the piston being driven by the diaphragm amplifiers shown.

The type head was positioned in one axis only by a digital actuator with two pistons (i.e., two binary bits or four positions). The actuator was coupled to the type head through an arm and a nylon cord driving a pulley under the yoke (See Figures 29 and 57).

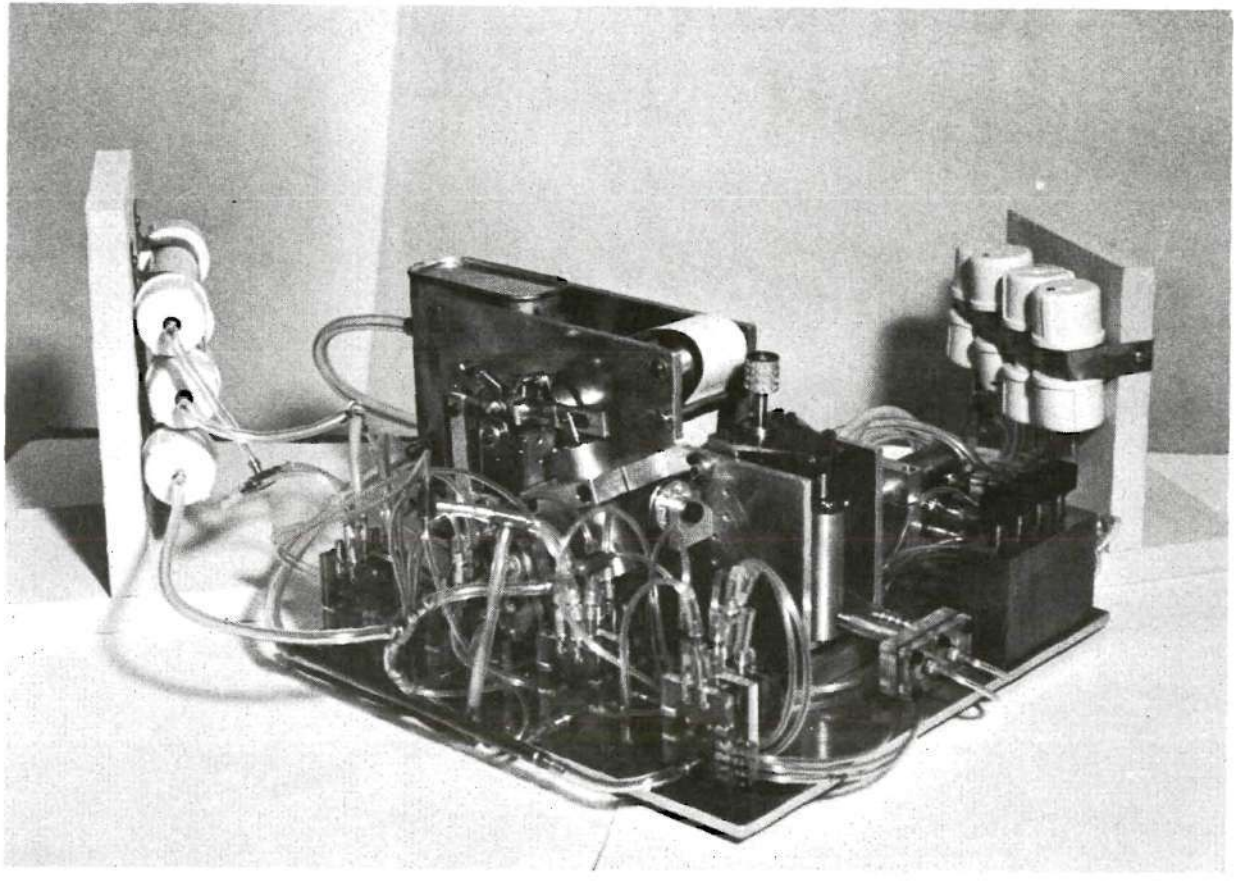

Figure 55. Demonstration Model

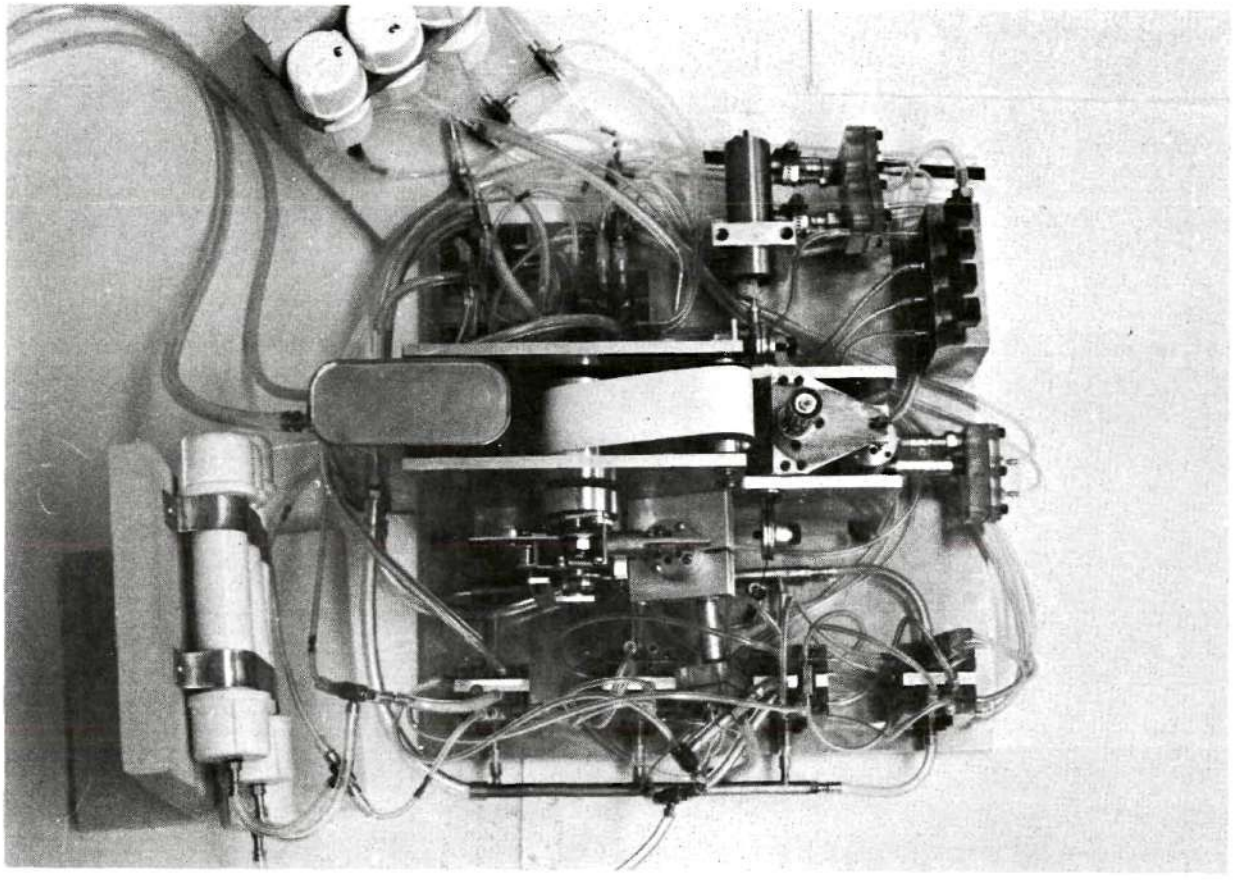

Figure 56. Demonstration Model - Plan View

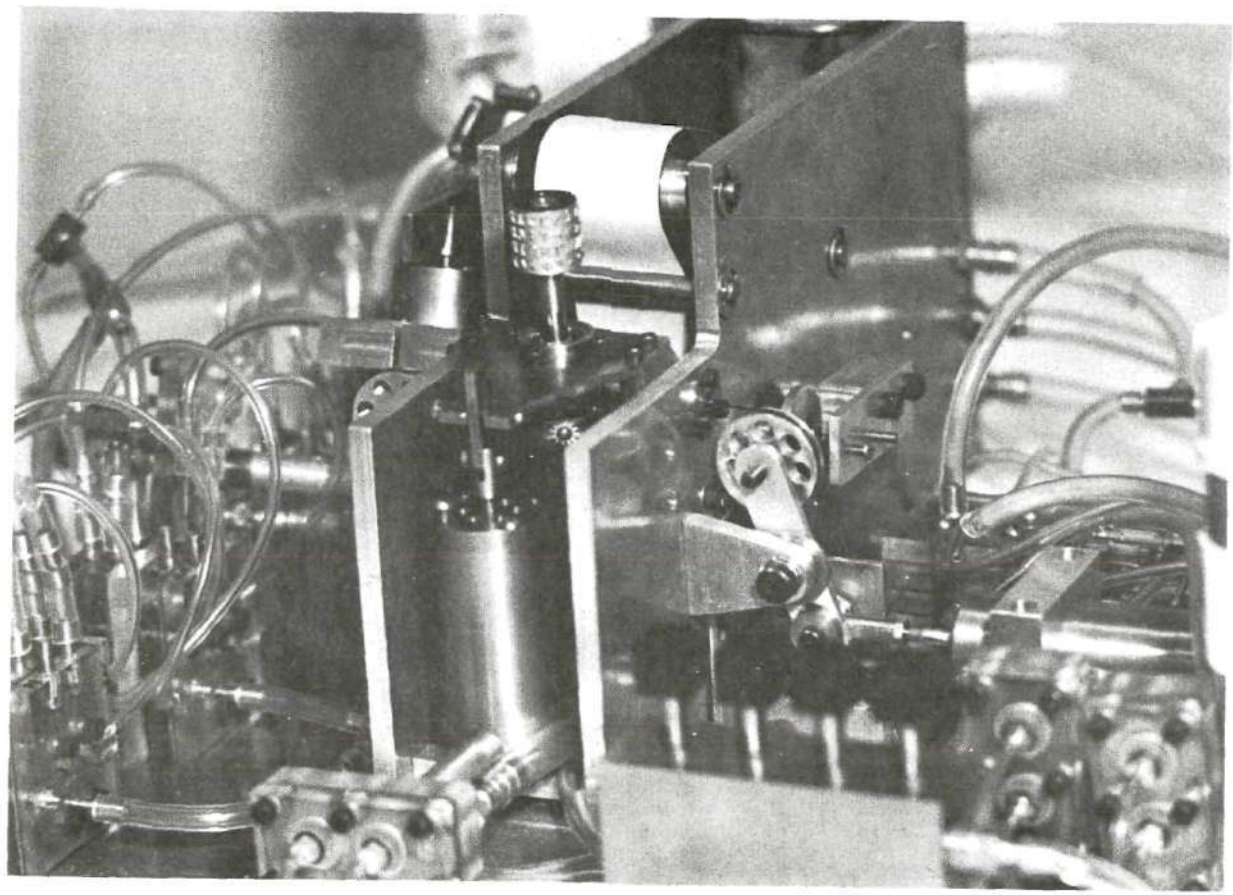

Figure 57. Demonstration Model - Actuator

A carriage and associated positioning means were not provided; however, a cylinder and rachet mechanism were incorporated to advance the paper tape after each print stroke. This cylinder was driven by the same diaphragm amplifier arrangement used for the other actuators, and is equivalent in function to the circuitry necessary to operate a carriage.

Fluidic encoder and control circuitry conforming to the design of Figure 15 was also included. The amplifier construction is illustrated by Figures 58 and 59. The control circuit was of necessity sufficiently complete for full typewriter, except that only two inhibit gates and final drive flip-flops were needed for the two-bit position actuator. The keyboard consisted of four keys of simple slide-valve construction, corresponding to the four-position binary actuator. A diagram of the components constructed is shown in Figure 60.

It was not considered feasible to construct a compressor-accumulator as described in the previous chapter. Air was supplied to the demonstrator from a high pressure supply through a regulator. A small accumulator was included to smooth pressure fluctuations and distribute air to the actuators and amplifiers.

Parameter Selection

The basic parameters defining the demonstration model were determined from the computer model described in Chapter VII. The results of the parameter study of that chapter were incorporated in the input data so that the demonstration model reflects the preferred design. The input data are summarized in Table 9, which parallels Table 4 in format

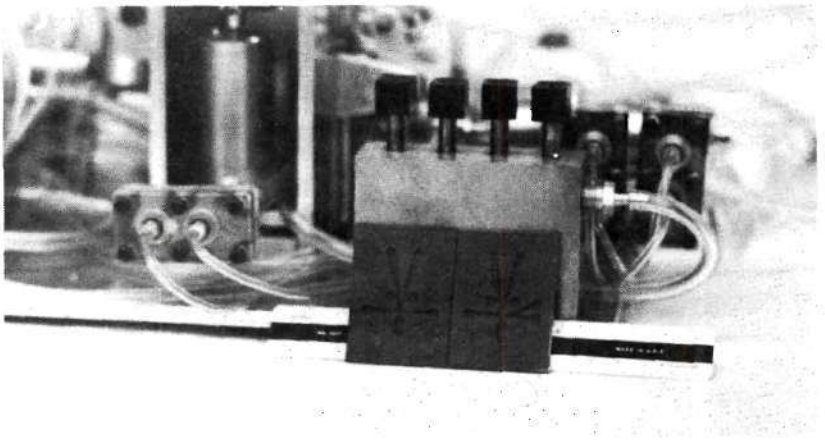

Figure 58. Fluid Amplifiers Etched in Dycril

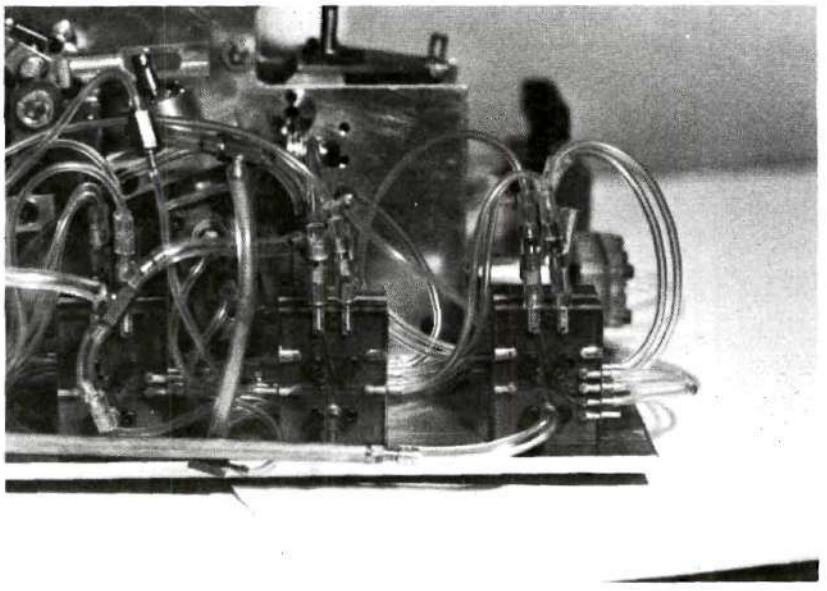

Figure 59. Fluid Amplifier Assembly and Connection

Table 9. Input to Computer Model for Demonstration Model Design

---

Overall System:

Recovery = σ = 0.25	Strouhal No. = N_{SL} = 15
Aspect ratio = η = 2.0	Supply flow temp. = T_S = 70°F
Reynolds No. = Re = 5000	Supply pressure = P_S = 3 psig
Characters/sec. = T_r^{-1} = 10	Specific wt. = = 0.1 lb/in^3

Interface: No. amplifiers = 0

Encoder: No. amplifiers = 2

Type Head:

Outside radius = r_c = 0.344 in.	End thickness = 0.0
Inside radius = r_i = 0.146 in.	Shaft radius = 0.125 in.
Length = ℓ_c = 0.625 in.	Shaft length = 2.25 in.

Rotation:

Pulley radius = r_{15} = 0.5 in.	Arm length = ℓ_5 = 1.0 in.
Pulley radius = r_{25} = 0.5 in.	Arm dist. = a_5 = 0.67 in.
Pulley thick. = 0.187 in.	Arm width = b_5 = 0.5 in.
Max. angle = $\theta_{15}(T_{15})$ = 2.355 rad.	Arm thick. = h_{a5} = 0.125 in.
Time ratio = τ_5 = 2.0	

Print:

Yoke length = b_8 = 2.0 in.
Yoke width = 1.65 in.
Yoke thickness = 0.125 in.
Kinetic energy = 0.088 in/lb
Time ratio = τ_7 = 1.67

Diaphragm Amplifiers:

Flow coeff = C = 0.8	Initial Tension = N_o = 0.1 lb/in

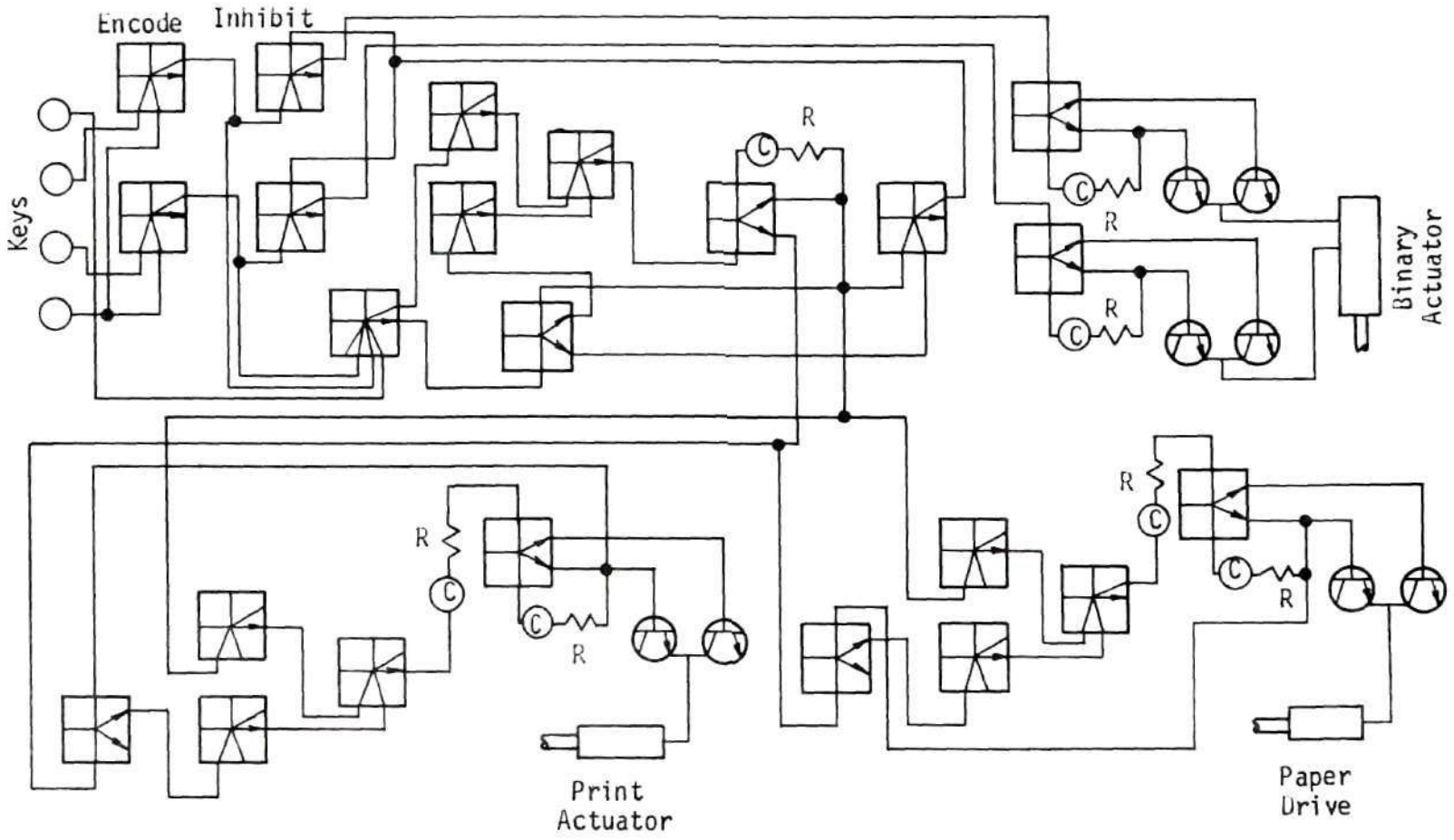

Figure 60. Demonstration Model Schematic

for the sake of comparison.

The Reynolds number was increased to 5000 and the aspect ratio to 2.0. The amplifiers were fabricated by photoetching with the Dupont Dycril process. The material thicknesses available were 0.009 inch, 0.017 inch and 0.042 inch, so that these were the only depths available. The Reynolds number of 5000 resulted in power jet widths (d) of 0.019 inch for the low pressure amplifiers, and 0.008 inch for the high pressure ones. During the course of developing designs for the amplifiers, considerable difficulty was encountered in achieving good pressure recovery with an aspect ratio of one and it was increased to two. This resulted in power jet dimensions of 0.009 inch X 0.017 inch for the high pressure amplifiers and 0.017 inch X 0.042 inch for the low pressure ones.

The type head dimensions of Table 9 correspond to the actual length and outside radius of the available head, with the inside radius computed to give approximately the actual weight for the given $\forall$.

The other dimensions of Table 9 are only slight modifications to those of Table 4 to correspond to convenient dimensions in the practical design of the demonstration model. Changes in parameters such as τ , T_r, etc. follow the results of Chapter VIII. As discussed in Chapter VIII, the stroke length of the print mechanism turns out to be rather long for a ten cps design. For the demonstrator, the print subsystem design for 30 cps was used, which has a much shorter stroke, and the print motion delayed accordingly.

A basic design speed of ten characters per second was chosen for

several reasons. First, this is roughly comparable to commercial machines. Second, the higher the operating speed, the more precision must be expected in both design and construction, and it was felt that limitations of time and funds did not permit such a design goal.

The parameters resulting from the computer computation are listed in Table 10.

The fluid amplifier designs used are shown in Figure 61 in actual size. The basic geometry is derived from the work of Warren [29]. A paper by Moses [40] was also helpful. The high and low pressure amplifier geometry is similar except for the venting employed. The original intent was to vent the amplifiers through the edge of the cover plates by channeling the vent flow as shown for the high pressure devices. This would allow the amplifiers to be stacked one on top of the other and reduce space requirements. This approach was successful for the high pressure devices, but not for the low pressure ones. Due to switching and stability problems, the low pressure amplifiers vents were designed to incorporate, in principle, some vortex vent ideas from Kwok [41]. The general idea is to allow the fluid flowing out the vent to form a vortex which has a smoother transition from flow to pressure energy, and results in matching to the load over a wider flow range.

Representative amplifier characteristics are given in Figures 62 and 63. For the low pressure device, maximum pressure gain was approximately four, with a corresponding flow gain of about four, measured with a slowly rising pressure at the conditions given. Measurements

Flip - Flop

2-input NOR gate

High Pressure

2-input NOR gate

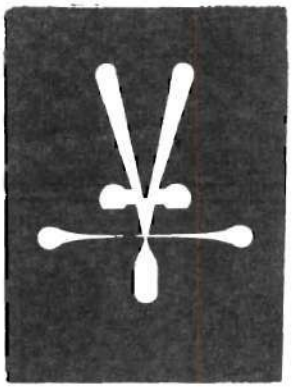

Flip - Flop

4-input NOR gate

Low Pressure

Figure 61. Fluidic Amplifier Geometry for Demonstration Model

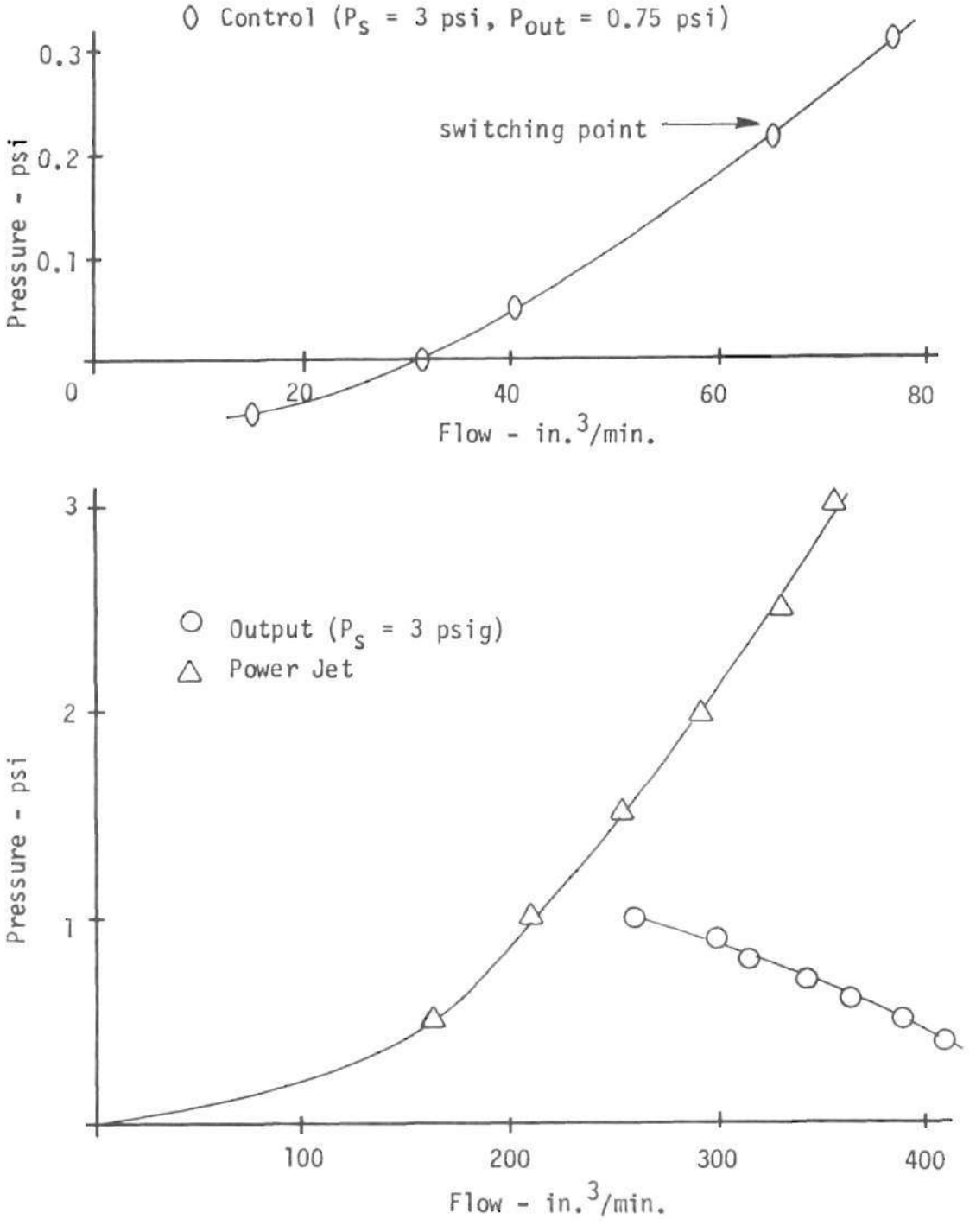

Figure 62. Low-Pressure Amplifier Characteristics

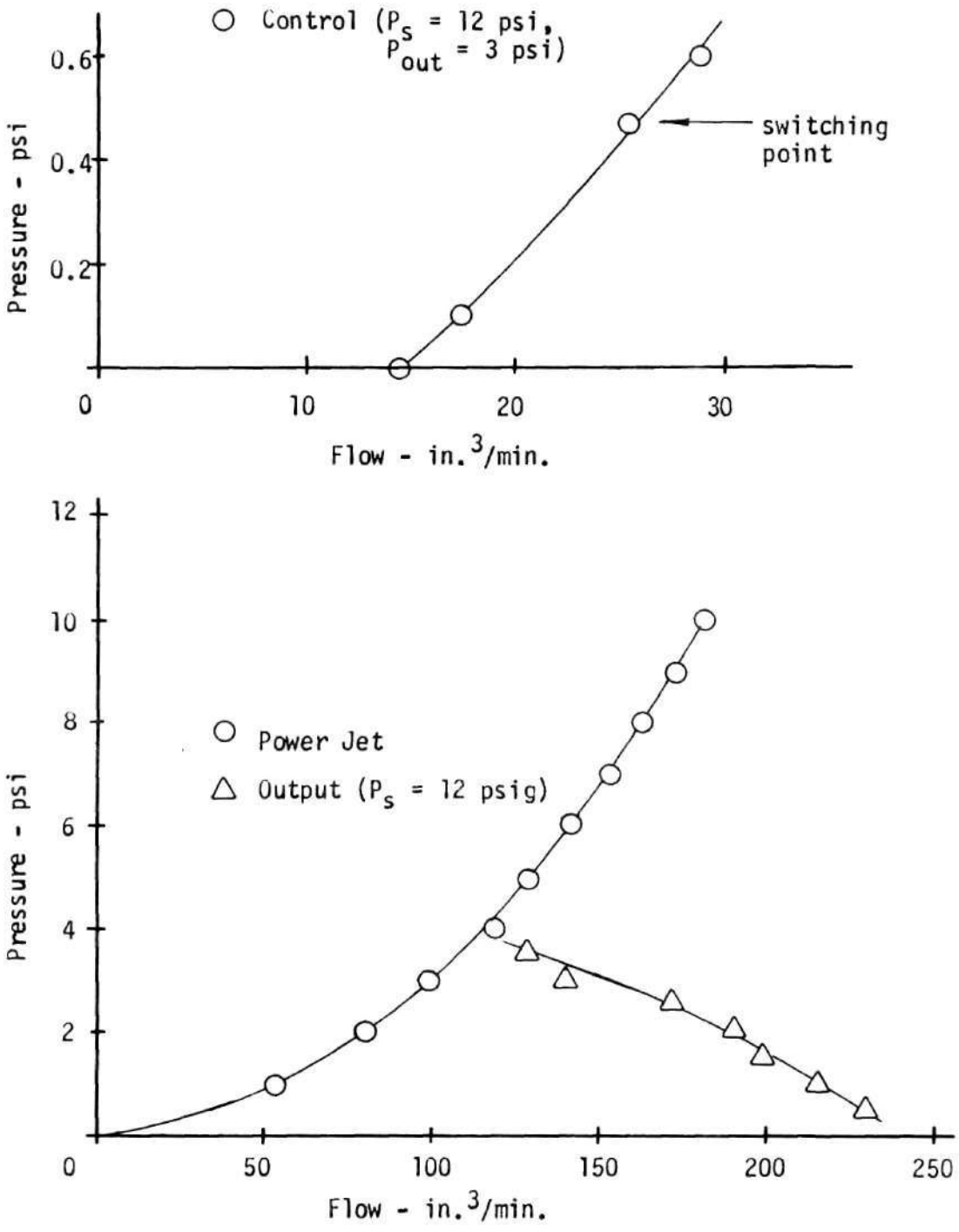

Figure 63. High-Pressure Amplifier Characteristics

Table 10. Predicted Demonstration Model Parameters

Low Pressure Amplifiers:

Nozzle width, d = 0.019 in.
Response time, t_r = 6.8 millisec.

High Pressure Amplifiers:

Nozzle width, d = 0.008 in.
Response time, t_r = 1.6 millisec.

Rotation:

Piston diameter = 0.359 in.
Piston travel = 0.393 in.
Spring constant = 0.086 lb/in

Print:

Piston Diameter = 0.774 in.
Piston travel = 0.697 in.
Type head travel = 0.656 in.
Spring constant = 3.43 lb/in

Diaphragm Amplifiers:

Radius = .185 in.

---

were made with simple U-tube manometers and calibrated rotameters. The high pressure devices had a pressure gain of approximately seven and a flow gain of about five. These gains satisfy the basic design requirements, although operation with blocked outputs was not possible without oscillation for either amplifier type. The four-input NOR of Figure 61 had essentially the same characteristics, although the lower control port had a lower gain than the others.

The fluidic circuitry for the demonstrator was built as in Figure 60 with only one modification in principle to that of Figure 15. Due to matching problems, the inhibit gates 1 and 2 were connected with their power jets supplied by the low pressure supply, P_s, instead of from the encoder output. The encoder outputs were used as control port signals to 1 and 2 and the inhibit signal from 13 was connected to the interaction region vent of 1 and 2. The control action thus obtained was the same, but was achieved in this slightly different manner. Pressure matching in the control circuitry was achieved with small bleed orifices where needed, and these were sized by experimentation. The RC time constants of Figure 15 were also chosen by experiment. The capacitors, whose size in proportion to the overall machine can be seen in Figures 55 and 56, ranged in volume from 4.2 in^3 to 1.3 in^3. Such volumes are quite feasible from the standpoint of machine size.

A repetition of the circuitry for the printing control shown in Figure 15 was added for the paper drive in the demonstrator. The same piston design was used for the print and paper drives. Since the paper drive in the demonstrator did not correspond to an actual typewriter mechanism, no special design was undertaken for it. Figure 58 shows two of the etched amplifiers, and Figure 59 illustrates the assembly and connection methods.

Performance

Performance of the fluidic portions of the demonstration model were as anticipated in terms of the logical operations. The timing functions were also satisfactory for the purposes of the demonstrator,

as will be seen from the resulting timing diagram to be given subsequently. The use of RC time constants presents one practical problem which requires careful design; however, the switching pressure derived from an RC combination should occur at about one or two time constants in order to avoid switching on the flat portion of the curve, since this can lead to variation in switching times. Restrictions imposed by other matching requirements sometimes make this difficult to achieve. In the demonstrator, there were instances of time period variations of approximately $\pm$ 10 per cent from operation to operation of a given RC circuit.

The binary actuator constructed according to Tables 9 and 10 had an unsatisfactory performance in that its stroke was slow and incomplete, particularly on the high-order piston. This can be attributed to several factors. First, the design spring constant was 0.086 lb/in, whereas the actual spring constant turned out to be 0.125 lb/in. Secondly, because of the small diameter (0.375 inch) of the actuator, it was difficult to machine the pistons and stops to the exact configuration assumed by the computer program. This resulted in the weight of the moving actuator parts being one ounce instead of the predicted 0.3 ounce. This increased the total effective mass by 15 per cent over that computed. The effect of these changes would be, according to Equation (80), to require a 3.7 psi supply pressure instead of 3.0. It was found by experiment that 0.75 psi was required to overcome static friction in the actuator, raising the required pressure to 4.45 psi. From the standpoint of static forces required, the predicted force required of the

piston at maximum stroke was 4.95 ounces. The predicted maximum force attainable ($P_S A$) was 5.28 ounces with a cylinder pressure of 3.0 psig. This points out that the dynamic model with the assumption of no friction had predicted parameters which met static requirements, but left little margin for error from the practical standpoint. In fact, the measured stroke was 8.25 ounces. This was due both to the increased spring constant and to binding in the mechanical connection between the piston rod end and the pivot arm.

It is apparent, then, that there were several reasons for the actuator performance. For the demonstration model, these were overcome in two ways. The piston diameter of the actuator was increased from 0.375 inch to 0.625 inch. These pistons were more accurate and relatively lighter in weight (in terms of the force generated by the piston), resulting in less leakage and smoother operation. Second, the piston rod-arm connection was improved to provide for better relative motion, and the piston rod was supported at the end throughout its travel to reduce a tendency to cock the pistons and increase frictional resistance. The resulting performance is shown in Figure 64a. The upper trace is the pressure in the high-order bit cylinder as measured with a Pitran* pressure transducer. Both bits were actuated in this figure. The pressure was essentially constant at 3.0 psig and the horizontal time scale of 20 milliseconds/division indicates a very rapid pressure rise, giving the almost square pressure pulse assumed in the theoretical

---

*Manufactured by Stow Laboratories

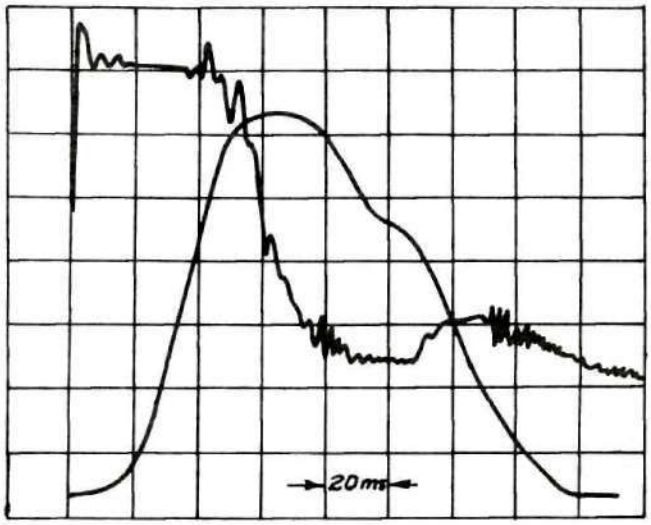

a) Binary Actuator

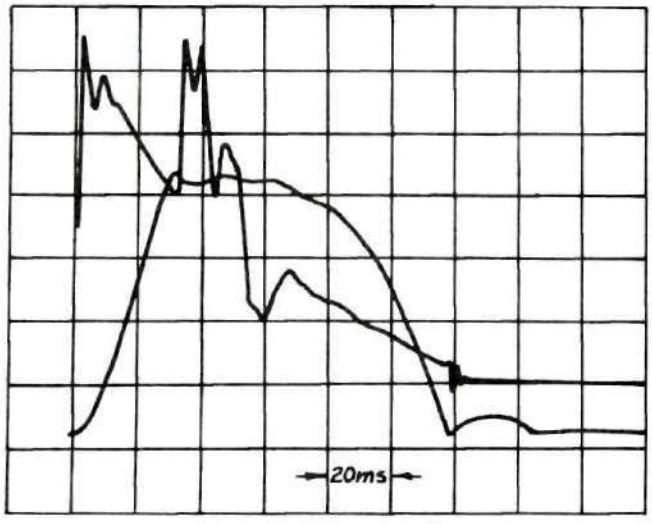

b) Print Actuator

Figure 64. Actuator Pressure and Motion Time Response

derivations. The lower trace of Figure 64a is the motion of the piston rod as measured by a photoelectric cell, and represents the maximum actuator stroke (both bits). A small vane attached to the rod was made to interrupt the light path illuminating the cell to produce a voltage indicative of rod position. The voltage versus position curve was approximately linear, so this trace is a reasonably good representation of the motion. The beginning and end of the forward and return strokes are represented accurately, of course. The pressure pulse is seen to be approximately 50 milliseconds long, corresponding to the design requirement, and the forward stroke time is also 50 milliseconds. The design required a return stroke time of 50 milliseconds also, but this was not achieved in this case. The actual time was about 75 milliseconds. This is due both to frictional effect, particularly the small amount of binding left in the pivot arm connection, and to a small amount of friction purposely introduced, which will be described later.

The performance of the print mechanism is shown by Figure 64b. The upper trace is the pressure in the cylinder and the lower one is the motion of the yoke supporting the type head, which is representative of the type head motion. The time scale is 20 milliseconds per division. Since the print mechanism was designed on the basis of 30 cps with $\tau = 1.67$, the forward stroke time should be about 20 msec. The time shown in the figure is about 30 msec. The return stroke time shown in Figure 64b is approximately 70 milliseconds, and there is a dwell of about 30 milliseconds. Theoretically, the return stroke should have been 13 milliseconds. The long return has several causes. First,

it is evident from the pressure trace that the cylinder pressure does not return to zero rapidly but retards the return motion. This could be due to improper operation of the exhaust diaphragm amplifier or to a slightly long timing pulse. Secondly, the link connecting the yoke to the piston rod was slotted to allow a free flight of the type head at the end of the stroke. The free flight was actually short (approximately 1/32 inch), but the slot was considerably longer, so that on the return the spring acting on the piston was not connected to the yoke until the piston neared the end of its return travel. This caused the type head return motion to be largely due to rebound from the platen, which was obviously not a desirable situation.

Also, in order to achieve the forward stroke time shown in Figure 64b, it was necessary to reduce the spring constant from the calculated 3.43 lb/in to 0.63 lb/in. This rather large difference can be ascribed to several causes. The effective mass was computed using some approximations which no doubt affected the performance. Also, friction was neglected, although this did not appear to be a significant factor in the performance. Probably the most significant factor was the choice of $\tau = 1.67$. This came about due to the arbitrary relation $\tau_7 = (5/6)\,\tau_5$ used in Chapter VII to develop Figure 46. In that instance, it was shown that $\tau_5 = 2$ was a good choice and $\tau_7 < \tau_5$ was required. These values for τ were carried over into the demonstration model before an important implication was realized. The energy balance at the end of the stroke ($t = T$) can be written

$$P_s A x(T) = 0.5 m[\dot{x}(T)]^2 + 0.5 k[x(T)]^2 \qquad (168)$$

By equating (81) and (84) and evaluating Equation (83) at $\tau = 2$, it can be shown that

$$P_s A x(T) = m[\dot{x}(T)]^2 \qquad (169)$$

Combining this with (168) and dividing through by X(T), the result is

$$P_s A = k x(T) \qquad (170)$$

The implication of this last expression is that, for $\tau = 2$, the applied force is equal to the spring force at the end of the stroke. Furthermore, if $\tau < 2$, the spring force is greater than the pressure force at the end of the stroke. In other words, the system is decelerating at the end of the stroke. This is not a good design condition, and τ must be increased by decreasing k. The value 1.67 for τ_7 is not actually required since the print subsystem was designed for 30 cps. This decrease in k may also have contributed to the long return stroke.

One further evaluation of the print subsystem performance was made. Figure 65 shows the print cylinder pressure in the upper trace and the type head velocity in the lower trace. The velocity was measured with a calibrated transducer consisting of a moving permanent magnet slug in an annular coil. Peak velocity shown is 30.8 in./sec. The theoretical velocity based on the computed effective mass is 65.9 in/sec from Equations (7) and (141). This velocity was sufficient to produce

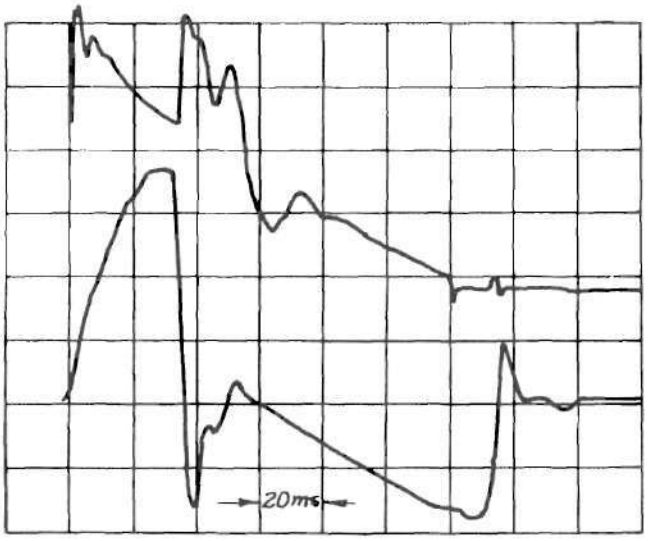

Figure 65. Print Actuator Pressure and Type Head Velocity

printing on a single-part form (i.e., one copy).

Figure 65 also serves to explain the shape of the pressure pulse. It is obvious that the type head struck the platen and reversed its motion by rebounding, which caused an increase in cylinder pressure since the timing pulse had not opened the exhaust diaphragm amplifier. Thus, a decrease in the pressure pulse width would probably have decreased the overall response time of the print mechanism.

The performance of the typewriter as a whole is illustrated in Figure 66, which is a timing diagram of the major functions. This diagram presents two sets of curves, the solid curves being a composite of oscilloscope traces of the various pressure signals and actuator

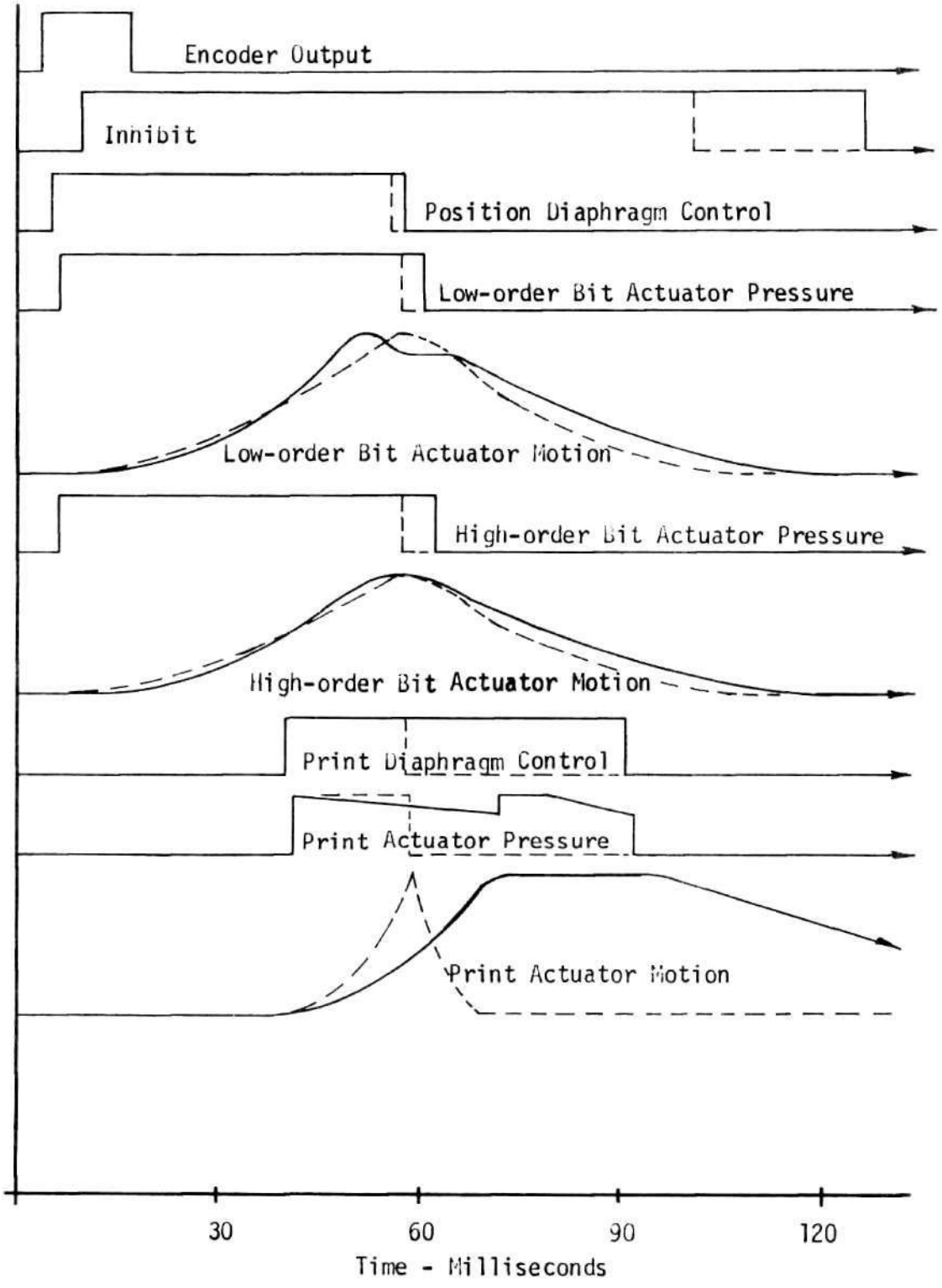

Figure 66. Demonstrator Timing Diagram

motions, all of which were referenced to a single key operation at zero time. The dashed curves represent theoretical performance. The pressure pulses and motion curves are slightly idealized for the sake of comparison. There is no magnitude scale, but the time scale is essentially correct. The measured binary actuator motions correspond closely to the theoretical and the encoder and inhibit signals are as expected. The print actuator motion is close to the design motion on the forward stroke, as discussed previously, but the pressure pulse and return stroke are longer than anticipated. Since the print subsystem was designed for 30 cps, a return motion considerably longer than theoretical could be tolerated for an overall performance of 10 cps. However, the response was slow enough to require extending the inhibit signal to 125 msec. This corresponds to an overall design of eight characters per second. A different timing of the print pressure pulse probably would have met the overall objective of 10 cps. Therefore, despite some modifications to certain parameters, principally the spring constant of the print subsystem and the binary actuator diameter, the overall machine performance in terms of speed of operation was close to the design speed.

The printing quality obtained was not of commercial caliber, as can be seen from Figure 67, but was sufficient to be encouraging. The letters set up to type out were X, Q, S and U, which are shown typed several times. These characters were typed rapidly in succession and are typical of the printing capability.

It will be observed that the type head angular positioning is not

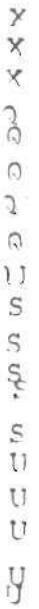

Figure 67. Typical Typed Output

completely repeatable. The variations are due to several factors, including friction effect, mechanical tolerance, and small variations in timing pulses. An additional factor which has not been discussed before was that of overshoot in the positioning mechanism. No provision was made in the simplified design procedure to account for rebound or overshoot in this subsystem, and overshoot was encountered in two ways. There was some overshoot in the binary actuator itself. For example, if the low-order bit was pressurized, it moved forward pushing the high-order piston in front. When the low-order piston hit its stop, the high-order piston was restrained only by the action of the spring communicated by the flexible cord. The high-order piston had a tendency to continue moving which pulled the type-head beyond its intended

position. Another contributing factor was overshoot of the type head, its shaft and cord-pulley. Again, due to the cord connection, it was possible for the rotational inertia of the type head assembly to continue past its intended position. The remedy taken for this overshoot problem was to introduce a small amount of coulomb friction on the cord between the type head and the spring. As can be seen from the typed characters, this did not completely alleviate the problem, but it helped considerably. This added friction did tend to increase the actuator response time, but the effect was not severe as can be seen from Figure 66.

Summary

A demonstration model designed on the basis of the mathematical models and computational methods of the previous chapters, and including the mechanisms exemplified by those computations was constructed. The type quality achieved was legible but not of commercial quality. The typing speed capability was approximately eight characters per second, compared to the predicted ten per second. This discrepancy was largely due to the printing subsystem performance which would have been improved by changing the timing of the control pressure pulse and the mechanical link between the piston and the yoke. Changes in the mechanical parameters from those predicted in order to achieve this performance were an increase in the binary actuator piston diameter, a reduction in the print return spring constant, and addition of a small amount of friction to the type head positioning cable.

The fluidic portions of the model operated satisfactorily from

standpoint of correct logical operations and proper timing sequence. Pressure pulses to the actuators had very fast rise times due to the low impedance diaphragm amplifiers, as predicted by the mathematical modeling.

The demonstrator showed, in general, that a fluidic typewriter could be constructed and have performance comparable to existing typewriters, and that the means used in previous chapters to arrive at an approximate design for a given performance criterion are useful if their limitations are kept in mind.

CHAPTER X

CONCLUSIONS AND RECOMMENDATIONS

Conclusions

Keeping in mind that the results of this investigation reflect the design criteria of minimum power consumption and maximum speed, as well as the basic mechanical configurations considered, some conclusions which bear on the feasibility of a fluidic typewriter and its overall design follow:

1. Diaphragm amplifiers used to drive the mechanical actuators reduce power consumption of the actuator - amplifier combination by an order of magnitude, and should be used instead of Coanda amplifiers.
2. Sequencing and control on a synchronous basis with RC time constants best satisfies the criteria and requires 26 Coanda amplifiers.
3. Time response of the Coanda amplifiers does not affect performance below approximately 30 characters per second.
4. Assuming four-input amplifiers are available, 110 Coanda amplifiers are required for a complete typewriter if stationary keys are incorporated.
5. The 49 amplifiers used for stationary keys have a high relative power consumption, especially at low design typing speeds.
6. Coanda amplifiers should be operated at minimum Reynolds

numbers and low aspect ratio. The range from d = 0.001 inch to d = 0.035 inch covers amplifiers which would be of interest for the typewriter. These are feasible and, with integrated circuit construction, present no problems from size or weight standpoints.

7. Amplifier supply pressure should be as high as possible to reduce actuator sizes, even though there is a slight increase in overall power consumption with increasing pressure at low typing speeds (15 cps).
8. The largest portion of the energy required for a print cycle goes to the fluidics at low speeds and to the positioning actuators at high speeds. Printing energy is relatively low at all speeds.
9. Actuator piston sizes in the range of one inch or less can be achieved for P_s = 3 psig. This presents little problem in terms of typewriter size or weight.
10. A rotary, sliding vane, positive displacement compressor is the best choice for the power supply.
11. The high intermittant flow requirements for high speeds (30 cps) result in compressor power consumption of approximately one-third horsepower. At 10 cps, the power is only 0.03 horsepower.
12. Based on power requirements, compressor size and actuator sizes, an upper limit on speed capability seems to be about 30 characters per second.

13. The print actuator should be part of the carriage assembly. Position actuators might also be part of the carriage for low speed designs.
14. A fluidic typewriter with the general design features described in previous chapters is feasible, and could be comparable to available commercial machines in size, weight and performance. Considerable development beyond that of this investigation would be required to achieve commercial performance.

Recommendations

Aside from general development of the fluidic typewriter towards commercialization, there are several areas in which further study could be made to provide useful theoretical background.

1. The transient motion of a piston moving in a cylinder and driven by a compressible fluid supplied through a transmission line. This would help improve high speed actuator design.
2. The problem in 1. could be extended to cover the binary actuator by including multiple pistons and inputs.
3. A basic limitation of fluidics in the type application studied here was the pressure recovery of Coanda amplifiers. Sarpkaya [42] has described high pressure recovery amplifiers, and their applicability should be considered.
4. The diaphragm amplifiers have advantages so long as the diaphragms are not damaged by high pressure. High pressure

(>3 psi) diaphragm amplifiers with good response should be investigated.

APPENDIX A

DERIVATION OF EQUATION (21)

Note that Equations (6) and (18) give

$$w = \rho_m q_m T \tau \tag{171}$$

Substituting (20) and (171) into (14) gives

$$\epsilon(T) = \frac{Y \exp\left(-\frac{w}{2R^2\tau}\right)}{\left(1 - \frac{Y^2}{4R^2}\right)^{0.5}} \sin\left[\frac{w}{YR\tau}\left(1 - \frac{Y^2}{4R^2}\right)^{0.5}\right] \tag{172}$$

Then, from Equation (19) and (20)

$$R^2 = \frac{4w(\tau-1)^2}{\pi^2 Y^2 \tau^2} \tag{173}$$

Substituting into Equation (172) gives

$$\epsilon(T) = \frac{Y \exp\left(-\frac{\pi^2 Y^2 \tau}{8w(\tau-1)^2}\right)}{\left(1 - \frac{Y^2\pi^2\tau^2}{16w^2(\tau-1)^2}\right)^{0.5}} \sin\left[\frac{\pi}{2(\tau-1)}\left(1 - \frac{\pi^2 Y^4 \tau^2}{16w^2(\tau-1)^2}\right)^{.05}\right] \tag{174}$$

The definitions of Equations (22) and (23) are directly from Equation (174), and result in Equation (21).

APPENDIX B

DERIVATION OF EQUATION (90)

The solution to Equation (4) at t = T is

$$x(T) = \frac{\rho_m A}{k}\left\{1 - \frac{\exp\left(-\frac{\rho_m A^2 T}{2q_m m}\right)}{\left(1 - \frac{\rho_m^2 A^4}{4q_m^2 km}\right)^{0.5}} \cdot \sin\left[\frac{k^{0.5} T}{m^{0.5}}\left(1 - \frac{\rho_m^2 A^4}{4q_m^2 km}\right)^{0.5} + \psi\right]\right\} \tag{175}$$

where

$$\psi = \tan^{-1}\left[\frac{1 - \frac{\rho_m^2 A^2}{4q_m^2 km}}{\frac{\rho_m A^2}{2q_m k^{0.5} m^{0.5}}}\right] \tag{176}$$

It can be seen from Equations (6), (18), (20) and (88) that

$$\frac{\rho_m A^2}{2q_m k^{0.5} m^{0.5}} = \frac{W(\tau-1)}{\pi R^2} \tag{177}$$

$$\frac{\rho_m A}{k} = \frac{4WT(\tau-1)^2}{\pi^2 R m^{0.5}} \tag{178}$$

and

$$\frac{\rho_m A^2 T}{2q_m m} = \frac{W}{2R^2} \tag{179}$$

A substitution in (175) gives

$$x(T) = \frac{4BRT(\tau-1)}{\pi m^{0.5}}\left[1 - \frac{\exp\left(-0.5\pi B(\tau-1)^{-1}\right)}{(1-B^2)^{0.5}}\sin\frac{\pi(1-B^2)}{2(\tau-1)}\right]$$

$$\psi = \frac{(1-B^2)^{0.5}}{B}$$

where

$$B = \frac{W(\tau-1)}{\pi R^2}$$

as in Equation (90)

If the first term on the right is factored to

$$\frac{4B^{0.5}(\tau-1)^{1.5}}{\pi^{1.5}} \cdot \frac{B^{0.5}RT(\tau-1)^{-0.5}}{\pi^{-0.5}m^{0.5}}$$

and B is replaced by Equation (90) in the right factor, the resulting Equation can be written as Equation (91).

APPENDIX C

DERIVATION OF MOMENT OF INERTIA OF TYPE HEAD

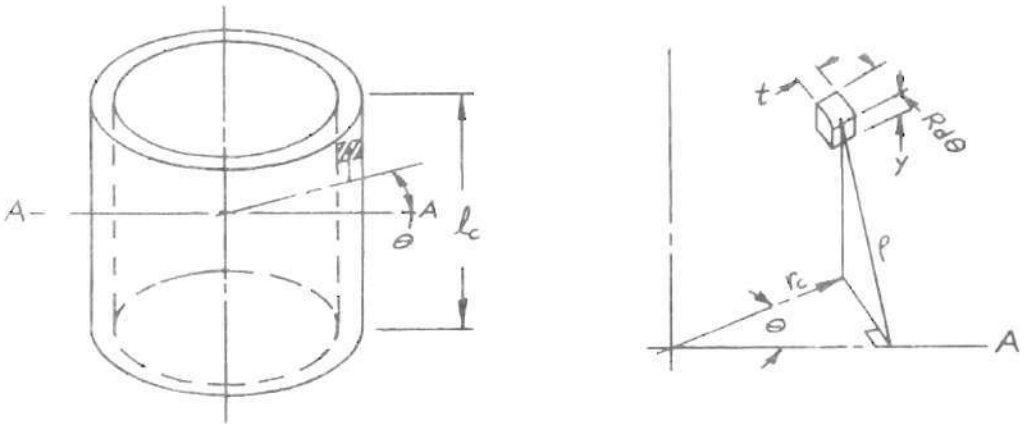

If the ends of the cylinder are neglected,

$$I_{AA} = \int \rho^2 dM$$

$$= \iint (y^2 + r_c^2 \sin^2\theta)\, \gamma_m t\, R d\theta dy$$

$$= 2\gamma_m r_c t \int_0^{2\pi} (y^2 + r_c^2 \sin^2\theta)\, dy d\theta$$

$$I_{AA} = \frac{\pi \gamma_m r_c t \ell_c^3}{6} + \gamma_m \pi \ell r_c^3 t$$

where γ_m is the density.

The mass of the cylinder is given by

$$m_c = 2\pi r_c t \gamma_m \ell_c$$

Thus

$$I_{AA} = \frac{m_c \ell_c^2}{12} + \frac{m_c r_c^2}{2}$$

BIBLIOGRAPHY

1. U. S. Patent 522,491; Pneumatic Type-Writing Machine, July 3, 1894.

2. U. S. Patent 543,164; Type-Writing Machine, July 3, 1895.

3. U. S. Patent 1,096,275; Pneumatic Type-Writer, May 12, 1914.

4. U. S. Patent 3,315,775; Fluid Actuated Typewriter, April 25, 1967.

5. R. N. Auger, "Turbulence Amplifier Design and Application", Proceedings of Fluid Amplification Symposium, Vol. 1, October, 1962, Harry Diamond Laboratories.

6. P. Bauer, "Pure Fluid Digital Logic With a Single Switching Element", Ibid.

7. P. Bauer, and E. E. Matzger, "Digital Data Handling Speeds With Pure Fluid (Pneumatic) Circuits", Proceedings of Fluid Amplification Symposium, Vol. II, October, 1965, Harry Diamond Laboratories.

8. B. Bliven, Jr., The Wonderful Writing Machine, Random House, 1964.

9. P. K. Chang, "Survey of Coanda Flow", Proceedings of Fluid Amplification Symposium, Vol. 1, October, 1962, Harry Diamond Laboratories.

10. R. A. Comparin, A. E. Mitchell, H. R. Mueller, and H. M. Glaettli, "On the Limitation and Special Effects in Fluid Jet Amplifiers", ASME Symposium on Fluid Jet Control Devices, November 1962.

11. R. A. Comparin, W. C. Jenkins, Jr., and R. B. Moore, Jr., "Jet Reattachment at Low Reynolds Numbers and Moderate Aspect Ratios", American Society of Mechanical Engineers, Paper No. 67-FE-25. May 8, 1967.

12. H. H. Glaettle, H. R. Mueller, and R. H. Zingg, "Remarks on the Limitations of Pure Fluid Elements", Proceedings of Fluid Amplification Symposium, Vol. 1, May 1964, Harry Diamond Laboratories.

13. B. J. Greenblott, "A Development Study of the Print Mechanism on the IBM 1403 Chain Printer", American Institute of Electrical Engineers, Conference Paper CP-62-381, Winter General Meeting,

14. H. F. Hrubecky, and L. N. Pierce, "The Effect of Geometric Changes upon the Switching Point in a Model Bistable Fluid Amplifier", Proceedings of Fluid Amplifications Symposium, Vol. I, May, 1964, Harry Diamond Laboratories.

15. J. Iseman, "Fluid Amplification. 9(rev.). Fluid Digital Logic Elements and Circuits", Harry Diamond Laboratories TR-1302, August 16, 1965. STAR N66-14948.

16. D. F. Jensen, H. R. Mueller, and R. R. Schaffer, "Pneumatic Diaphragm Logic", Advances in Fluidics, Proceedings of 1967 Fluidics Symposium, ASME.

17. D. F. Jensen, "Static Operating Characteristics of Diaphragm Pneumatic Logic Devices", Ibid.

18. S. Katz, E. T. Winston, and P. Hanes, "The Response of a Bistable Amplifier to a Step Input", Proceedings of Fluid Amplification Symposium, Vol. I, May, 1964, Harry Diamond Laboratories.

19. G. V. Lemmon, and E. R. Phillips, "Development of Two Pure Fluid Timers", Proceedings Fluid Amplification Symposium, Vol. II, May, 1964, Harry Diamond Laboratories.

20. G. A. Maley, and J. Earle, The Logic Design of Transistor Digital Computers, Prentice-Hall, Inc., 1963.

21. R. E. Olsen, "Reattachment of a Two-Dimensional Compressible Jet to an Adjacent Plate", ASME Symposium on Fluid Jet Control Devices, November, 1962.

22. K. N. Reid, Jr., "Dynamic Interaction of a Fluid Jet and Receiver Load System", Proceedings of Fluid Amplification Symposium, Vol. IV, October, 1965, Harry Diamond Laboratories.

23. E. F. Richards and S. D. Graber, "Transition to Turbulence and Wall Attachment of Miniature Jets", Ibid.

24. H. E. Riordan, "High Speed Pneumatic Digital Operations with Moving Elements", Proceedings of Fluid Amplification Symposium, Vol. I, October 1962, Harry Diamond Laboratories.

25. H. T. Saghafi, "Static Design of Pneumatic Logic Circuits", Proceedings of Fluid Amplification Symposium, Vol. II, May, 1964, Harry Diamond Laboratories.

26. D. A. Small, "Optimizing Element Size for Speed and Power Consumption", ASME Paper 67-WA/FE-39, November 12, 1967.

27. M. L. Walker, Jr., and R. P. Trask, II, "Feasibility Study of a Laminar Nor Unit", Advances in Fluidics, Proceedings of the 1967 Fluidics Symposium, ASME.

28. W. H. Walston, Jr., "Transient Response of a Fluid Line with and without Bleeds", Proceedings of Fluid Amplification Symposium Vol. II, October, 1965, Harry Diamond Laboratories.

29. R. W. Warren, "Some Parameters Affecting the Design of Bistable Fluid Amplifiers", Proceedings of Symposium on Fluid Jet Control Devices, ASME, November 28, 1962.

30. R. W. Warren, "Wall Effect and Binary Devices", Proceedings of Fluid Amplification Symposium, Vol. I, October 1962, Harry Diamond Laboratories.

31. Daryl L. Letham, "Fluidic System Design, 7. Turbulence Amplifiers", Machine Design, July 7, 1966.

32. Raymond N. Auger, "How to Use Turbulence Amplifiers for Control Logic", Reprint No. 935, Control Engineering.

33. C. B. Schuder and R. C. Binder, "The Response of Pneumatic Transmission Lines to Step Inputs", Trans. of the ASME, Journal of Basic Engineering, December, 1959, p. 578.

34. B. C. Kuo, Automatic Control Systems, Prentice Hall, Inc. 1962.

35. A. H. Shapiro, The Dynamics and Thermodynamics of Compressible Fluid Flow, Volume I, Ronald Press, New York, 1953.

36. J. F. Blackburn, Ed., Fluid Power Control, MIT Press, 1960.

37. C. R. Wiley, Jr., Advanced Engineering Mathematics, McGraw-Hill, Inc. 1966.

38. D. G. Shepard, Principles of Turbomachinery, The Macmillan Company, New York.

39. H. F. Lehmkuhl, "Rotary Compressors 1 to 25 Horsepower, Design and Performance", Symposium on Positive Displacement Compressors, ASHRAE, January 30, 1967.

40. H. L. Moses, and D. S. McRee, "Switching in Digital Fluid Amplifiers", ASME Paper No. 69-FLCS-31, June 16, 1969.

41. Clyde C. K. Kwok, "Vortex Flow in a Thin Cylincrical Chamber and its Applications in Fluid Amplifier Technology", Rept. No. 66-8, Department of Mechanical Engineering, McGill University, September, 1966.

42. T. Sarpkaya, "The Performance Characteristics of Geometrically Similar Bistable Amplifiers", Trans. of the ASME, Journal of Basic Engineering, June, 1969.

VITA

Richard Austin Whisnant was born in Asheville, North Carolina on February 9, 1935. He is the son of Mr. and Mrs. John K. Whisnant of Shelby, North Carolina. Richard attended elementary and secondary schools in Asheville and Buncombe County, North Carolina, and was graduated from Sand Hill High School, Buncombe County, North Carolina in June, 1952. He attended Georgia Institute of Technology from 1952 to 1957 on the Cooperative Plan and was awarded the degree Bachelor of Mechanical Engineering in June, 1957.

Following graduation Mr. Whisnant was employed by the Westinghouse Electric Corporation, New Products Laboratory, at Pittsburgh, Pennsylvania. During this time he was engaged in new product development in the areas of thermoelectricity, ultrasonic cleaning and electrodynamic loudspeakers. In 1962, he accepted a position with the Deering Milliken Research Corporation, Spartanburg, South Carolina, where he did textile process development. During 1964, Mr Whisnant joined the Sea Technology Corporation of Sarasota, Florida. The principal activity there was the development of electronic shrimp fishing gear. In 1965, he returned to Deering Milliken Research Corporation and the following year entered the Graduate School of the Georgia Institute of Technology.

Mr. Whisnant was awarded the degree Master of Science in Mechanical Engineering in June, 1968, and continued his work toward the Doctor of Philosophy in the School of Mechanical Engineering. While completing

the requirements for the doctorate, Mr. Whisnant accepted, in February, 1970, the position of Senior Research Engineer with the Burlington Industries Research Center at Greensboro, North Carolina, where he is presently employed.

In June, 1957, Mr. Whisnant was married to the former Kathleen Elaine Sanford of Asheville. They have two daughters, Lisa and Kathy. He is a member of Tau Beta Pi, Pi Tau Sigma, the American Society of Mechanical Engineers, the Institute of Electrical and Electronic Engineers, and is a Registered Professional Engineer in Pennsylvania.